RECOVERY OF TUNGSTEN FROM TUNGSTEN BEARING COMPOUNDS

A THESIS SUBMITTED TO
THE GRADUATE SCHOOL OF NATURAL AND APPLIED SCIENCES
OF
MIDDLE EAST TECHNICAL UNIVERSITY

BY

METEHAN ERDOĞAN

IN PARTIAL FULFILLMENT OF THE REQUIREMENTS
FOR
THE DEGREE OF DOCTOR OF PHILOSOPHY
IN
METALLURGICAL AND MATERIALS ENGINEERING

FEBRUARY 2013

Approval of the thesis:

RECOVERY OF TUNGSTEN FROM TUNGSTEN BEARING COMPOUNDS

submitted by **METEHAN ERDOĞAN** in partial fulfillment of the requirements for the degree of **Doctor of Philosophy in Metallurgical and Materials Engineering Department, Middle East Technical University** by,

Prof. Dr. Canan Özgen   _____
Dean, Graduate School of **Natural and Applied Sciences**

Prof. Dr. C. Hakan Gür   _____
Head of Department, **Metallurgical and Materials Engineering**

Prof. Dr. İshak Karakaya   _____
Supervisor, **Metallurgical and Materials Engineering Dept., METU**

Examining Committee Members:

Prof. Dr. Naci Sevinç   _____
Metallurgical and Materials Engineering Dept., METU

Prof. Dr. İshak Karakaya   _____
Metallurgical and Materials Engineering Dept., METU

Prof. Dr. Yavuz Topkaya   _____
Metallurgical and Materials Engineering Dept., METU

Prof. Dr. Tayfur Öztürk   _____
Metallurgical and Materials Engineering Dept., METU

Assoc. Prof. Dr. Hasan Okuyucu   _____
Materials Engineering Dept., YBU

Date: 01.02.2013

I hereby declare that all information in this document has been obtained and presented accordance with the academic rules and ethical conduct. I also declare that, as required by these rules and conduct, I have fully cited and referenced all material and results that are not original to this work.

Name, Last name: Metehan Erdoğan

Signature:

ABSTRACT

RECOVERY OF TUNGSTEN FROM TUNGSTEN BEARING COMPOUNDS

Erdoğan, Metehan
Ph.D., Department of Metallurgical and Materials Engineering
Supervisor: Prof. Dr. İshak Karakaya

February 2013, 80 pages

Extensive research in recent years has failed to develop any essentially new method of large scale tungsten production. A new tungsten powder production technique from calcium tungstate ($CaWO_4$) has recently been reported. In this thesis, this technique was further explored from the aspects of electrochemical reduction mechanism and kinetics, applicability to scheelite concentrates and industrial production.

Cyclic voltammetry, constant potential and constant current electrochemical reduction tests were performed to determine the reversible cell potential. Analyses of the experimental results revealed that at least 2.2 V was required to compensate the potentials for the accompanying cell reaction and the electrode polarizations. A cell reaction was proposed by associating the experimental results and the Gibbs Energy changes of the possible reactions.

An experiment (mixture) design was created to optimize the process parameters of the electrochemical reduction of $CaWO_4$ to W in molten $CaCl_2$-NaCl eutectic mixture. Temperature, applied voltage and the length of Kanthal wire winding of the $CaWO_4$ pellets were selected as the process parameters and allowed to vary between the predetermined minimum and maximum values. The rates of the electrochemical reductions were interpreted from the variations of current and total charge vs. time graphs under different conditions. The analysis pointed out $640^{\circ}C$ and 2.81 V from the created mixture design for the fastest reduction and it was seen that the effect of Kanthal wire winding on the output current was less pronounced when compared to the other two parameters.

Another set of experiments was performed by full factorial design to investigate the cleaning procedure needed to remove calcium containing byproducts after electrochemical reduction experiments. Three levels were determined prior to the experiments for the selected three parameters; temperature, acid concentration and exposure time. Main effect and interaction graphs for calcium percent as a function of process parameters were plotted. Calcium contents of the samples were determined by XRF measurements.

A 300 g/day capacity tungsten production line was manufactured to take the process one step closer to industrialization. Problems at larger scale were addressed as incomplete reduction, oxidation of graphite and corrosion of cathode materials. After careful research, AISI 316 Ti steel was found to impart sufficient resistance to highly corrosive environment. Oxidation of graphite anode inside the cell was lowered to acceptable levels by continuous nitrogen flow.

Metallic tungsten powder was obtained from rich and flotation concentrates of Uludağ Etibank Volfram Plant (closed in 1989) together with mainly iron. It was seen that tungsten and iron do not make compounds at the temperatures used for reduction (600-750°C).

A basic diffusion model in the electrolyte was developed to better understand the decrease in current values and incomplete reduction encountered during large scale production. The model was used to simulate the recorded current vs. time graphs of selected experiments.

Keywords: Tungsten, scheelite, CaWO$_4$, electrochemical reduction, electrodeoxidation.

ÖZ

TUNGSTEN İÇEREN BİLEŞİKLERDEN TUNGSTEN KAZANIMI

Erdoğan, Metehan
Doktora, Metalurji ve Malzeme Mühendisliği Bölümü
Tez Yöneticisi: Prof. Dr. İshak Karakaya

Şubat 2013, 80 sayfa

Son yıllarda yapılan yoğun çalışmalar, endüstriyel boyutta tungsten üretimi için kayda değer bir teknik geliştirmeyi başaramamıştır. Kısa bir süre önce kalsiyum tungstattan ($CaWO_4$) tungsten tozu üretimi üzerine yeni bir teknik bildirilmiştir. Bu tezde, bu teknik, elektrokimyasal indirgenme mekanizması ve kinetiği ile şelit konsantrelerine ve endüstriyel uygulamaya aktarılabilirliği üzerinden incelenmiştir.

Denge hücre potansiyelini belirlemek üzere tekrarlı voltametri, sabit potansiyel ve sabit akım elektrokimyasal indirgeme testleri yapılmıştır. Deney sonuçlarının irdelenmesi, hücre reaksiyonu ve elektrot polarizasyonları için gerekli potansiyeli karşılamak için, en az 2.2 V'ye ihtiyaç duyulduğunu göstermiştir. Deney bulguları ve olası reaksiyonların Gibbs Enerji değişimlerinin birleştirilmesiyle, bir hücre reaksiyonu önerilmiştir.

Erimiş $CaCl_2$-NaCl ötektik karışımı içerisinde, $CaWO_4$'ün W'ya elektrokimyasal indirgenmesi işlemindeki değişkenlerin, en uygun değerlerinin bulunması için bir deney tasarımı (mixture design) yapılmıştır. İşlem değişkenleri olarak sıcaklık, uygulanan voltaj ve $CaWO_4$ peletlerin sarıldıkları Kanthal tel uzunluğu seçilmiş ve bu değişkenler, önceden belirlenen üst ve alt limitler dahilinde değiştirilmiştir. Elektrokimyasal indirgenme hızı, değişik koşullar altında kaydedilen akım ve toplam yükün zamanla değişimi grafiklerinden çıkarılmıştır. Oluşturulan deney tasarımı üzerinden yapılan incelemeler, en hızlı indirgeme için, 640^oC ve 2.81 V'yi işaret etmiş ve Kanthal tel ile sarma işleminin hücre akımı üzerindeki etkisinin, diğer iki değişkene göre daha önemsiz olduğu görülmüştür.

Tam-faktöriyel (full-factorial) yöntemiyle tasarlanan bir diğer deney takımı, elektrokimyasal indirgeme deneyleri sonrası, kalsiyum içeren yan ürünlerin bertaraf edilmesi için gereken temizleme işleminin incelenmesinde kullanılmıştır. Seçilen üç değişken olan sıcaklık, asit konsantrasyonu ve işlem süresi için üç farklı değer belirlenmiştir. Kalsiyum yüzdesinin işlem değişkenlerine göre değişimini gösteren direk etki ve etkileşim grafikleri çizilmiştir. Örneklerin kalsiyum içerikleri XRF ölçümleriyle belirlenmiştir.

Tekniği endüstriyelleşmeye bir adım daha yaklaştırmak için 300 g/gün kapasiteli bir tungsten üretim hattı kurulmuştur. Bu ölçekte sorunlar; tam indirgenmeme, grafitin oksitlenmesi ve katot malzemelerinin korozyonu olarak tespit edilmiştir. Titiz incelemeler sonucu, AISI 316 Ti çeliğinin, son derece korozif olan ortama yeterli direnci gösterdiği bulunmuştur. Grafit anodun hücre

içerisinde oksitlenmesi ise, sisteme sürekli azot akışı sağlanmasıyla kabul edilebilir değerlere indirilmiştir.

Uludağ Etibank Volfram Tesisi (1989 yılında kapanmıştır) zengin ve flotasyon konsantrelerinden metalik tungsten üretimi, başlıca safsızlık olarak demirle birlikte gerçekleştirilmiştir. Tungsten ve demirin indirgeme deneylerinde kullanılan sıcaklıklarda (600-750°C) bileşik oluşturmadıkları görülmüştür.

Akım değerlerindeki düşüşü ve büyük ölçekte karşılaşılan tam indirgenmemeyi daha iyi anlayabilmek için, elektrolit içerisinde temel bir difüzyon modeli geliştirilmiştir. Bu model, seçilen deneylerde kaydedilen akım-zaman grafiklerine benzetim yapmakta kullanılmıştır.

Anahtar Kelimeler: Tungsten, şelit, $CaWO_4$, elektrokimyasal indirgeme, elektrodeoksidasyon.

To my family,

ACKNOWLEDGEMENTS

TABLE OF CONTENTS

LIST OF TABLES

TABLES

LIST OF FIGURES

FIGURES

CHAPTER 1

INTRODUCTION

Tungsten is classified as a strategic metal which is defined as "integral to the national defense, aerospace or energy industry; and subject to potential supply restrictions". There are just 48 strategic metals in this category. As a consequence, import of tungsten was restricted with the Missile Technology Control Regime (MTCR) [1] and Wassenaar Arrangement [2]. Türkiye is a party of both agreements. Like rare earth metals, Chinese government restricted sales of APT and the price is now nearly eight times higher than the price in 2002. As a result, tungsten could prove good investment for Türkiye, who has notable tungsten potential.

Today, it has been estimated that, nearly two thirds of total tungsten ore reserves are scheelite [3]. However; in spite of its relatively low abundance, most of the industrial tungsten powder is produced from wolframite mineral. Although the reserve of scheelite is much higher than that of wolframite, the difficulties encountered in the alkaline dissolution process to transfer scheelite into tungsten trioxide severely restrict the widespread use of scheelite in tungsten extraction [4]. In response to the rapid exhaustion of wolframite reserves in recent years (especially in China), the development of new technologies for producing tungsten from scheelite are highly desired. The aim of this study was to explore a new tungsten production technique based on electrochemical reduction of calcium tungstate in molten chloride salt solutions. High tungsten prices and difficulties encountered in the current tungsten production technique as will be discussed later were the main motivations for the study. The process is already patented [5-7] and possessing great potential as a promising tungsten and nano tungsten powder production technique.

CHAPTER 2

LITERATURE REVIEW

2.16 The Element Tungsten

There is no free elemental tungsten in the earth's crust and its abundance is very low (approximately 1 ppm). It is the element 74 of Periodic Table and has the symbol "W".

In addition to having the highest melting point and the lowest thermal expansion coefficient of all metals, tungsten also comes into prominence with its very high density, thermal creep resistance, moduli of compression and elasticity, good electrical and thermal conductivity, and good high temperature mechanical properties. Tungsten is one of the most important metals for thermo-emission applications because of its high electron emissivity, thermal and chemical stability. Some of the important properties of tungsten is given in Table 2.1 [3]. These unusual properties of tungsten arise from the half-filled 5d electron shells (see Table 2.1) with a very high binding energy of the tungsten in the bcc tungsten crystal which is caused by the strong, unsaturated covalent bonds.

Table 2.1: Some of the important properties of W [3].

Electron Configuration	$\{Xe\}\ 4f^{14}\ 5d^4\ 6s^2$
Crystal Structure	Body-Centered Cubic A2
Lattice Parameter	a=3.16524 Å (298 K)
Atomic radius (metallic)	137 pm
Density	19.25 g/cm^3 (298 K)
Melting Point	3422±15°C
Vapor Pressure (2000°C)	8.15×10^{-8} Pa
Boiling Point	5700±200°C
Specific heat capacity	135 J•kg^{-1}•K^{-1} (298 K)
Enthalpy of fusion	46 kJ•mol^{-1}
Enthalpy of sublimation	≈ 860 kJ•mol^{-1}
Coefficient of Thermal Expansion	4.32-4.68×10^{-6}•K^{-1} (298 K)
Electrical Resistivity	5.28 μΩ•cm
Thermal Conductivity Coefficient	1.75 •W•cm^{-1} •K^{-1}(298 K)
Modulus of Elasticity	390-410 GPa (298 K)
Hardness	300-650 HV30

Casting tungsten ingots is not applied because of the extremely high melting point of the metal which can be seen in Table 2.1. Therefore, tungsten products (sheet, rod, wire, pins, etc.) are fabricated by powder metallurgy. Some major steps of the technology, which were adopted from ceramics, are given in Figure 2.1. As can be seen in this figure, tungsten powder is alloyed, pressed into desired shapes, sintered and worked (rolling, forging, swaging, wire drawing, etc.) to the desired end form.
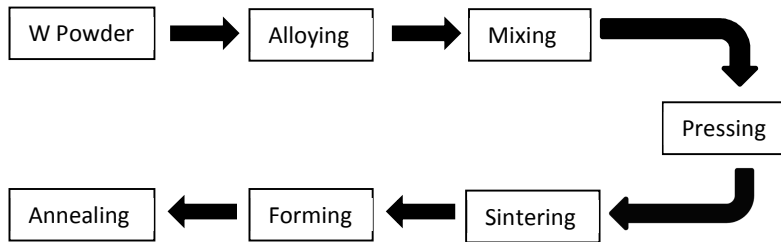
Figure 2.1: Basic flowsheet of tungsten powder metallurgy.

2.1.1 Application Areas [3]

As a result of its exceptional physical and chemical properties due to half-filled 5d electron shells (d5s1), tungsten and tungsten alloys are indispensable in many technological applications. The major usage of tungsten is in the manufacture of cemented carbides whose main ingredient is WC. Cemented carbides are composites in which carbide particles are cemented by a binder matrix. Therefore they combine the high hardness and strength of the tungsten carbide (WC) with the toughness and plasticity of a metallic binder (Co, Ni, and Fe). A large portion of cemented carbides are used in wear applications.

The second important consumption area is the use of tungsten as the alloying element in iron and steel industry. Tungsten, as a carbide-forming element, increases strength, hardness, wear resistance and toughness of the steel. It finds uses in stainless, tool, heat resisting and full alloy steels as well as superalloys. The use of tungsten in iron and steel industry lost its supremacy gradually over time, especially with the growing market of hardmetals. Nevertheless, steel industry is today still the second largest tungsten consumer.

Tungsten mill products, especially used in lamp industry and for electric and electronic contacts, are another important usage of the metal. Furthermore, tungsten compounds are in use for chemical applications and products such as catalysts, pigments, paints and lubricants. Tungsten metal is also required for some other special applications such as vacuum metallizing and substituting poisonous lead and tungsten oxides in smart windows and optical glasses.

In addition, tungsten and carbon fiber composites are the only applicable materials which can withstand extreme operation conditions of heat exchangers used in nuclear fusion reactors. Tungsten is one of the most promising materials to be used in commercial power plants, which will possibly be a huge energy source for the future. Apart from these major sectors, tungsten and tungsten alloys find usage in many special applications in modern technology like circuit breakers and switchgears for high voltage, catalysts, pigments or as important additives in functional materials.

2.1.2 Pricing

Recent tungsten price fluctuations are given in Figure 2.2 [8]. As it can be seen in this figure, tungsten prices have increased significantly in 2005, from a level of 80 US$/MTU in 2004 to 230 US$/MTU in mid-2005. Another jump in prices is seen in 2011 from 245 to 460 US$/MTU. Prices are generally quoted per metric ton unit ("MTU" - one hundredth of a metric ton of 1,000 kilograms) of contained tungsten trioxide (WO_3). One MTU contains 10 kilograms of tungsten trioxide (WO_3) and/or 7.93 kilograms of tungsten (W).

World tungsten supply is dominated by China. However, China at the same time is the world's largest tungsten consumer. The amount of tungsten consumed in China for domestic market has exceeded the amount exported since 2008 [9]. According to the USGS report [9], the Chinese Government was expected to continue to limit exports and increase tungsten imports to conserve its resources and meet domestic demand. As a result, tungsten prices seem to continue its increase in future.

2.1.3 Sources

Although there are many tungsten minerals, only scheelite, ferberite, hübnerite and wolframite are economically notable. The concentration of commercial tungsten ores are between 0.3 and 1 % WO_3 [3]. Among these minerals, scheelite is the most important raw material for the production of tungsten metal and compounds. Scheelite possesses bluish white fluorescence under short wavelength UV radiation which is quite valuable in ore prospection and mining. Some of the important properties of scheelite are given in Table 2.2 [3].

Ferberite, hübnerite and wolframite all belong to the wolframite group. They are all tungstate minerals of varying composition (Fe, Mn, W). The important properties of the wolframite group minerals are given in Table 2.3 [3].

Tungsten resources are geographically widespread. China has the largest tungsten reserves of the world. There are also significant tungsten resources in Canada, Russia, and the United States. World's tungsten resources are compiled in Figure 2.3. As can be seen in this figure, Türkiye has nearly 1.5% of total tungsten ore reserves [10].
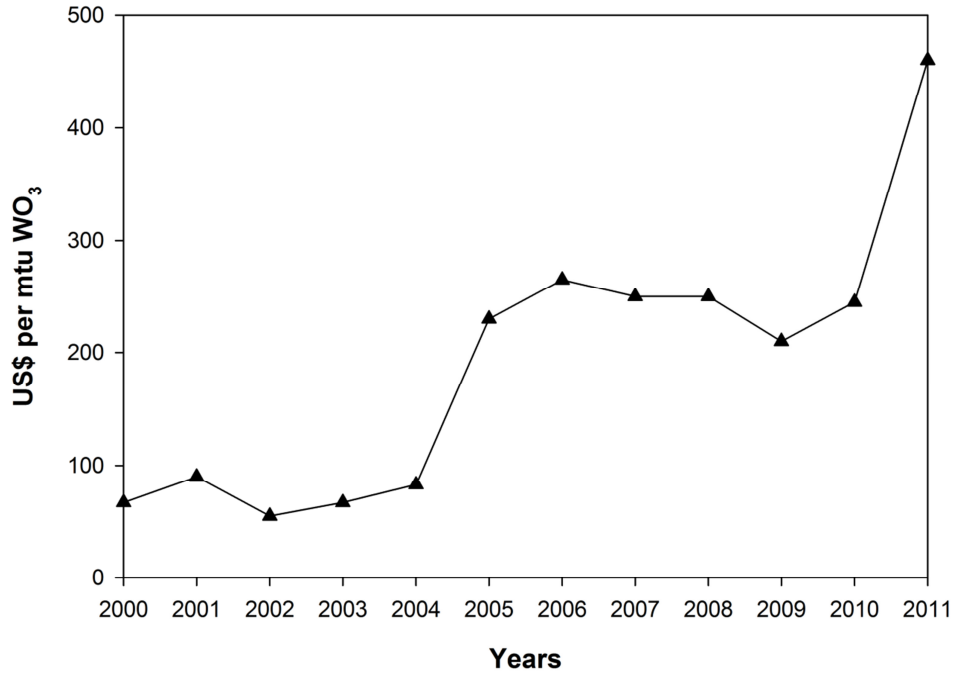
Figure 2.2: Approximate tungsten (ammoniumparatungstate) price fluctuations between 2000 and 2011 [8].

Table 2.2: Some of the properties of scheelite [3].

Formula	$CaWO_4$
WO_3 content (%)	80.6
Crystal Structure	tetragonal dipyramidal
Lattice Parameters	
a (Å)	5.24-5.26
c (Å)	11.37-11.40
c/a	2.163-2.169
Specific gravity	5.9-6.1
Color	colorless, white, yellow, tan, orange, red, blue, black
Tenacity	very brittle
Luster	vitreous or resinous
Fracture	uneven
Hardness (Mohs)	4-5
Magnetism	Nonmagnetic
Streak	White
Diaphaneity	transparent or translucent

Table 2.3: Some of the properties of wolframite group minerals [3]

Property	Ferberite	Wolframite	Hübnerite
Formula	$FeWO_4$	$(Fe,Mn)WO_4$	$MnWO_4$
WO_3 content (%)	76.3	76.5	76.6
Mn Content (%)	0-3.6	3.6-14.5	14.5-18.1
Fe Content (%)	18.4-14.7	14.7-3.7	3.7-0
Crystal Structure	monoclinic	monoclinic	monoclinic
Lattice Parameters			
a (Å)	4.71-4.76	4.77-4.79	4.85
b (Å)	5.68-5.70	5.73-5.74	5.77
c	4.92-4.95	4.98-4.99	4.98
β	90°	$90^{o}26^{l}$	$90^{o}53^{l}$
Density (g/cm^3)	7.5	7.0-7.5	7.2-7.3
Color	black	dark grey to black, brownish black	red, reddish brown to black
Tenacity	very brittle	very brittle	very brittle
Luster	submetallic to metallic	submetallic to metallic	submetallic to adamantine
Fracture	uneven	uneven	uneven
Hardness (Mohs)	4.5-5	4.5-5	4.5
Magnetism	sometimes feebly magnetic	slightly magnetic	-
Streak	dark brown, black	dark brown	brownish red to greenish yellow
Diaphaneity	opaque to translucent in cleavage plates	opaque	opaque to translucent
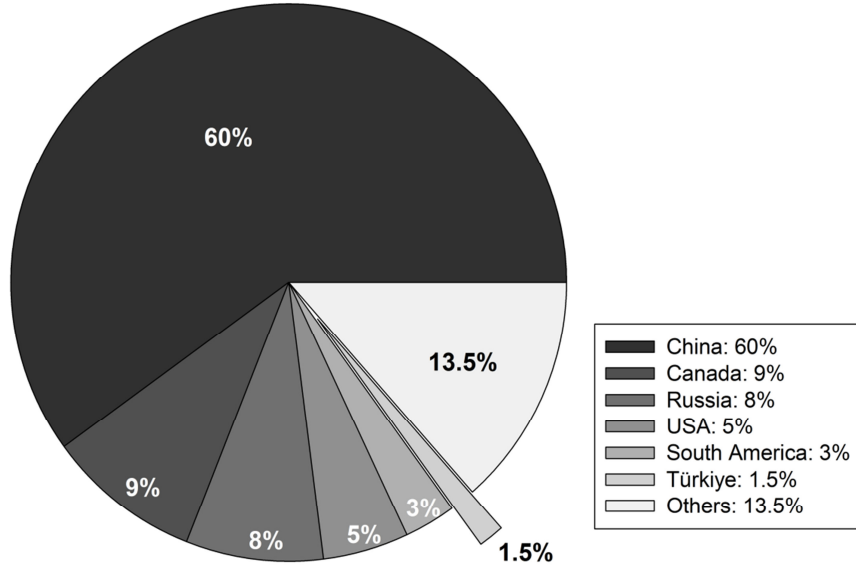
Figure 2.3: Tungsten Reserves (W content: 3 million tons total) [3]. Türkiye was added from another source [10].

2.1.4 Tungsten Potential of Türkiye

There are 28 tungsten ore reserves in Türkiye, mainly around Bursa-Uludağ-Kozbudaklar, Elazığ-Kebandere-Soğanlıköy-Nallıziyaret, Çanakkale-Çakıroba-Hamdibey, Niğde-Gümüşler, Yozgat-Akdağ mines [10]. Some of the tungsten ore reserves of Türkiye are compiled in Table 2.4 [10].

Table 2.4: Tungsten ore reserves of Türkiye [10].

Place	Grade (WO$_3$%)	Total Reserve (tons)	W content (tons)
Bursa-Uludağ	0.437	14,384,336	49,854
Bursa-Kozbudaklar	0.3	210,000	500
Elazığ-Keban-Soğanlıköy	0.2	255,000	383
Elazığ-Keban-Keban D.	0.2	5,000	8
Niğde-Gümüşler	0.1	100,000	79
Ç.kale-Yenice-Hamdibey	0.5	3,000	12
Bilecik-Söğüt-Dudaş	0.04	10,000	3

The biggest of these reserves is the Uludağ scheelite deposit. In the inventory of Maden Tetkik Arama Enstitüsü (MTA) prepared in 1978 [11], the reserve was estimated at about 14 million tons.

A similar estimation was reported in reference [10]. Although tungsten content of Uludağ reserve is low, it is above the commercial lower limit (0.2 % WO_3). It should be noted that the richest tungsten ore reserves contain 2-3 % WO_3. Therefore tungsten minerals should be concentrated whatever their grades are.

Tungsten mineral was mined regularly in Türkiye in the plant constructed by Etibank in 1977 in Uludağ. Eti Holding Uludağ Tungsten Plant was founded to produce 2,983 tons/year scheelite concentrate containing 65% WO_3, 12,000 tons/year pyrite, 4,500 tons/year garnet and 1,200 tons/year magnetite concentrates [10]. However, the plant was closed down in 1989 due to technological problems and low tungsten prices. Since then, tungsten ore has not been mined in Türkiye. Three types of scheelite concentrates were produced in the plant between 1977 and 1989; rich, flotation and poor. Typical chemical compositions of the concentrates are given in Table 2.5 [12].

Table 2.5: Compositions of the concentrates of Uludağ Etibank Tungsten Plant [12].

Mineral	Rich Concentrate (%)	Flotation Concentrate (%)	Poor Concentrate (%)
$CaWO_4$	75	30	18
$CaCO_3$	1-2	45-50	15-17
FeS_2	5	7	45
Fe_2O_3	2-3	<1	<1
Fe_3O_4	2	1	<1
$(Fe,Mn)WO_4$	1-2	1	2-3
ZnS	<1	1-2	4
SiO_2	<1	<1	3-5
Total Gangue	7-9	48-55	24-30

Türkiye has a demand for tungsten especially in the form of tungsten carbide and ferrotungsten. This demand was reported in 2000 [10] as 50 tons ferrotungsten and 25 tons tungsten carbide.

Tungsten is classified as a strategic metal which is defined as "integral to the national defense, aerospace or energy industry; and subject to potential supply restrictions". There are just 48 strategic metals in this category. As a consequence, import of tungsten was restricted with the Missile Technology Control Regime (MTCR) [1] and Wassenaar Arrangement [2]. Türkiye is a party of both agreements. Like rare earth metals, Chinese government restricted sales of ammoniumparatungstate (APT) and the price is now nearly eight times higher than the price in 2002 (see Figure 2.2). As a result, tungsten could prove good investment for Türkiye, who has notable tungsten potential as can be seen in Table 2.4.

2.2 Industrial Production

Most of the time industrial production of tungsten starts with formation of the important intermediate product "ammoniumparatungstate" (APT, formula: $(NH_4)_{10}(H_2W_{12}O_{42})4H_2O$). Flowsheet considerations associated with the APT production from the ore can be seen in Figure 2.4. Today's only technically important method for tungsten powder production is the hydrogen reduction of tungsten oxides at temperatures between 700 to 1100 ^{o}C in a streaming hydrogen atmosphere. Therefore APT is mostly converted into tungsten oxides first and then reduced to tungsten metal (see Figure 2.5). The overall reduction reaction can be given as:

$$WO_3 \text{ (s)} + 3H_2 \text{ (g)} = W \text{ (s)} + 3H_2O \text{ (g)} \qquad \text{Eq. 2.1}$$
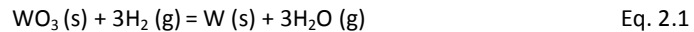
As starting materials, besides the trioxide, tungsten blue oxide (WO_{3-x}) or tungstic acid (H_2WO_4) are also in use. In fact, the reduction of WO_3 to W as described by the simple equation above is in reality a rather complex process. The reduction process proceeds in distinct stages, through the formation of all stable oxides:

$$WO_3\text{(yellow)} \rightarrow WO_{2.9}\text{(blue)} \rightarrow WO_{2.72}\text{(violet)} \rightarrow WO_2\text{(brown)} \rightarrow W\text{(gray)}$$
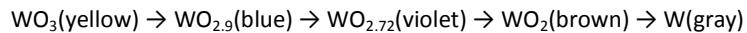
By changing the reduction parameters the powder properties like average grain size, grain size distribution, grain shape, agglomeration, etc. can be regulated within a considerable wide range. Tungsten powder sizes are available from 0.1 to 100 μm on the market. The purity of the tungsten powder is usually determined by the purity of the starting APT. In ASTM B 777-99, four classes of tungsten powder are specified with respect to W content, as given in Table 2.6.

Disadvantages of the current tungsten production technique:

As can be seen in Figure 2.4 and Figure 2.5, production of tungsten oxides from tungsten concentrates is a complicated and time consuming procedure, involving many steps. In addition, hydrogen reduction of tungsten oxides has certain difficulties:

1) There is considerably low driving force for the process at the temperatures of reduction. For a large negative Gibbs energy change (large driving force) for the reduction reaction, the line of the reductant must be far below the line of the reduced metal on the corresponding Ellingham Diagram. However, as it can be seen from Figure 2.6, H_2-H_2O line is only slightly below W-WO_3 line at the temperatures of reduction [13].

2) It is conducted with continuous external heat supply.

3) Hydrogen is a difficult gas to handle.

```
┌─────────────────────────┐          ┌─────────────────────────┐
│  Low Grade and Mixed Ore or │         │   High Grade Ore or Oxidized │
│       Residues           │          │         Scrap            │
└─────────────────────────┘          └─────────────────────────┘
            │                                      │
            ▼                                      ▼
┌─────────────────────────┐          ┌─────────────────────────┐
│    Soda Roast & Leach    │─────╲    │  Soda or Caustic Autoclave │
│                          │      ╲   │         Leach            │
└─────────────────────────┘       ╲  └─────────────────────────┘
            │                       ╲            │
            ▼                        ╲           ▼
┌─────────────────────────┐          ┌─────────────────────────┐
│       Purification       │───╲      │       Purification       │
└─────────────────────────┘    ╲     └─────────────────────────┘
            │                    ╲              │
            ▼                     ╲             ▼
┌─────────────────────────┐       ╲   ┌─────────────────────────┐
│   CaWO₄ Precipitation    │        ╲  │ Liquid or Solid Ion Exchange │
└─────────────────────────┘           └─────────────────────────┘
            │                                      │
            ▼                                      │
┌─────────────────────────┐                       │
│ Decomposition to Tungstic Acid │                 │
└─────────────────────────┘                       │
            │                                      │
            ▼                                      │
┌─────────────────────────┐                       │
│  Dissolution in Ammonia  │                       │
│        Solution          │                       ▼
└─────────────────────────┘                       │
            │                                      │
            ▼                                      ▼
┌─────────────────────────┐          ┌─────────────────────────┐
│      Crystallization     │          │      Crystallization     │
└─────────────────────────┘          └─────────────────────────┘
            │                                      │
            ▼                                      ▼
┌─────────────────────────┐          ┌─────────────────────────┐
│ Ammoniumparatungstate (APT) │       │ Ammoniumparatungstate (APT) │
└─────────────────────────┘          └─────────────────────────┘
```

Here the boxes read: CaWO$_4$ Precipitation.

Figure 2.4: Flowsheet of APT production from the ore. (Arrows between the two columns indicate alternative roots.)

```
                              ┌─────────────────────┐
                              │         APT         │
                              └─────────────────────┘
                                         │
                                         ▼
Nitrogen or                   ┌─────────────────────┐
Nitrogen + Hydrogen    ━━▶    │      Calcining      │
                              └─────────────────────┘
                                         │
                                         ▼
                              ┌─────────────────────┐
                              │   Tungsten Oxide    │
                              └─────────────────────┘
                                         │
                                         ▼
Hydrogen               ━━▶    ┌─────────────────────┐    ━━▶    Hydrogen+H₂O
                              │      Reduction      │
                              └─────────────────────┘
                                         │
                                         ▼
┌────────┐          ┌──────────────────────────┐          ┌─────────┐          ┌──────────────────┐
│ Users  │   ◀━━    │   Tungsten Metal Powder   │   ━━▶    │ Mixing  │   ━━▶    │ Tungsten Carbide │
└────────┘          └──────────────────────────┘          └─────────┘          └──────────────────┘
                                                                ▲
                                                                ┃
                                                          Pure C powder
```
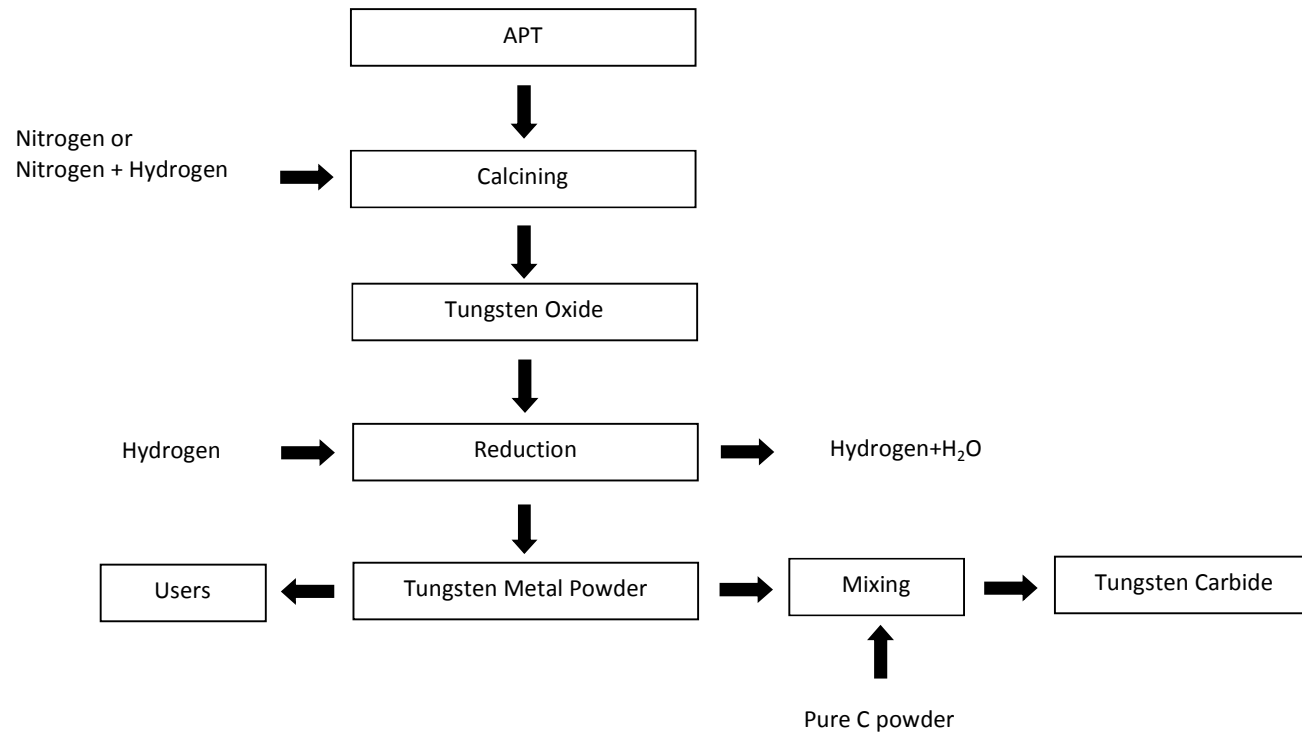
Figure 2.5: Tungsten production from APT. (Most of the metal is then used in the manufacture of tungsten carbides.)

Table 2.6: Composition, density and hardness values of four classes defined in ASTM B 777-99 standard.

Class	Nominal W weight (%)	Density g/cc	Hardness Rockwell C max.
1	90	16.85-17.25	32
2	92.5	17.15-17.85	33
3	95	17.75-18.35	34
4	97	18.25-18.85	35
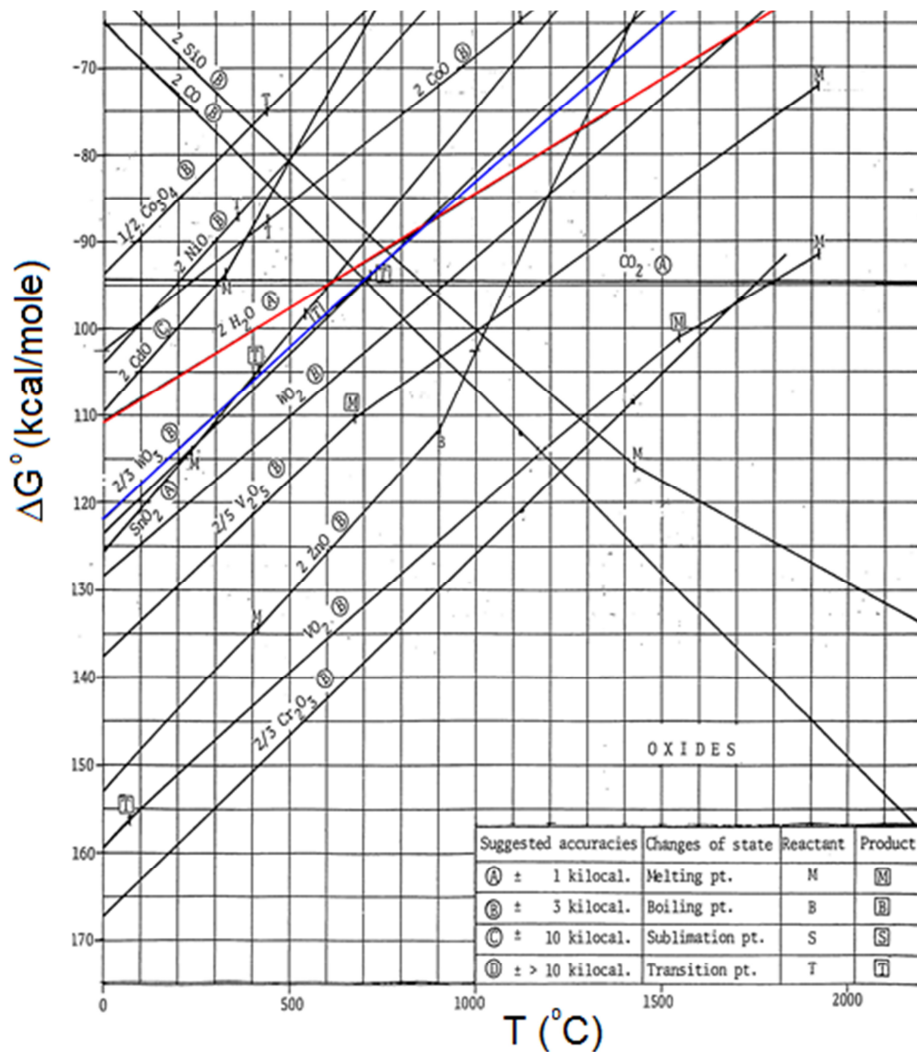
Figure 2.6: Ellingham Diagram for metal-metal oxide systems. (W-WO$_3$ line is in blue and H$_2$-H$_2$O line is in red, reproduced from [13].)

However, in tungsten production, the major concern is product purity because good ductility and fabricability of tungsten depend strongly on the purity of the metal. Since hydrogen is easily obtainable, it is used industrially as a reductant for tungsten oxides instead of carbon or other reducing agents to obtain cleaner solid product and avoid other side reactions. In some cases (e.g. tungsten used as an alloy addition), the purity requirement is less stringent, and carbon may be used for the reduction process but the resultant powder usually contains some silicon, iron, carbon, sulphur, and phosphorus impurities.

Metallothermic reduction has also been used in small scale or for some special purposes, but after reduction, a refining process such as electro-refining is necessary. Another drawback of metallothermic reduction is that the final shape of the product is not fine powder. This leads to difficulties during consolidation in subsequent powder metallurgy processes.

There have also been some studies to produce high purity tungsten metal by the electrolysis of various molten salts, but none have been successful on a commercial scale. In general molten salt electrolysis for electrodeposition of metals have some problems in common, such as; dendritic deposition, consequent oxygen contamination of products upon exposure to air, and redox cycling reactions of multi-valent metal ions that become even more active in molten salts because of high temperatures. For tungsten electrowinning, the most important problem is the large particle size of the electrowon tungsten. This leads to a relatively porous product when consolidated by the classical pressing and sintering techniques.

2.3 Electrochemical Reduction of Metal Compounds

Molten salt processing is used in metal extraction for more than a century. Metals having very stable compounds cannot be produced by gas-based pyro-reduction, metallothermic reduction, hydrometallurgical methods or aqueous electrochemical techniques. In these cases, where production by other routes is not feasible due to thermodynamic, kinetic or economic constraints, the option is limited to electrowinning of the metal by the electrolysis of various molten salts. However fused salt electrolysis is satisfactory only for low melting point metals which are deposited in the liquid state. High melting point metals can be electrowon in the solid state because the reduction temperature is less than the melting point. But this results in dendritic deposition which is prone to oxidation.

The classical molten salt electrolysis involves dissolution of the starting material, containing the metal to be electrowon, in the electrolyte. A subsequent electrowinning of the metal from the solution takes place by direct current reduction. Therefore, there had been some attempts to produce metals from their oxides by dissolving the metal oxide in fluoride melts because fluorides are regarded to be better at dissolving oxides than chlorides. However, most of the time these studies failed to develop a commercial large scale production because fluorides usually melt at higher temperatures and they are far more corrosive. Until quite recently, the only molten salt process involving electrochemical reduction of oxides industrially was the Hall-Heroult process for the electrowinning of aluminum from alumina.

A novel process was reported recently which enables the production of metals from their oxides by electrolysis in fused salts [14]. The process is called as FFC (Fray-Farthing-Chen) Cambridge process and it is claimed to be more suitable for electroreduction of the high-melting transition metal oxides and actinides.

In metal-oxygen systems oxygen can take two forms; chemically bound oxygen as oxide or dissolved oxygen as solid solution. Calcium oxide is the most stable metal oxide, therefore calcium is used as a very effective deoxidant in metal-oxygen systems. The general form of the reaction can be written as:

$$M(O) + Ca = M + CaO \qquad \text{Eq. 2.2}$$

Therefore, equilibrium oxygen content of the metal can be calculated from:

$$[O] = \left(\frac{a_{CaO}}{a_{Ca}}\right)\left(\frac{1}{f_O}\right) exp\left(\frac{\Delta G^\circ}{RT}\right) \qquad \text{Eq. 2.3}$$

ΔG° = Standard Gibbs Energy change of the reaction,

f_O = Activity coefficient of oxygen in the metal,

a_{CaO} = Activity of calcium oxide referred to pure state as the standard state

a_{Ca} = Activity of calcium referred to pure state as the standard state

From the above equation, it is clear that for a given system with constant f_O, the lower the $\frac{a_{CaO}}{a_{Ca}}$ ratio gets, the lower the oxygen concentration in the metal will be. However, with time CaO formed, makes a thick coating around the metal surface and inhibits further reduction by interrupting the contact between the metal and calcium. Therefore, $\frac{a_{CaO}}{a_{Ca}}$ ratio becomes quite high at the reaction interface. This problem can be overcome by conducting the reduction in a medium in which both Ca and CaO can dissolve. At this point molten salts are incorporated into the process because alkaline earth chlorides have very high solubility for their respective oxides. Therefore if the process is conducted in the molten medium (CaCl$_2$ in the case of Ca reduction), the CaO dissolves in the molten salt flux and no longer acts as barrier. Finally electrochemistry is incorporated into the process because the process will require continuous supply of Ca on to the metal and removal of CaO from the melt in order to keep $\frac{a_{CaO}}{a_{Ca}}$ ratio low at the reaction interface.

For the first time, Ward and Hoar [15] had removed oxygen, sulphur, selenium and tellurium from molten copper by electrochemical technique. Graphite was used as the anode and the electrolyte was BaCl$_2$. A potential, which was above the decomposition potential of BaCl$_2$, was applied to remove the non-metallic impurities. The overall cell reaction was assumed to be:

$$BaCl_2 = Ba + Cl_2 \qquad \text{Eq. 2.4}$$

Elemental Ba produced at the cathode surface was considered to react with impure copper according to the below reaction:

$$Cu_2X + Ba = 2Cu + BaX \qquad \text{Eq. 2.5}$$

where X is O, S, Se or Te.

Similar to above application, Okabe et al have developed many techniques for removal of oxygen from titanium in calcium saturated calcium chloride melts [16-18]. They could achieve the lowest oxygen impurity level of about 10 ppm, when the reductant Ca metal was generated in-situ by electrolysis of calcium chloride. The calcium metal produced by the electrolysis reacts with oxygen in titanium to give calcium oxide. This CaO dissolves in calcium chloride, and is electrolyzed to regenerate Ca for further reduction. The cell arrangements in both cathodic refining techniques ([15], [16-18]) were identical and given in Figure 2.7.
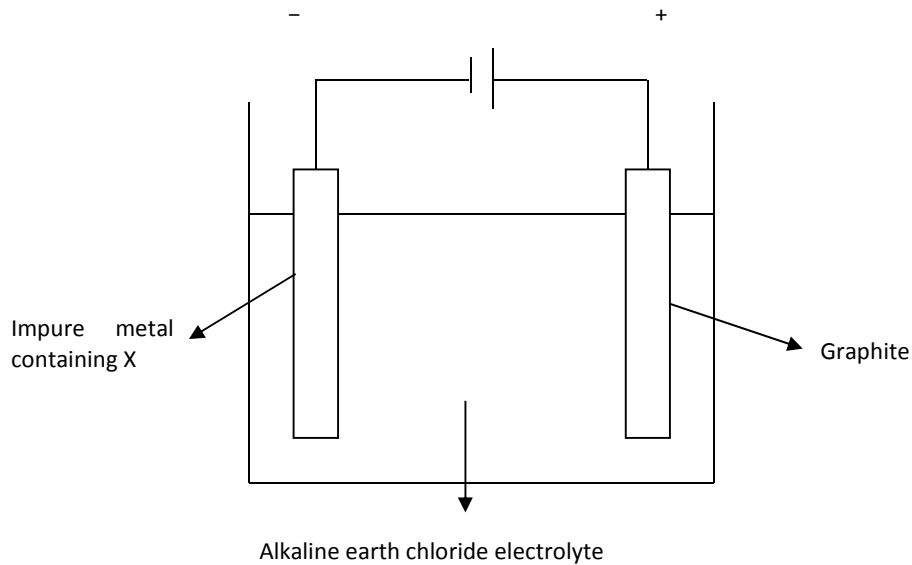
Figure 2.7: Cell Arrangement of Cathodic Refining Technique

Chen and Fray have also done similar experiments on cathodic refining of copper [19] and titanium [20]. They applied potentials which were lower than the decomposition potential of the salts, but they could still achieve deoxygenation. As a result of these observations, they concluded that, electrolysis of the salt to produce Ca or Ba and their chemical reaction with the oxygen (or the impurity element X) were not necessary for the deoxygenation. Removal of oxygen (or the impurity element X) takes place via its cathodic ionization and following discharge at the anode. Therefore, the generalized electrode reactions for element X that is going to be removed are:

$$X + ne^- = X^{n-} \text{ (cathode reaction)} \qquad \text{Eq. 2.6}$$

$$X^{n-} = X + ne^- \text{ (anode reaction)} \qquad \text{Eq. 2.7}$$
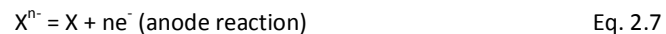
Fray–Farthing–Chen (FFC) Cambridge Process is a high temperature electrochemical reduction process in molten salts to obtain metals or alloys from the starting material as oxide, sulphide, carbide or nitride. However almost all the work so far has been for metal production from their oxides. The cell arrangement for FFC Cambridge process, given in Figure 2.8, is very similar to the cathodic refining technique discussed above. Electrolysis is conducted between the graphite rod anode and the metal oxide cathode in the molten salt media containing $CaCl_2$ as the major component. By the application of a voltage, which is lower than the decomposition potential of the molten salt but higher than the decomposition potential of the metal oxide, the oxygen ions leave the metal oxide cathode and move towards the graphite rod anode, forming CO and/or CO_2 depending on the temperature. The reactions are:

$$M_xO_y + 2ye^- = xM + yO^{2-} \text{ (Cathodic reaction)} \qquad \text{Eq. 2.8}$$

$$yO^{2-} + yC = yCO + 2ye^- \text{ (Anodic reaction)} \qquad \text{Eq. 2.9}$$

$$M_xO_y + yC = xM + yCO \text{ (Overall reaction)} \qquad \text{Eq. 2.10}$$
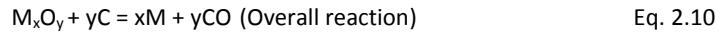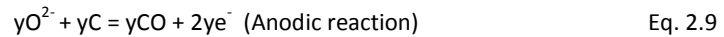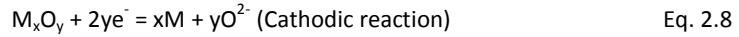
By the FFC Cambridge process, Ti [21], Cr [22], Si [23], Cu [24], Al, B, Fe, V, Nb, U, Nd, Zr, Hf, Ce, and Ni [25-28] have already been produced in laboratory experiments. In addition, Dring et al.[29] and Bhagat et al.[30] have reported that Ti–W alloys were produced via electrochemical reduction of TiO_2–WO_3 mixed oxide preforms in molten calcium chloride electrolyte at 900^oC. However, Erdoğan and Karakaya [31] reported formation of gaseous WO_2Cl_2 while trying to reduce WO_3 at 900^oC with very similar experimental conditions. The reaction was given as:

$$2\ WO_3\ (s) + CaCl_2\ (l) = CaWO_4\ (s) + WO_2Cl_2\ (g) \qquad \text{Eq. 2.11}$$
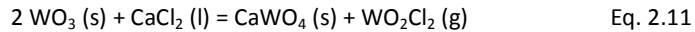
X-ray diffraction pattern of the gaseous product, which deposited to the cooler parts of the reaction tube as yellow powders in the above study, is given in Figure 2.9 [31] . As it can be seen in this figure, when the peaks of hydrated forms of calcium chloride are omitted, the deposited yellow powder was tungsten oxychloride (WO_2Cl_2).

Bhagat et al. [30] also mention the loss of WO_3. However, they claim these losses were to the electrolyte as a result of formation of oxychloride and chloride phases and did not report gaseous WO_2Cl_2 formation. A large negative Gibbs Energy change of -54899 J at $900^{\circ}C$ [32, 33] indicates almost completion of Eq. 2.11. To verify the extent of gaseous WO_2Cl_2 formation, equilibrium composition of the system at 900^oC was determined by thermodynamic computations. Using 2.5 grams WO_3 added to 100 grams of $CaCl_2$, as was the case in the related article [31], the equilibrium composition of the phases were calculated. According to the reaction, almost 50% (wt.) of the starting tungsten in the form of WO_3 was lost from the cathode as WO_2Cl_2 vapor. The FACT (Facility for the Analysis of Chemical Thermodynamics) computer program [33] was used to perform Gibbs energy minimization in equilibrium composition determination. The output of the program, giving the composition of the equilibrium phases for above conditions, is shown in Figure 2.10. Therefore tungsten trioxide cannot be reduced electrochemically at high temperatures without loss using above procedure, because it reacts with calcium chloride by liberating volatile tungsten oxychloride.
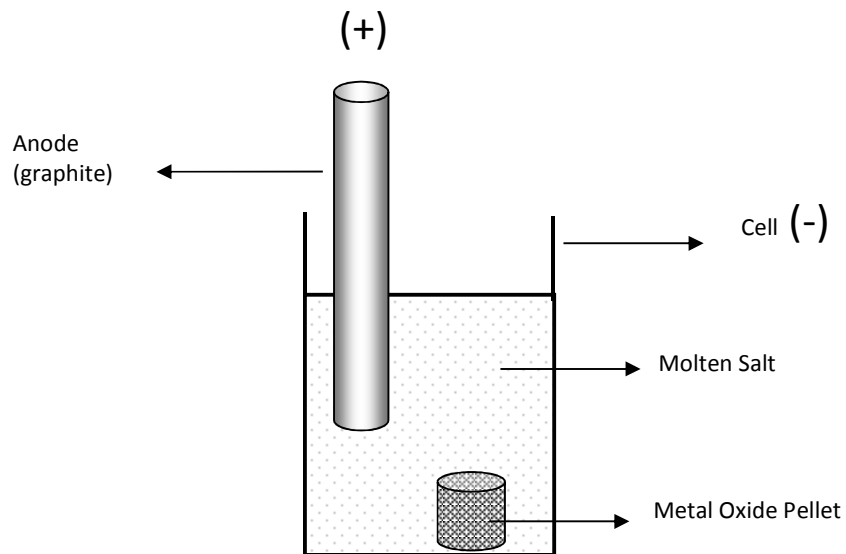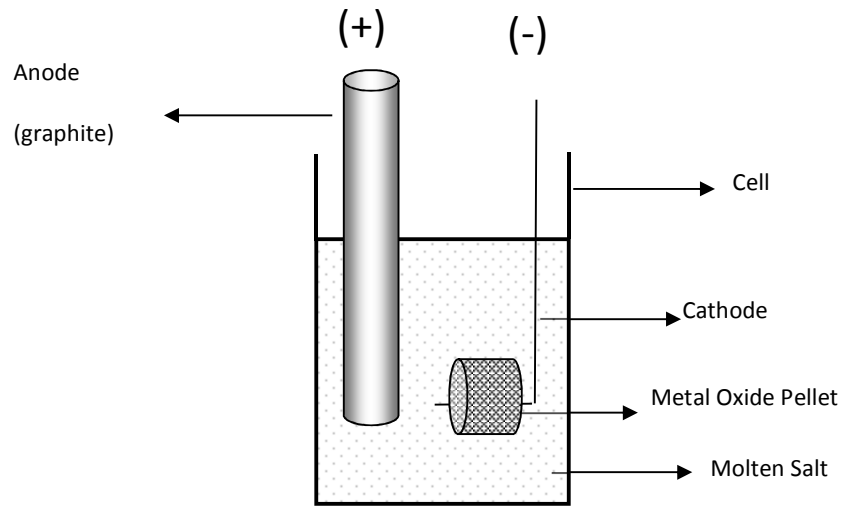
Figure 2.8: Two different cell arrangements of FFC Cambridge process. In the upper one, a wire is used as the current collector. In the lower one, crucible itself is made the current collector.
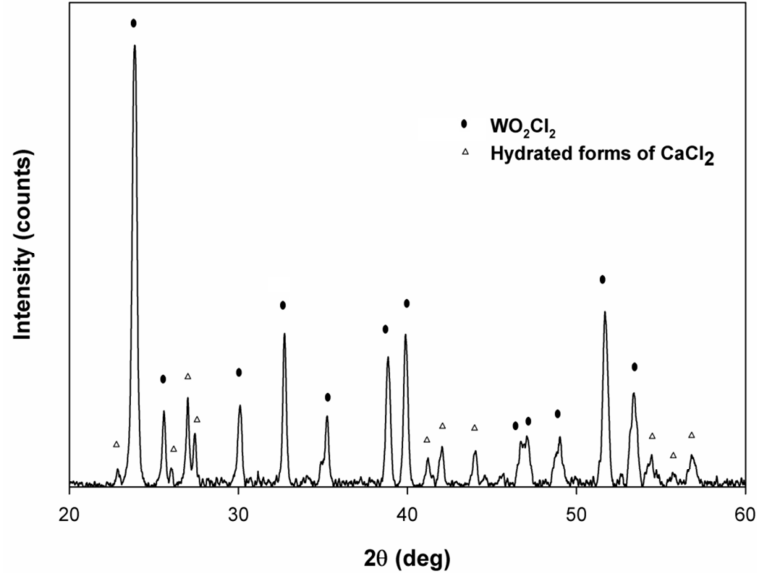
Figure 2.9: X-ray diffraction pattern of the deposited yellow powder, scraped from the walls of the cell vessel. Reproduced from [31] by the license obtained from Springer.

T = 1173 K, P = 1 atm, (gram) 2.5 WO$_3$ + 100 CaCl$_2$ =

0.51895 litre (99.999 vol% WO$_2$Cl$_2$
+ 0.36558E-03 vol% CaCl$_2$
+ 0.23359E-03 vol% Cl
+ 0.79773E-04 vol% WCl$_4$
+ 0.43944E-04 vol% Cl$_2$
+ 0.40481E-04 vol% WCl$_2$
+ 0.40935E-06 vol% OWCl$_4$
+ 0.72924E-08 vol% WCl$_5$

+ ....
(1173.00 K, 1 atm, gas_ideal)

+ 99.402 gram CaCl$_2$
(1173.00 K, 1 atm, L1, a= 1.0000)

+ 1.5523 gram (CaO)(WO$_3$)_scheelite
(1173.00 K, 1 atm, S1, a= 1.0000)

+ 0.00000 gram WO3
(1173.00 K, 1 atm, S2, a=0.58484E-01)

+ 0.00000 gram WO3
(1173.00 K, 1 atm, S1, a=0.57602E-01)

Figure 2.10: Equilibrium composition of the phases calculated by FACT program when 2.5 grams of WO$_3$ and 100 grams of CaCl$_2$ were brought together at 900°C. Reproduced from [31] by the license obtained from Springer.

The disappearance of the sample from the cathode could also be explained with reference to above observations, because some of the starting WO_3 was lost as WO_2Cl_2 and the remaining was converted to $CaWO_4$ according to Eq. 2.11. About 15 mole % solubility of $CaWO_4$ in calcium chloride at $900°C$ [34] explains why all of the reduced sample could not be found on the cathode. Furthermore, X-ray diffraction of the reduced sample collected from the cell indicated the presence of metallic tungsten [31, 35]. Therefore it was concluded that, in the experiment, tungsten was obtained as a result of electroreduction of $CaWO_4$ rather than WO_3. In other words, $CaWO_4$, which was formed according to Eq. 2.11, could be reduced to tungsten by electrodeoxidation [31].

In order to stop the reaction (Eq. 2.11) and verify above conclusions, $CaWO_4$ was formed before the electrochemical reduction and further studies were done by using $CaWO_4$ as the starting material [31]. As it was stated earlier, $CaWO_4$ has about 15 mole % solubility in calcium chloride at $900°C$ [34]. This imposed a restriction on the temperature range over which electrochemical reduction experiments can be done. Solubility of $CaWO_4$ could be reduced considerably by using a low electrolysis temperature of about $600°C$ [31]. In order to have calcium chloride molten at such low temperatures, it was mixed with sodium chloride which does not have any significant $CaWO_4$ solubility at that temperature [36]. Therefore, $CaCl_2$-NaCl mixture with eutectic composition, which melts at $504°C$ [37] is completely molten at the selected operating temperature of $600°C$. An approximate solubility of $CaWO_4$ in this electrolyte was determined as 1 % mole at $600°C$, by extrapolation of the liquidus surface of $CaCl_2$-$CaWO_4$-NaCl phase diagram to $600°C$ [31].

Erdoğan and Karakaya [31] reported for the first time that $CaWO_4$ can be electrochemically reduced to tungsten, without dissolving $CaWO_4$ in the electrolyte, in $CaCl_2$ containing molten salt solutions. Following this, Tang et all [4] repeated the same process and reported production of fine tungsten powder having particle size less than 200 nm. Their contribution to the process was the washing stage applied at the end of the reduction process, in the same melt at a higher temperature (1123 K, 1-hour washing). By this way, they reported that, any $CaWO_4$ that could possibly be left unreduced, was completely dissolved in the electrolyte. In 2011, Hang, Nguyen and Fray [4] reported WC production using a very similar experimental setup to one used by Erdoğan and Karakaya.

Production of tungsten from $CaWO_4$ by molten salt electrolysis in molten chloride salts was an old idea [38, 39] which has still been investigated [40]. In these studies, the starting materials were first dissolved in the electrolyte, which usually requires higher temperatures than $600°C$. However, the most important problem arises from the dendritic deposition of tungsten at the cathode. Since tungsten is solid at the process temperatures and deposited from a liquid phase, the final product is usually not suitable for subsequent pressing and sintering processes. Furthermore, the deposited material has to be scraped from the cathode, which brings extra difficulty.

Yet in the process mentioned above [5-7, 31, 35], the starting materials are not dissolved in the electrolyte and reduced in solid state with the removal of non-metallic substances. Therefore, the resulting material is obtained in powder form at the end of the process. The fact that pure $CaWO_4$ can be more easily produced from tungsten concentrates -when compared to tungsten oxides- and the possibility that the process can be directly applied to scheelite ($CaWO_4$) concentrates, increase the expectations on the process. Today, it is assumed that nearly 70% of total tungsten ore reserves are scheelite [3] and current tungsten production technique is accepted to be more suitable for tungsten production from wolframite than scheelite [4]. Another advantage of the process is the nano particle size of the produced tungsten powder [4, 31]. When all these factors are put together with the restrictions imposed by the Chinese government and increasing tungsten prices, such a new promising tungsten production technique should be investigated to adapt laboratory scale success to industrial production.

CHAPTER 3

EXPERIMENTAL

3.1 Laboratory Experiments

3.1.1 Constant Voltage and Constant Current Reduction Experiments

The two electrode cell used in constant voltage reduction experiments is schematically shown in Figure 3.1.
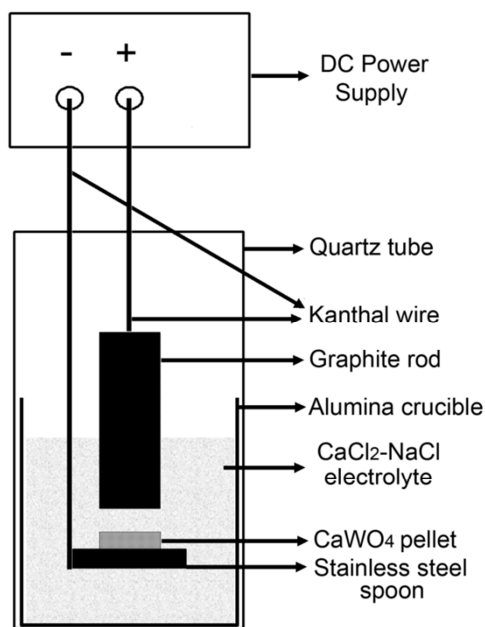
Figure 3.1: The schematic view of the experimental setup for constant voltage electrolysis experiments.

The $CaWO_4$ pellet, forming the cathode, was positioned onto a stainless steel spoon electrode, which was welded to the end of a 3 mm Kanthal wire (N80) current collector. This wire was covered by an alumina insulator near the bottom of the cell to prevent any short circuit problem during experiments. A 100 mm long, 13 mm diameter graphite rod (A10134, Alfa Aesar) was used as the anode material and it was attached to the end of a 3 mm Kanthal wire. An alumina crucible (100 mm long, 4 cm outside diameter), positioned into a quartz vessel (60 cm long, 5 cm inside

diameter), was used to hold the electrolytic cell. The cell vessel was covered at the top by a Teflon lid, which had four holes on it. The hole at the center was used to install the Kanthal wire connected to the graphite rod anode and the other three holes were located around this central hole. Two of the holes were used for argon inlet and gas outlet and the remaining hole was used to place the cathode assembly. Rubber o-rings were applied to each hole. By this way, cathode and anode connections were vertically movable without gas leak. Quartz cell vessel was placed into a vertical tube furnace to a depth of about 40 cm. Upper portion of the cell vessel remained outside the vertical tube furnace during the electrolysis. Therefore, the necessary electrode movements were made possible by electrode leads extended from the top of the cell vessel. Furthermore, electrical and gas connections at a temperature close to room temperature enabled an easier operation.

Two different $CaWO_4$ powders were used for laboratory experiments. One was prepared by mixing CaO and WO_3. A commercially available WO_3 powder (95410, Fluka) was selected as one of the starting materials. It was mixed with an equimolar calcium oxide (CaO) powder in a mixer for 60 minutes. Then, this powder mixture was heated to 1200∘C and held for 360 minutes to convert the whole powder into $CaWO_4$ according to the reaction:

$$CaO \text{ (s)} + WO_3 \text{ (s)} = CaWO_4 \text{ (s)} \hspace{3cm} \text{Eq. 3.1}$$
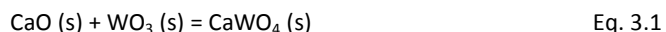
The other $CaWO_4$ powder used in laboratory scale experiments was commercially available 248665, Sigma-Aldrich $CaWO_4$ powder. SEM micrographs of the synthesized and commercially available $CaWO_4$ powders are given in Figure 3.2. As can be seen in this figure, commercially available $CaWO_4$ powder had a smaller particle size and the particles were more spherical.

(a)   **(b)**
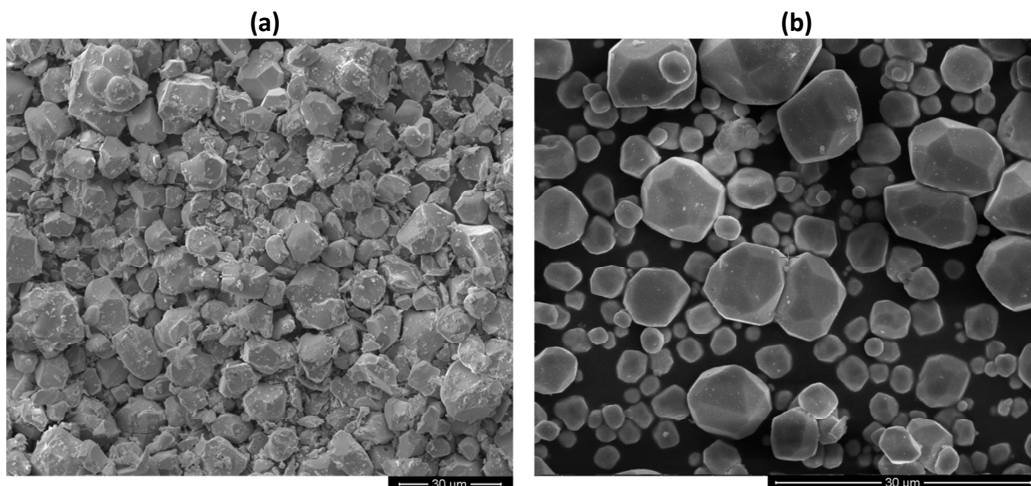
Figure 3.2: SEM micrographs of (a) synthesized and (b) commercially available 248665, Sigma-Aldrich CaWO₄ powder.

The flow sheet considerations of pellet preparation procedure for synthesized and commercially available $CaWO_4$ powders are given in Figure 3.3. The pellets used in constant voltage reduction

experiments were prepared via the following route: Firstly, the $CaWO_4$ powder was impregnated with 2% by mass of a binder; polyethylene glycol (PEG). Secondly, the components were mixed for 40 minutes and then left to dry in air at room temperature for 24 hours. Following the sieving stage, the pellets were formed by die pressing the powder under 2 tons of load and PEG was removed by holding the pellets at $600^{o}C$ for 150 minutes. Since the melting point of pure $CaWO_4$ is around $1600^{o}C$ [32], $600^{o}C$ was too low for the $CaWO_4$ powder to sinter. The pellets were 2.5 g in weight, 1.5 cm in diameter and 0.3 cm in height.

```
┌─────────────────────────────────────────┐
│                  CaWO₄                    │
└─────────────────────────────────────────┘
                    ↓
┌─────────────────────────────────────────┐
│            Impregnating with PEG          │
└─────────────────────────────────────────┘
                    ↓
┌─────────────────────────────────────────┐
│             Mixing for 40 minutes         │
└─────────────────────────────────────────┘
                    ↓
┌─────────────────────────────────────────┐
│         Drying for 24 hours in air at R.T.│
└─────────────────────────────────────────┘
                    ↓
┌─────────────────────────────────────────┐
│                  Sieving                  │
└─────────────────────────────────────────┘
                    ↓
┌─────────────────────────────────────────┐
│               Die Pressing                │
└─────────────────────────────────────────┘
                    ↓
┌─────────────────────────────────────────┐
│    Holding the pellets at 600°C for six hours │
└─────────────────────────────────────────┘
                    ↓
┌─────────────────────────────────────────┐
│           Sylindirical CaWO₄ pellets      │
└─────────────────────────────────────────┘
```
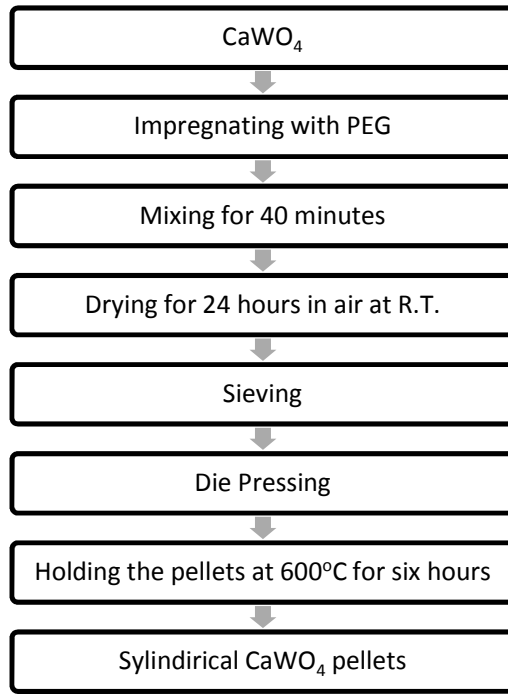
Figure 3.3: Flow sheet considerations of pellet preparation procedure.

$CaCl_2$ (12095, Riedel-de-Haën)–NaCl (13423, Riedel-de-Haën) salt mixture at eutectic composition was used as the electrolyte. Both salts were dried prior to each experiment without producing oxides and hydroxides of the salts.

It requires close experimental attention to obtain anhydrous, oxide free $CaCl_2$. Therefore, it was first heated to 110°C at $10^{°}C$/min and held for three hours. Then, the temperature was ramped to 400°C at $1^{°}C$/min and held for 24 hours. All the process was conducted under vacuum and by this way, physically and chemically bound moisture in $CaCl_2$ could be removed. The phase diagram with possible phase boundaries, shown by the dashed lines, for $CaCl_2$-H_2O system at low HCl pressure (10^{-3} atm), is shown in Figure 3.4 [41]. With reference to Figure 3.4, it can be concluded that above procedure, involving dehydration at low pressures, could yield oxide free anhydrous $CaCl_2$. On the other hand, NaCl was just heated to $110^{°}C$ and held at this temperature for 24 hours. The phase boundary between NaCl and NaOH is shown in Figure 3.5 [41]. As it is apparent from the figure, unlike $CaCl_2$, the equilibrium partial pressure of water to form NaOH is extremely high.
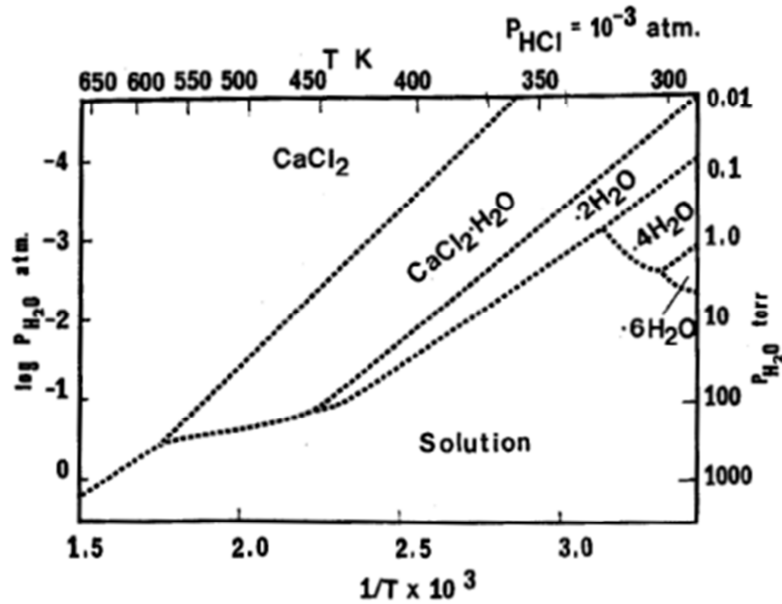
Figure 3.4: Approximate equilibrium diagram for the CaCl$_2$-H$_2$O system at an HCl partial pressure of 10^{-3} atm. showing possible phase boundaries between the hydrates and the solution. Ca(OH)$_2$ is off scale at the lower left. Reproduced from [41].
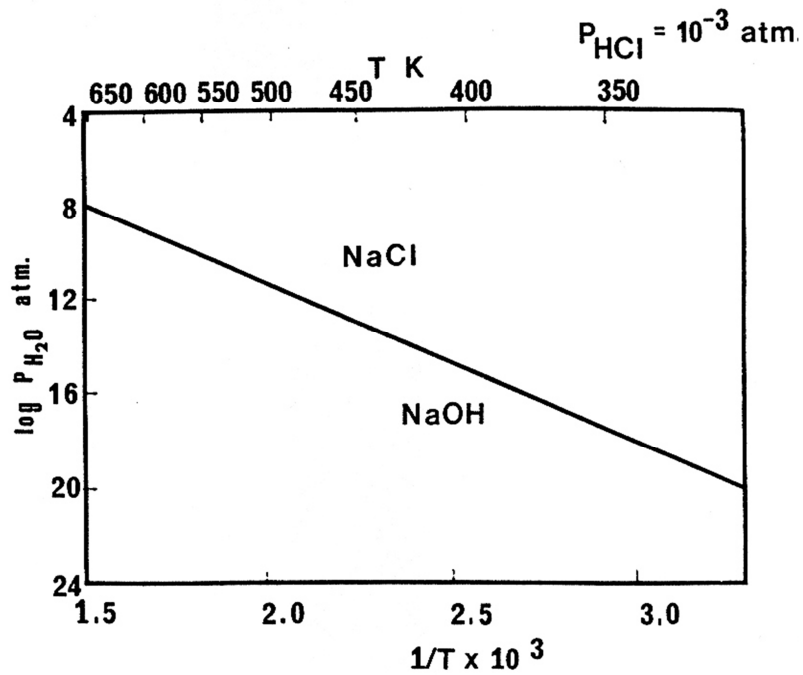
Figure 3.5: Equilibrium diagram for the NaCl-H$_2$O system at an HCl partial pressure of 10^{-3} atm. Reproduced from [41].

Because the eutectic mixture of CaCl$_2$-NaCl, which has 48 mole % NaCl, melts at 504°C [33] the electrolyte with this composition was in molten state when the temperature reached 600°C as can be seen in Figure 3.6. The electrodes were lowered and immersed into the electrolyte. Sufficient time was given for the temperature to stabilize and concentration to homogenize as a result of the mixing action of electrodes. Then, the electrodes were clamped to the rectifier (Agilent N 6700) leads and the current was turned on. Applied voltages and corresponding currents were digitally collected and recorded by a computer. In the experiments, applied potentials did not exceed 3.2 V. These voltages are by far lower than the decomposition potentials of CaCl$_2$ and NaCl ($E^o_{CaCl_2} = -3.4$ V, $E^o_{Nacl} = -3.37$ V) when the overvoltages, IR drop, and the voltage drops along the electrode leads are also considered. An argon gas flow of 100 ml/minute was used to provide an inert atmosphere in the cell vessel and also argon was used as a carrier gas to take gaseous electrolysis products out of the cell vessel.
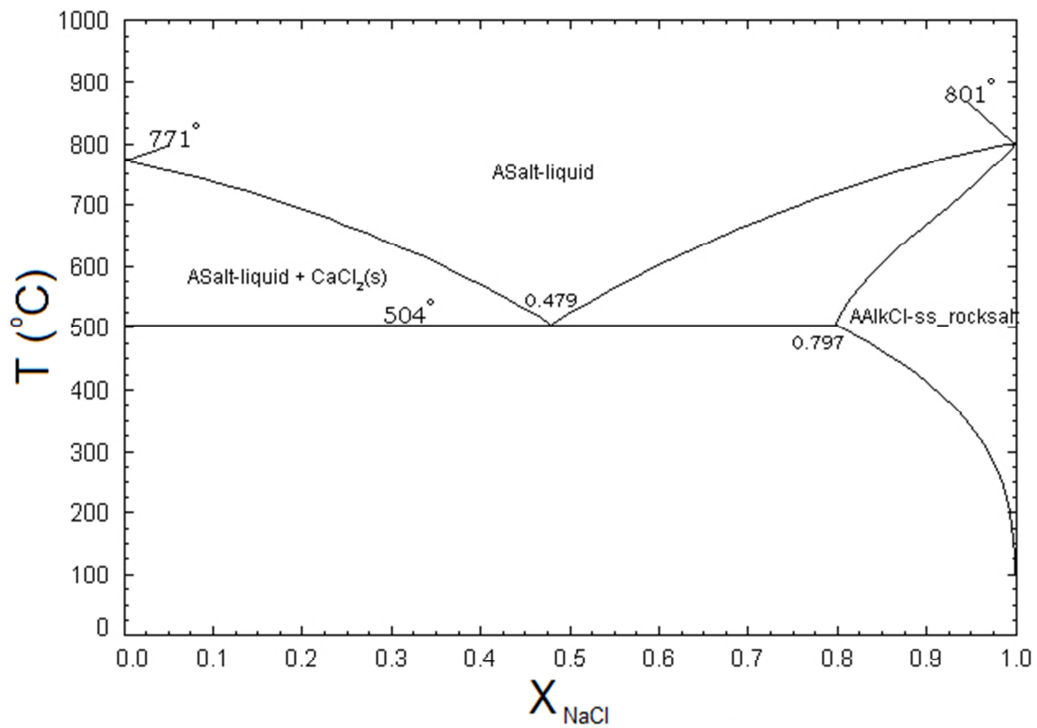
Figure 3.6: Phase diagram of CaCl$_2$-NaCl system (Reproduced from [33]).

3.1.2 Cyclic Voltammetry Experiments

The schematic view of the experimental setup used in cyclic voltammetry is given in Figure 3.7.
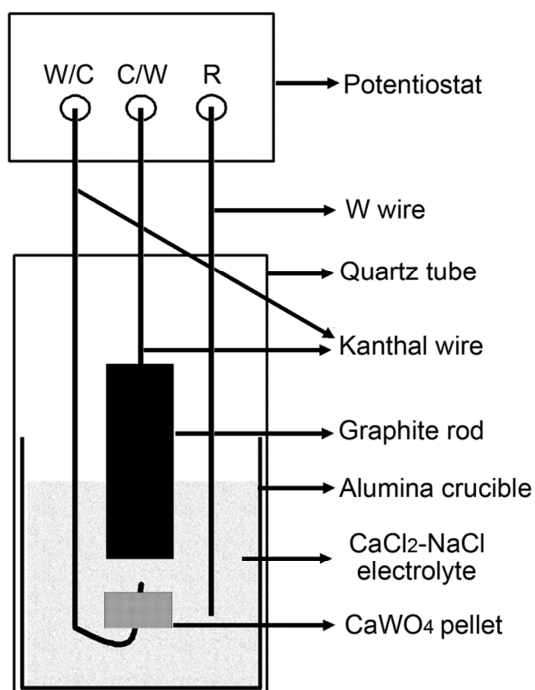
Figure 3.7: The schematic drawing of the experimental setup for the cyclic voltammetry experiments. Reproduced from [42] by the license obtained from Springer.

The $CaWO_4$ pellets for the cyclic voltammetry experiments were prepared according to the same powder processing procedure as described in the previous paragraph up to the heating stage. However, after die pressing the $CaWO_4$ powder, the green bodies were sintered for two hours at 1200^oC. Following sintering, a small hole was drilled through the pellet to attach the pellet onto a Kanthal (N 80) wire to form the assembled cathode. The anode material, the electrolyte and the temperature of the cyclic voltammetry experiments were the same as the previously mentioned constant voltage electrolysis experiments. In this electrochemical cell, depending on the electrode reaction under consideration; either the $CaWO_4$ pellet cathode or the graphite anode was made the working electrode (W). When one was used as the working electrode, the other was used as the counter electrode (C). A three electrode cell, which is commonly used for cyclic voltammetry studies, differs from that of the conventional two electrode cell with the use of a reference electrode (R) that must be corrosion resistant to the electrolyte. Tungsten, molybdenum, Kanthal and stainless steel were reported to be satisfactory in molten chlorides [22]. However, when stainless steel or Kanthal is used, the experiments should be completed in a short period of time, because these materials do not export sufficiently stable potentials for long durations. Therefore,

in this study, a tungsten wire was used as the reference electrode. The cyclic voltammetry experiments were conducted by a GAMRY Reference 3000 type potentiostat.

Nearly in all of the electrochemical reduction studies of metal oxides, sintered porous pellets were used [22, 23, 43, 44]. By this way, while the sintered body provides good contact between the oxide particles, the porous structure of the pellet eases the transportation of oxygen in the solid oxide phase [22]. Furthermore, in many of these studies, the metal oxide cathode materials were attached to the current collector by means of a hole drilled in the middle of the pellets. This cathode design requires that the pellets should have sufficient strength which can be gained by sintering.

However, the advantage of using only mechanically compressed pellets over sintered pellets in the electrochemical reduction of $CaWO_4$ was already demonstrated [31]. It was shown that, only mechanically compressed $CaWO_4$ pellets placed on a spoon-like electrode were reduced completely to tungsten, whereas; reduction occurred only at the surfaces of the sintered $CaWO_4$ pellets with the same cathode design. The spoon-like cathode design works well in the electrochemical reduction of $CaWO_4$ because of the high density of this material. When lighter materials -especially the ones with densities less than or equal to the electrolytes- are considered, there is a high probability that the electrolyte will penetrate between the current collector and the pellet causing the loss of electrical contact. Use of such an electrode is crucial when the cathode materials are used without sintering because they can easily disintegrate during reduction. However, because of the previously mentioned problem, its use is confined to the materials with considerably higher densities than the electrolytes.

It was therefore decided to use only mechanically compressed $CaWO_4$ pellets in the constant voltage electrochemical reduction experiments. In the cyclic voltammetry experiments, use of a spoon-like electrode was found to cause problems with the current measurements, probably because of the large volume of stainless steel immersed into the electrolyte. Consequently, sintered pellets were prepared and attached to the current collector for cyclic voltammetry experiments.

3.1.3 HCl Cleaning Treatment Experiments

The necessity for a cleaning procedure by dilute HCl solution, after electrochemical reduction of $CaWO_4$, to remove the calcium compounds was already suggested [31, 35]. In this study, this procedure was further investigated by full factorial experimental design. Temperature, acid concentration and exposure time were selected as the process parameters. Three levels were determined for each parameter and the full factorial experimental design required 27 experiments under these conditions. The experiment sequence and values of the process parameters for each experiment are given in Table 3.1.

All the experiments were performed in glass beakers with 250 ml solution and 4 grams of as reduced powder. Magnetic stirring was applied during each experiment and the stirring rate was constant at 500 rpm. X-ray diffraction analysis result of the as reduced powder is given in Figure 3.8. As reduced powder (stock) contained 33.4 % Ca according to the XRF analysis. The stock used in this part was obtained from large scale experiments that will be discussed next.

Table 3.1: The experiment sequence and values of the process parameters for each experiment.

Exp. No	T (^{o}C)	C (M)	t (min.)
1	55	0.2	60
2	55	0.4	120
3	40	0.2	60
4	55	0.1	60
5	25	0.4	30
6	55	0.2	30
7	40	0.2	120
8	55	0.4	60
9	40	0.4	120
10	25	0.2	30
11	55	0.1	30
12	55	0.2	120
13	40	0.1	120
14	40	0.4	30
15	25	0.1	30
16	25	0.2	120
17	55	0.1	120
18	25	0.2	60
19	25	0.1	120
20	40	0.2	30
21	25	0.4	120
22	25	0.4	60
23	25	0.1	60
24	40	0.1	30
25	40	0.1	60
26	40	0.4	60
27	55	0.4	30
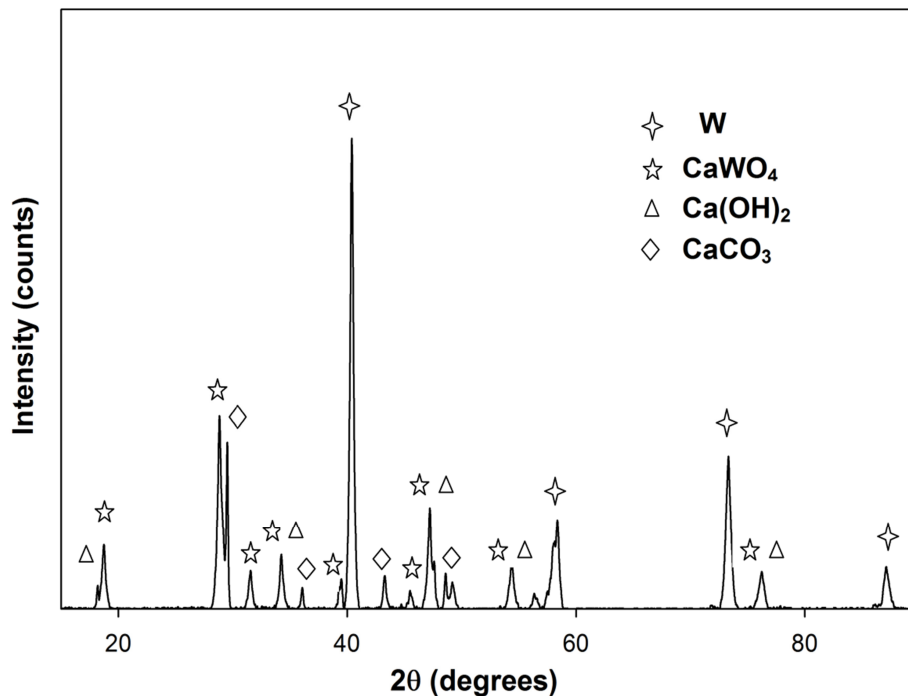
Figure 3.8: X-ray diffraction analysis result of the as reduced powder

3.2 Large Scale Experiments

A tungsten production line was designed and manufactured with the aim of 300 g tungsten production per day. The three dimensional drawing of the furnace constructed can be seen in Figure 3.9. The external dimensions of the furnace were 500 mm diameter and 500 mm height. It had three rows of resistance wires at the side walls and one row at the bottom. By this way, it became possible to heat the furnace by the resistances positioned at the side walls or at the bottom alone or using both of the resistances. The resistance wires were installed to the refractor materials as shown in Figure 3.10.

A stainless steel (AISI 316 Ti) vessel was placed into the furnace to hold the salt bath. It had 360 mm outer diameter, 4 mm thickness and 360 mm height. The $CaWO_4$ (Noah, 18418) powder was introduced to the molten salt within a stainless steel (AISI 316 Ti) tray, when the target temperature of 600^oC was reached. The three dimensional drawings of the tray and the vessel are given in Figure 3.11. The tray (330 mm outside diameter and 30 mm height) was placed into the vessel as seen in this figure. The vessel and the tray used in the first test were not AISI 316 Ti stainless steel. They were AISI 306 stainless steel, readily available in shops selling kitchenware and were not manufactured specifically for this purpose. The reason for using these materials for the first test was to have easy replacement and avoid use of vessels which may have defects at seams formed by welding. It was found that, use of AISI 316 Ti stainless steel vessel and the tray improved the operation.
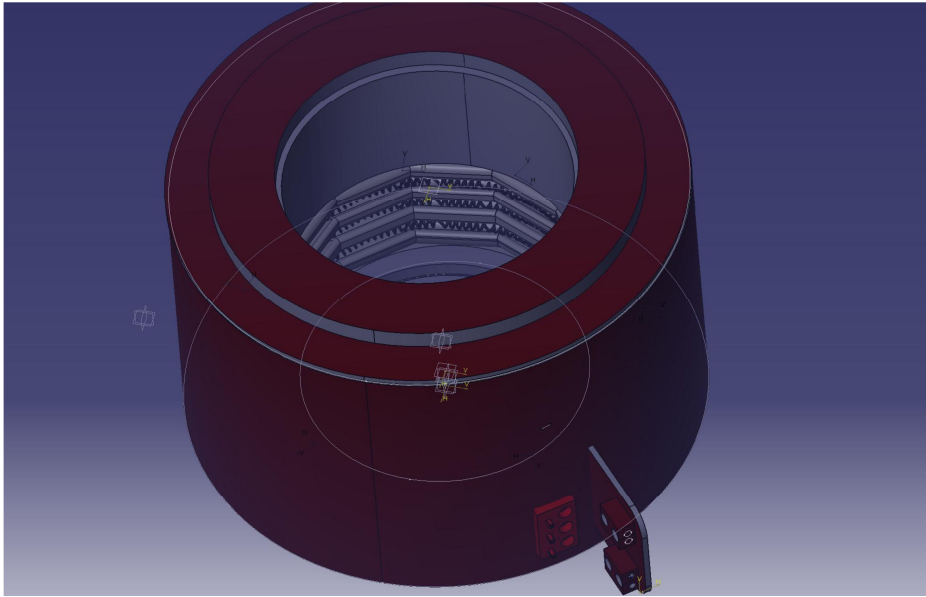
Figure 3.9: The three dimensional drawing of the furnace constructed for large scale tests.

(a)

(b)
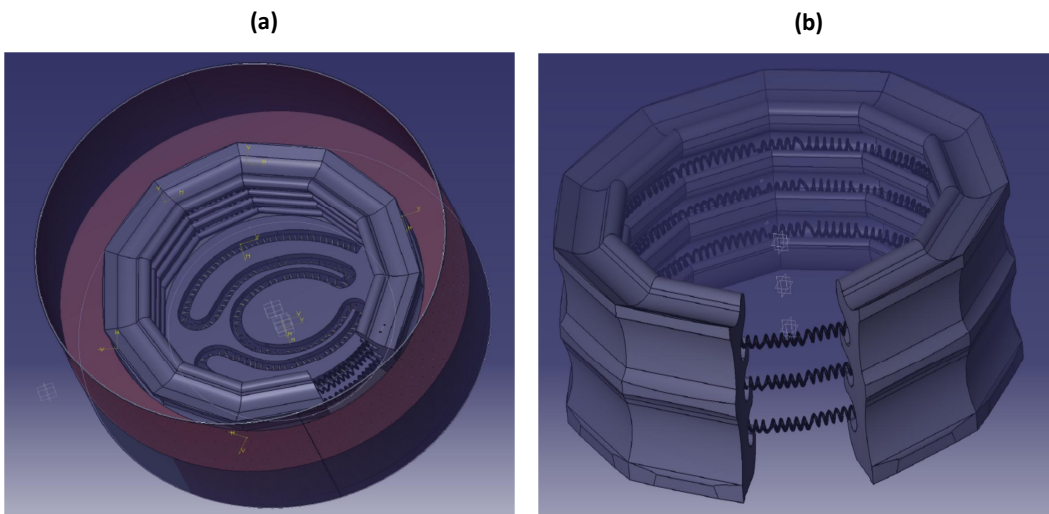
Figure 3.10: Resistance wires (a) at the bottom and (b) at the side walls of the furnace constructed for large scale tests.
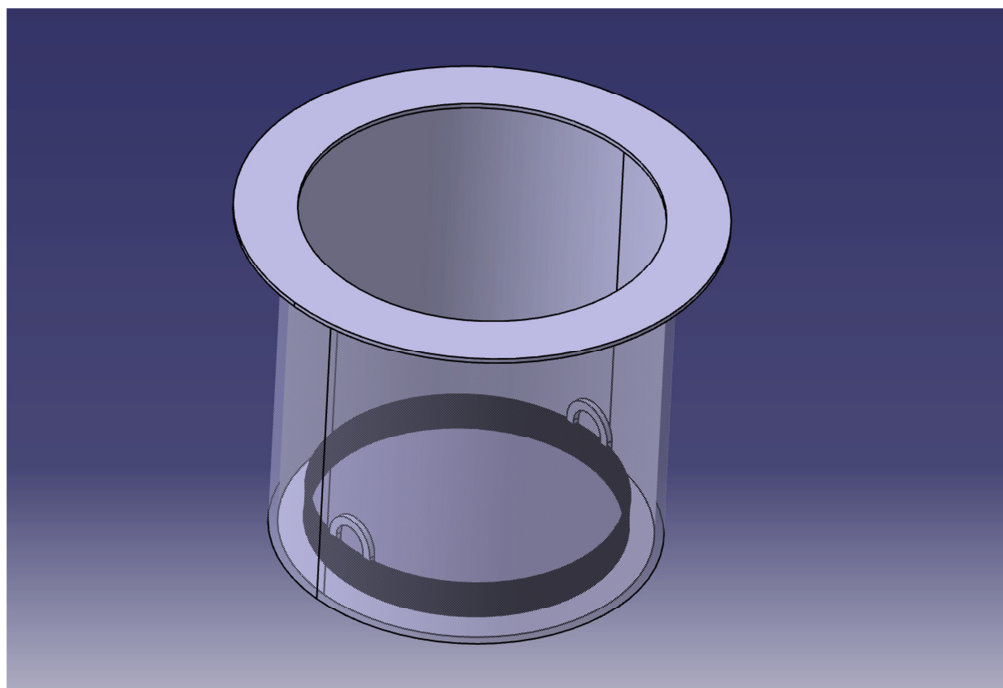
Figure 3.11: Three dimensional drawings of the tray (inside) which was used to introduce the CaWO₄ powder and the vessel (outside) which was used to hold the salt bath.

A graphite rod with 100 mm diameter was used as the anode material. In order to move the graphite rod vertically, an elevator system was built next to the furnace. The system was composed of an arm to hold the graphite anode at the center of the furnace, an infinite screw and an insulator nut system placed into a U profile. An AC electric motor and a redactor were used to rotate the screw at low speed to move the anode up and down slowly. The nut system carrying the arm that was holding the graphite anode was made of Kestamid to insulate the elevator system while supplying electrical current to the anode directly. The three dimensional drawing of the elevator system is given in Figure 3.12. When the AC motor is started, the fixed screw rotates and the nut -consequently the graphite rod- moves vertically, in this system. The rotation of the screw from left to right or right to left was controlled by a two-way switch. A photograph of the complete large scale tungsten production system manufactured in this study can be seen in Figure 3.13. Side and top view drawings of the system are given Figure 3.14.

Technical grade $CaCl_2$ (Solvay) and NaCl (Üçleroğlu) salts were mixed to obtain a salt solution of eutectic composition as the electrolyte. Melting of the salt mixture was completed in 48 hours and most of the H_2O that $CaCl_2$ contained was removed at low temperatures. An air flow was provided during heating to aid dehydration.

SEM photograph and EDX analysis of the CaWO₄ (Noah, 18418) powder used in the experiments are given in Figure 3.15 and Figure 3.16, respectively. As it can be seen in Figure 3.16, the powder contains about 1.4 % wt. Na which was probably caused by the soda roasting and leaching step given in Figure 2.4.
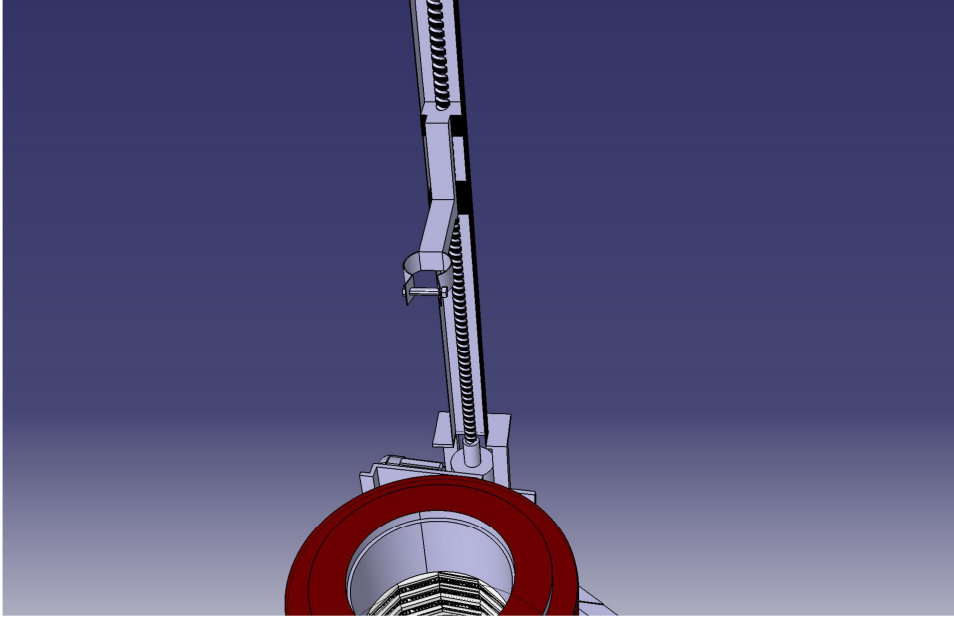
Figure 3.12: The three dimensional drawing of the elevator system.

Figure 3.13: A photograph of the complete large scale tungsten production system manufactured in this study.
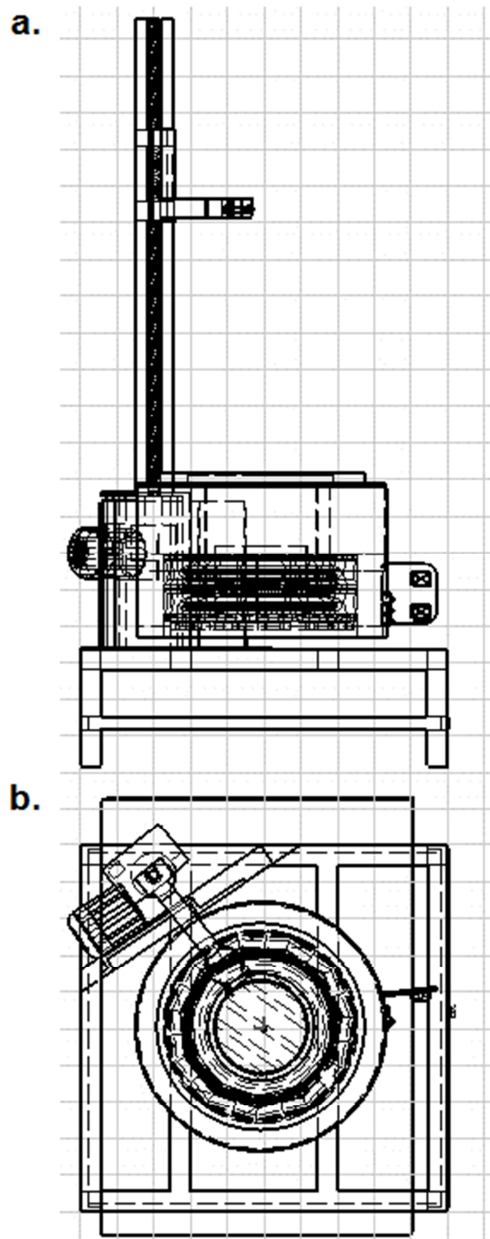
Figure 3.14: a) Side and b) top view drawings of the system manufactured.
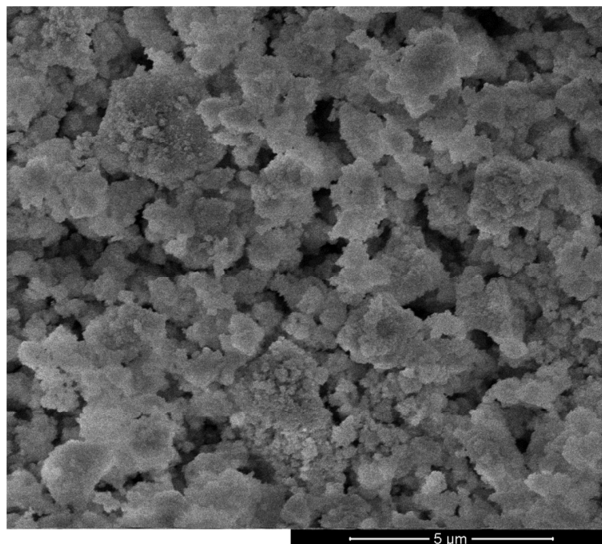
Figure 3.15: SEM micrograph of the CaWO$_4$ (Noah, 18418) powder.
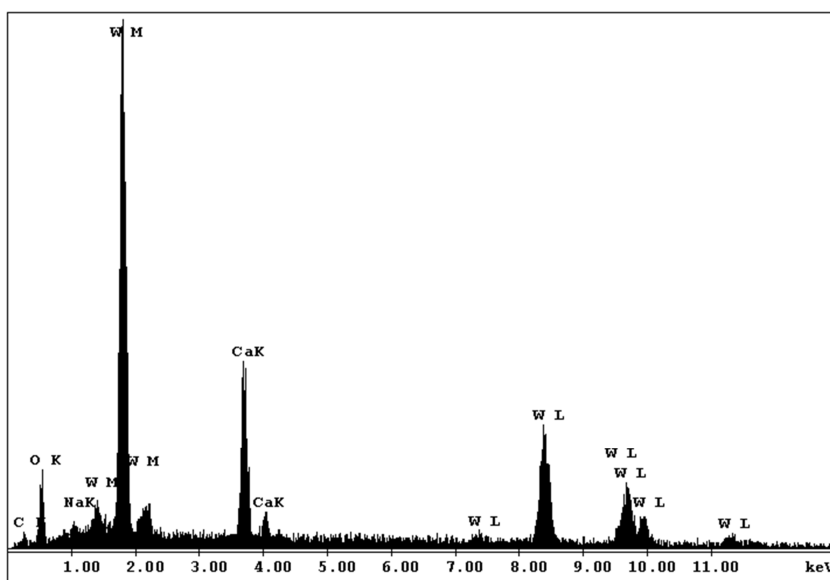

```
EDAX ZAF Quantification (Standardless)
Element Normalized
SEC Table : Default

Element   Wt %    At %    K-Ratio    Z        A        F
  C K     4.11    13.78   0.0101    1.1600   0.2111   1.0003
  O K    22.57    56.79   0.0369    1.1432   0.1430   1.0000
  NaK     1.40     2.45   0.0032    1.0730   0.2133   1.0002
  CaK    14.31    14.37   0.0818    1.1115   0.5113   1.0052
  W L    57.61    12.61   0.5107    0.8434   1.0511   1.0000
  Total 100.00   100.00
```

Figure 3.16: EDX analysis of the CaWO$_4$ (Noah, 18418) powder.

3.3 Characterization

In the characterization of raw materials, intermediate and final products of laboratory and large scale tungsten production experiments, scanning electron microscope (Nova NanoSEM 430), XRF (Bruker S8 Tiger), particle size analyzer (Malvern Mastersizer 2000) and X-ray diffractometer (Rigaku D/Max2200/PC) were used.

XRF analyses were conducted without standard based calibrations by QUANT-EXPRESS program. With standardless analysis, all parameters are based upon theoretical equations, the fundamental parameter database, and precise modeling of the detector, X-ray tube, and geometry. QUANT-EXPRESS was reported to comprise a unique multipurpose calibration prepared by the manufacturer using innumerable certified standards [45].

XRD analyses were performed by Rigaku diffractometer using CuKα radiation. Data were acquired with a scan rate of 2°/min and sampling width of 0.02°. X-ray data were refined by the Rigaku software.

In some cases, elemental analyses were performed by the use of an energy dispersive system (EDS) that is attached to Nova NanoSEM 430 scanning electron microscope.

CHAPTER 4

RESULTS AND DISCUSSION

4.1 Tungsten Production by Electrodeoxidation

The current vs. time graphs of the constant voltage electrolysis of $CaWO_4$ for three different experiments are shown in Figure 4.1.
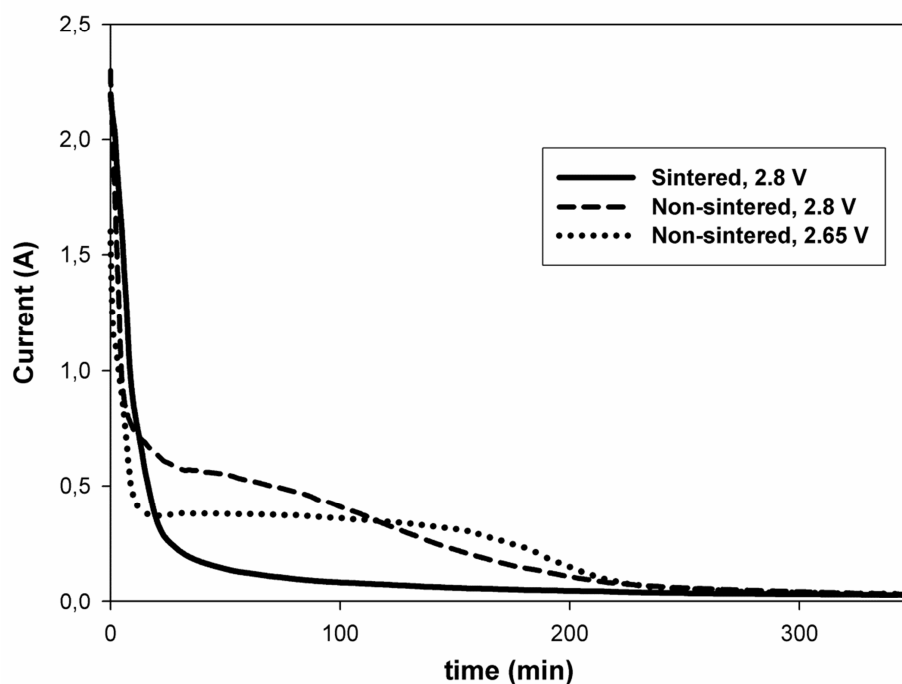
Figure 4.1: Current vs. time graphs of CaWO₄ electroreduction with the sintered pellet under a voltage difference of 2.8 V and with the non-sintered pellets at voltages 2.8 and 2.65 volts. Reproduced from [31] by the license obtained from Springer.

Two of the curves belong to the electroreduction of non-sintered pellets; one was reduced at 2.8 V and the other at 2.65 V. The remaining curve was obtained from the electroreduction of a sintered pellet, under a potential difference of 2.8 V. The pellets were identical in weight and geometry for all experiments. As it can be seen in this figure, the current vs. time plots of all runs begin with a peak current and thereafter the current decreases with time. Higher initial current values were probably because electroreduction of the pellets start from the regions at which $CaWO_4$ pellets are in contact with the stainless steel current collector and then proceeds to the

inner regions. In other words, reduction starts where the pellet, molten salt and the current collector are in contact with each other. The rapid decrease of the current values after the initial period, which is evident from Figure 4.1, could be attributed to the increase in resistance due to increase in conduction path in the porous pellet.

The lowest current values recorded during electroreduction of sintered pellet indicated the lowest fraction of reduction after the initial period. This was also evident from the observation that, the sintered pellet preserved its shape after the electrolysis and the reduction took place only at the surfaces of the pellet and $CaWO_4$ was left unreacted in the inner regions. Higher current values were observed during electroreduction of non-sintered pellets and they increased with increasing applied potential during electrolysis. As it can be seen in Figure 4.1, a plateau has been formed between 15 to 150 minutes, indicating the establishment of steady state, when 2.65 V potential was applied. In the case of 2.8 V potential application, faster decrease in size of unreacted part of the pellet and increase in conduction path results in continuous decrease of current.

In the experiments with the non-sintered pellets, the pellets were found to have lost their integrity but the reduced samples could be obtained in powder form inside the stainless steel spoon cathode. The samples were taken from the cathode by removing the solidified salt with water. They were then filtered and dried. X-ray diffraction spectrum of one of the reduced samples is given in Figure 4.2-a. With reference to this figure it can be said that mechanically compressed $CaWO_4$ pellets were reduced completely to tungsten. The presence of byproducts; $CaCO_3$ and $Ca(OH)_2$ can also be seen in this figure.

Formation of $CaCO_3$ was eliminated by flushing the cell vessel with argon gas after the completion of electrolysis experiments. Figure 4.2-b shows the X-ray diffraction spectrum of a sample after an experiment in which the vessel was flushed with argon gas. The reduced samples taken from cathode containing $Ca(OH)_2$ with or without $CaCO_3$ were subjected to a cleaning process to obtain tungsten metal powder. This was achieved by treating the reduced sample with a dilute hydrochloric acid solution. It was observed that tungsten was sufficiently inert in such a solution, whereas $Ca(OH)_2$ and/or $CaCO_3$ can easily and completely be removed. Figure 4.3 shows the X-ray diffraction result of a cathode sample that was treated with 0.2 M HCl solution. As it can be seen in this figure, all the peaks except those belonging to tungsten disappeared.

The particle size analysis results and SEM photographs of the starting non-sintered $CaWO_4$ pellet and produced metallic tungsten powder are given in Table 4.1 and Figure 4.4, respectively. It can be seen in Figure 4.4-a that particle size of the $CaWO_4$ is in agreement with the results of particle size analysis, showing majority of the particles are smaller than 40 μm and the average particle size is about 14 μm. Particle size of the electrochemically produced W powder was not clear as it is seen in Figure 4.4-b due to necking between parts of about 100 nm size. This explains the particle size analysis results which showed that the average particle size was about 4 μm. Another factor for above observation is that the particles have very high surface energies and high tendencies to agglomerate because they have very small size. Power of the particle size analyzer was probably unable to separate the agglomerated particles.
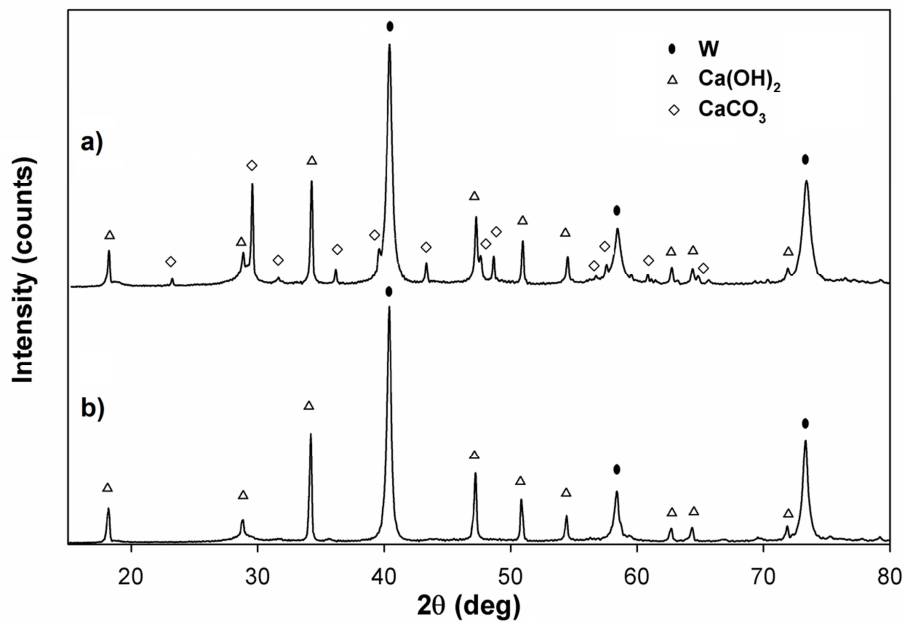
Figure 4.2: X-ray diffraction results of the electroreduced CaWO₄ samples taken from the cathode; a) without flushing the cell with argon and b) after flushing the cell with argon. Reproduced from [31] by the license obtained from Springer.
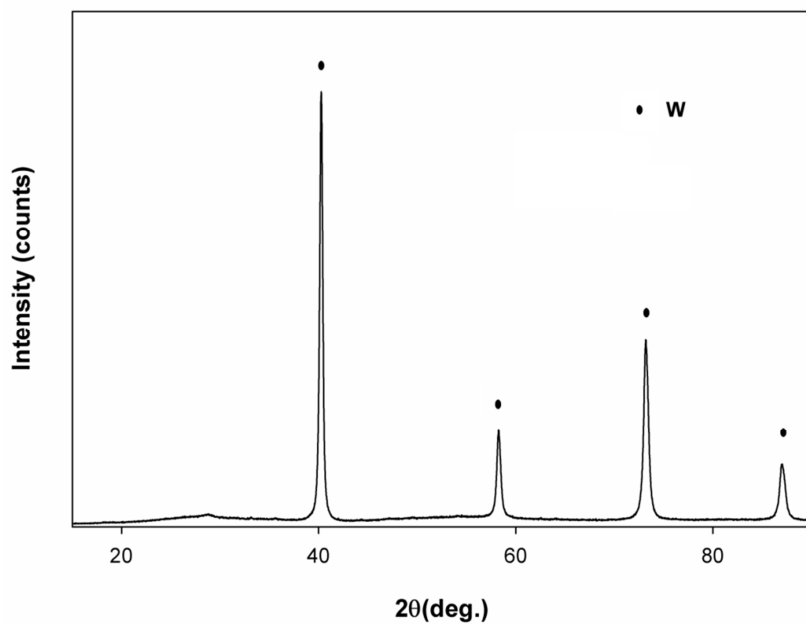
Figure 4.3: X-ray diffraction spectrum of a sample treated with 0.2 M HCl solution. Reproduced from [31] by the license obtained from Springer.

Table 4.1: Particle size analysis results of the starting non-sintered CaWO$_4$ pellet and produced metallic tungsten powder. 0.1, 50 and 90 are corresponding to the 10%, 50% and 90% of the particles, respectively.

	d(0.1) (µm)	d(50) (µm)	d(90) (µm)
CaWO$_4$	1.99	13.96	39.626
W	1.155	3.799	10.722
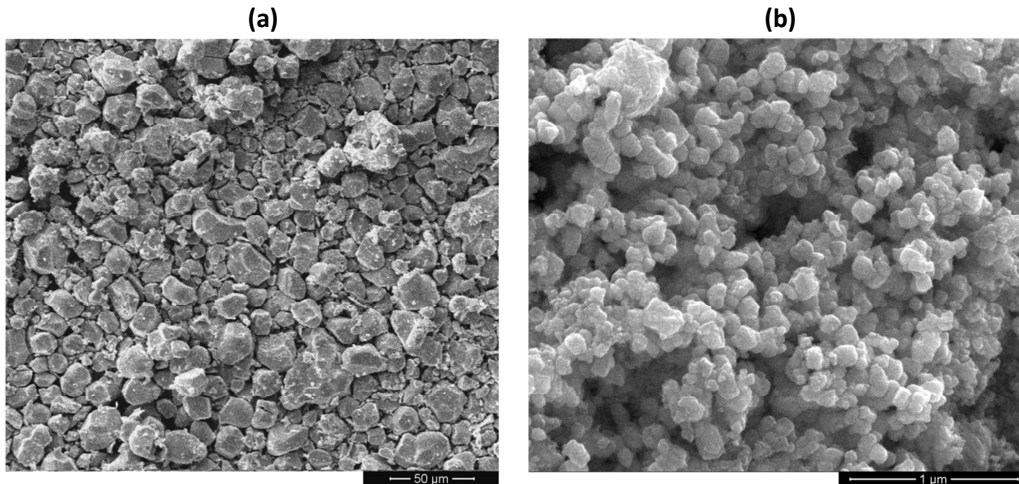
Figure 4.4: SEM photographs of the a) non-sintered CaWO$_4$ pellet and b) electrochemically produced tungsten powder. Reproduced from [31] by the license obtained from Springer.

4.2 Determination of the Reduction Mechanism of CaWO$_4$ in Molten CaCl$_2$-NaCl Salt Solution

The electrochemical reduction experiments were performed at 600°C by applying four different constant potential differences between the CaWO$_4$ cathode and the graphite anode in molten CaCl$_2$-NaCl eutectic salt solution. Current values were recorded as a function of time during each experiment and they are given in Figure 4.5. In the presentation of the results, current values were directly used instead of current densities because the pellets were identical in shape and geometry for all of the experiments. The plots revealed the positive influence of the applied voltage on the output current as expected. All the curves start with a current peak and then decrease steadily to lower values. In the experiments at 2.5 V and 2.65 V, the current values form a plateau at about 0.2 A and 0.4 A respectively. At higher voltages, i.e. 2.8 V and 2.95 V plateau formation was not observed, probably because of the absence of steady state due to faster reduction.
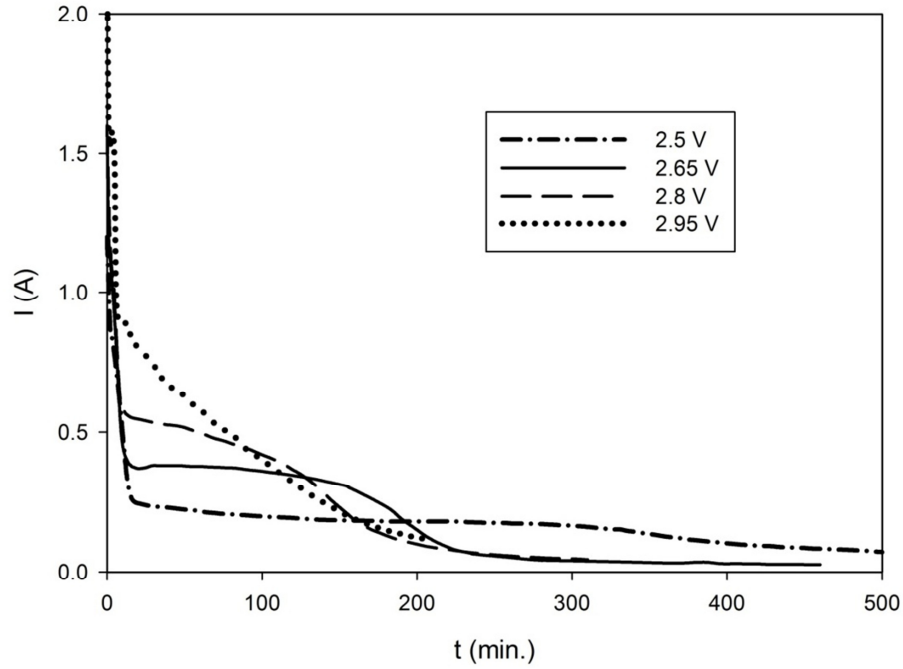
Figure 4.5: Electrochemical reduction experiments of the CaWO$_4$ pellets at different applied constant voltages in eutectic CaCl$_2$-NaCl electrolyte at 600°C. Reproduced from [42] by the license obtained from Springer. The data for 2.65 and 2.8 V applied constant voltages were repeated from [31] by the license obtained from Springer.

The required potential for a reaction to take place in an electrochemical cell is always greater than that of the theoretical potential of the reaction. When current is passing through the cell, resistances of the cell and the electrical connections together with the overvoltages caused by the kinetics of electrode reactions consume some of the applied potential. Accordingly, the total applied potential for the present electrochemical cell can be given as:

$$E_{applied} = E_{reaction} + E_{electrical\ connections} + E_{electrolyte} + E_{pellet} + \eta \qquad \text{Eq. 4.1}$$

$E_{reaction}$ is the theoretical potential required for the reduction reaction and given by the following equation;

$$E_{reaction} = -\frac{\Delta G_{reaction}}{nF} \qquad \text{Eq. 4.2}$$

where $\Delta G_{reaction}$ represents the Gibbs Energy change of the reaction, n the number of Faradays involved in the reaction and F the Faraday's constant.

Voltage drops along the electrode leads, $E_{electrical\ connections}$, were measured by short-circuiting the electrodes in a molten Pb pool and applying currents within the range of current values recorded in the constant voltage electrochemical reduction experiments. The resulting voltage vs. current graph can be seen in Figure 4.6. By this way, the voltage drop along the electrode leads was obtained for any current value and used to calculate the net cell voltage, E_{net}, which is defined as;

$$E_{net} = E_{applied} - E_{electrical\ connections} \qquad \text{Eq. 4.3}$$
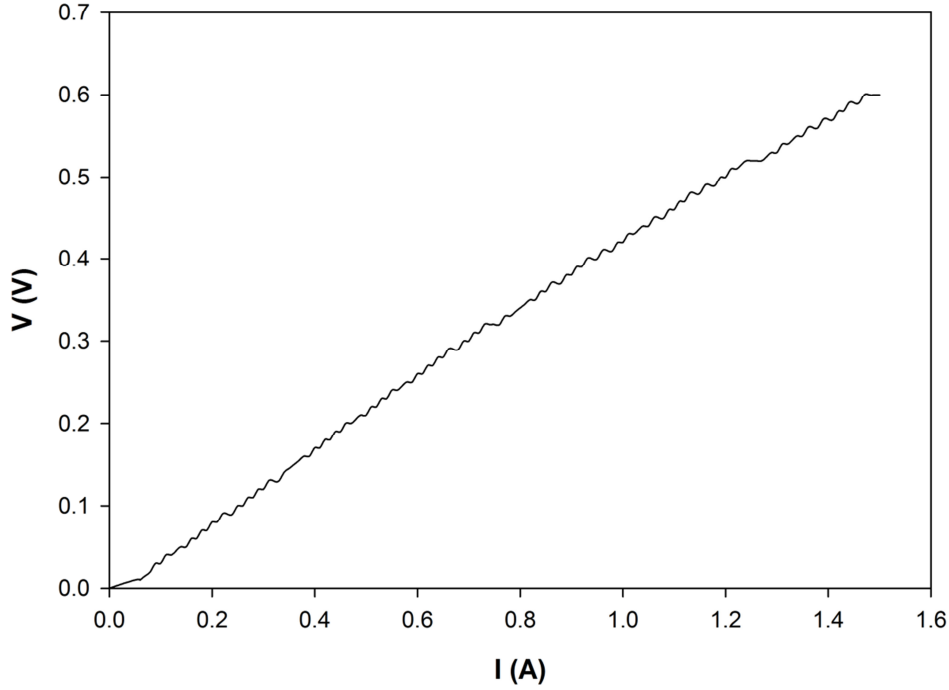
Figure 4.6: Recorded voltage values ($E_{electrical\ connections}$) as a function of applied current (I), obtained by short-circuiting the electrodes in a molten Pb pool at 600°C.

$E_{electrolyte}$ and E_{pellet} are ohmic voltage drops of the electrolyte and the pellet and they are given by multiplication of their resistance and the current passing through the cell.

As being associated with the current, the ohmic voltages will be zero when there is no current passing through the cell. Therefore, it is clear from Eq. 4.1 and Eq. 4.3 that extrapolation of the regression line of the E_{net} vs. I plot to zero current gives the value of the theoretical potential required for the reduction reaction plus the anodic overvoltage. It should be noted that the current dependency of the anodic overvoltage is logarithmic and its dependency can be neglected for low current density values recorded in this study. Likewise, the slope of the above regression line gives the sum of the resistances of the electrolyte and the pellet.

For the present study, cathodic overvoltage could be neglected especially when the low current density values recorded in this study are considered. Therefore, the overvoltage, η, component of

the Eq. 4.1 could be regarded to be the anodic overvoltage which is mainly caused by CO_2 evolution at the anode. The required activation overvoltages for such new phase formations are usually presented by the Tafel equation;

$$\eta = a + b \log i \qquad\qquad \text{Eq. 4.4}$$

where a and b are the Tafel coefficients and i is the current density.

In the light of above information, E_{net} vs. I plots were constructed from the data of Figure 4.5 for two cases; one for the initial stage and the other for the later stage. It is worthwhile to note that the $CaWO_4$ pellets exhibit a certain resistance to the flow of current and corresponding voltage drops should be considered in the computations. However, from the examination of Figure 4.5, it can be deduced that the resistances of the pellets are much less pronounced at the initial stages of the experiments where higher currents were recorded. This kind of I-t graphs are seen in nearly all of the electrochemical reduction studies of metal oxides [22, 23, 31, 43, 44]. In the case of TiO_2 electrolysis, the high-current period observed at the initial stages of the experiments was explained with reference to the electrochemical insertion of Ca^{+2} ions in TiO_2 to form $CaTiO_3$ [43]. However, in this study, $CaWO_4$ was directly used as the starting material instead of WO_3; thereby insertion of Ca^{+2} ions was not possible. It was also proposed that the reduction starts from the regions where the three phases; the pellet, the electrolyte and the current collector are in contact with each other and then proceeds into the pellet [46]. Accordingly, rapid decrease of the current values apparent in Figure 4.5 can be attributed to the resistance of the pellet which became effective after the direct contact between the $CaWO_4$ powder and the current collector was lost. Consequently, the slope of the regression line of E_{net} vs. I graph plotted for the initial stage was expected to reflect the resistance of the electrolyte only. For the initial stage, the currents, corresponding to the passage of 0.0052 Faradays (502.6 Coulombs) of electrical charge, - when only about 10% of the pellets were theoretically reduced- were plotted as a function of net cell voltages. The list of calculated values and the resulting E_{net} vs. I plot are given in Table 4.2 and Figure 4.7, respectively. As it can be seen in Figure 4.7, extrapolation of the regression line to zero current yielded the sum of $E_{reaction}$ and η as 2.22 V and the slope gave the electrolyte resistance as 0.35 Ω.

Table 4.2: The list of calculated values for the initial stages (10% theoretical reduction) of the experiments.

$E_{applied}$ (V)	$E_{electrical\ connections}$ (V)	E_{net} (V)	I (A)
2.5	0.16	2.34	0.39
2.65	0.24	2.41	0.55
2.80	0.31	2.49	0.71
2.95	0.41	2.54	0.97
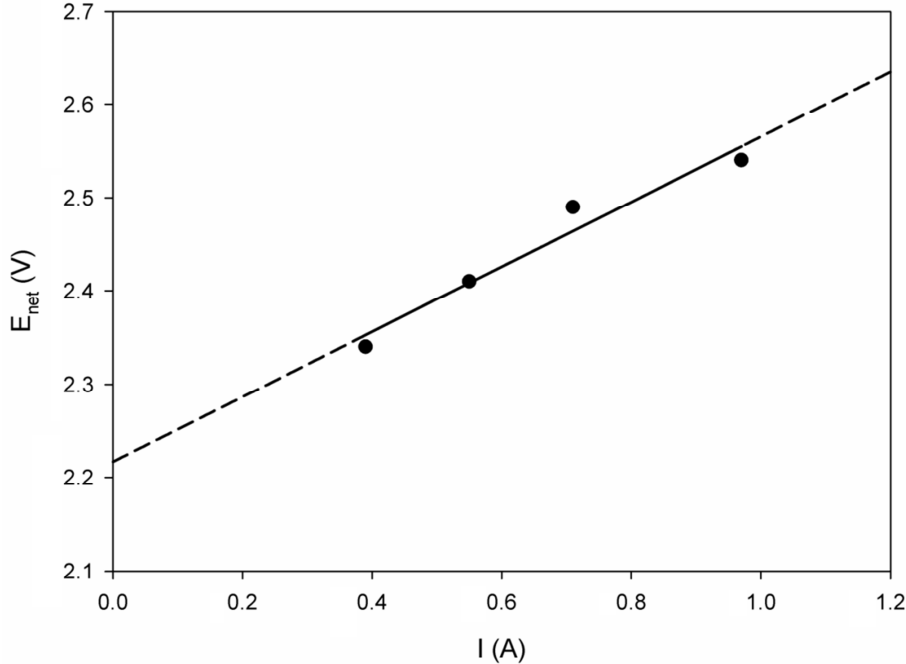
Figure 4.7: Net cell voltage as a function of current values for the initial stages (10% theoretical reduction) of the experiments. Reproduced from [42] by the license obtained from Springer.

The specific resistance of the eutectic $CaCl_2$-NaCl melt at $600^{\circ}C$ was reported to range between 0.68 and 0.81 Ω.cm [47]. Using 1.91 cm^2 cross-sectional areas of the pellets and 1 cm anode-cathode distance of the cell, the specific resistance of the molten salt solution was calculated as 0.67 Ω.cm. This value can be regarded to be consistent with the literature considering the small polarization present during cell operation.

However, it should be pointed out that, at the initial stages, the pellet resistance to the flow of current is lower when compared to the later stages of the electrochemical reduction process. Tang et al [4] claim that the increase in the resistance of the pellets can be explained with reference to the less-interconnected structure of produced fine particles. Presence of calcium compounds which are generated together with the reduced particles [31, 35] can be shown as another factor responsible for this behavior.

For this reason, the above study was repeated for a later stage of the experiments. Accordingly, the current values corresponding to the passage of 0.035 Faradays (3377.5 Coulombs) were determined and plotted against the net cell voltages. Nearly 68% of the starting $CaWO_4$ was theoretically reduced when 0.035 Faradays of electrical charge passed through the cell. The related calculations and the resulting E_{net} vs. I plot are given in Table 4.3 and Figure 4.8 respectively.

44

Table 4.3: The list of calculated values for the later stages (68% theoretical reduction) of the experiments.

| $E_{applied}$ (V)	$E_{electrical\ connections}$ (V)	E_{net} (V)	I (A)
2.5	0.07	2.43	0.18
2.65	0.13	2.52	0.33
2.80	0.17	2.63	0.41
2.95	0.22	2.73	0.51
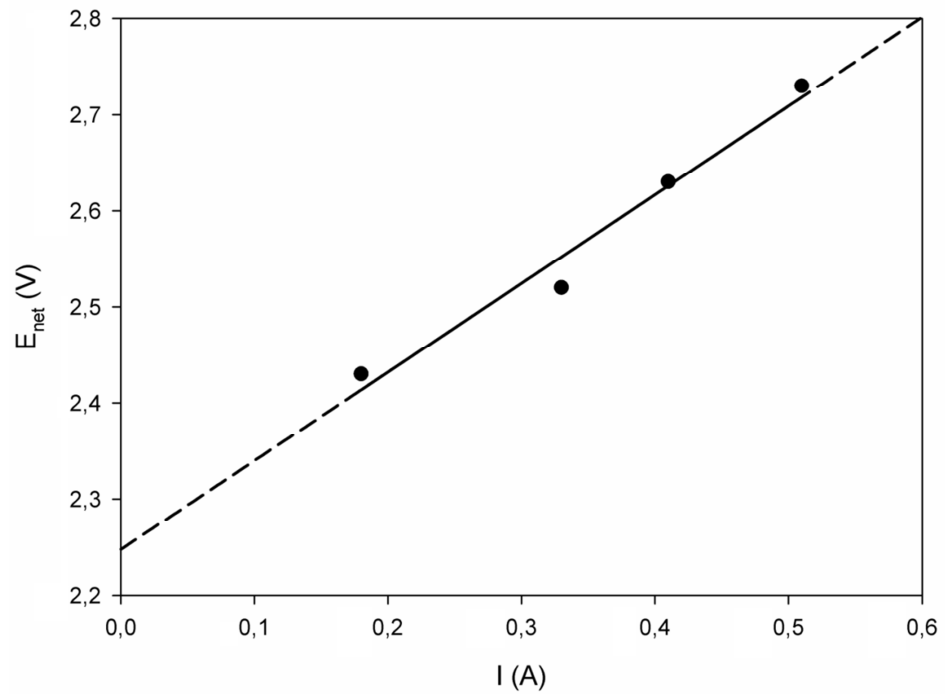
Figure 4.8: Net cell voltage as a function of current values for the later stages (68% theoretical reduction) of the experiments. Reproduced from [42] by the license obtained from Springer.

Extrapolation of the regression line of the plot presented in Figure 4.8 to zero current gave 2.25 V which is very close to 2.22 V obtained from Figure 4.7. Therefore, it can be proposed that the same mechanism is operative both at the initial and later stages of the electrochemical reduction experiments. However, the slope of the regression line in Figure 4.8 was calculated as 0.92 Ω, which is 0.57 Ω greater than the value obtained from the previous diagram. This was expected and already discussed that the pellets do not exhibit a remarkable resistance at the initial stages of the experiments. Therefore, the difference of 0.57 Ω between the resistances calculated from Figure 4.7 and Figure 4.8 was attributed to the resistance of the pellets, which became significant after the initial period when relatively higher-currents fall down.

In order to verify above findings and gain additional information on the reduction mechanism, a two electrode cyclic voltammetry (CV) experiment was performed at 600°C. Similar to the constant voltage electroreduction experiments, CaCl$_2$-NaCl molten salt solution at eutectic composition was used as electrolyte. The potential between the CaWO$_4$ pellet and the graphite rod was scanned in the 0 to -3.5 V range at 20 mV/s rate. The resulting voltammogram is given in Figure 4.9.
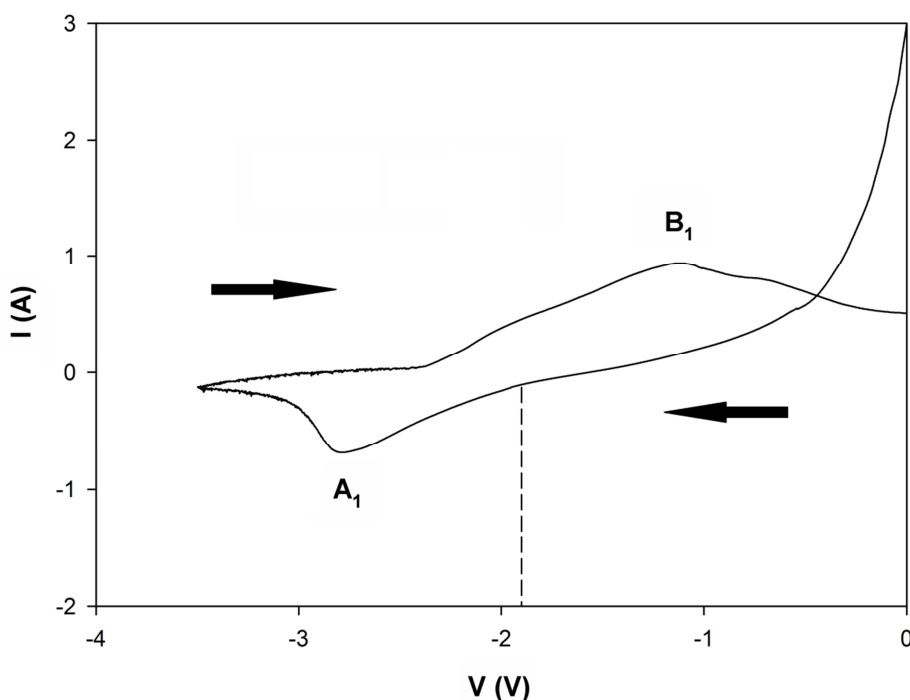
Figure 4.9: CV result between the CaWO$_4$ pellet and the graphite rod. Scan rate; 20 mV/s; scan range: 0 to -3.5 V, temperature; 600°C and electrolyte; eutectic CaCl$_2$-NaCl solution. The arrows indicate the scan directions. Reproduced from [42] by the license obtained from Springer.

The CV recorded showed that only non-faradaic currents flow until about -1.90 V. At this value, the current starts to increase, indicating that the applied potential is approaching the reduction potential, and forms a reduction peak A$_1$ at about -2.81 V. Therefore, from the midpoint of the onset and the peak potentials [48], -2.36 V was calculated as the reduction potential which can be

seen in Figure 4.9. Since the CV was recorded with the two electrode cell, overvoltages and voltage drops due to resistances are also included within this value. The resistance of the electrolyte was previously calculated as 0.35 Ω from Figure 4.7. For the Kanthal (N 80) wires used in the cathode and the anode assemblies, the total resistance was calculated as 0.12 Ω at $600^{o}C$ by using the data given in the literature [49]. Since the resistance of the graphite rod is very small, and the potentiostat excluded the voltage drops along its connections, the overall resistance of the cell was expected to be around 0.47 Ω. Using 0.34 A current value at -2.36 V, the voltage drop caused by the resistance of the cell can be calculated as 0.16 V. When the voltage drop due to resistance of the cell was excluded, a potential difference of -2.20 V was obtained. Consequently, this voltammogram can be considered to be in accordance with the results obtained from the constant potential study which pointed out about 2.22 V potential differences at zero current. Upon reversing the potential scan, the CV showed no reaction until -2.4 V. At this value, the current started to increase and formed an oxidation current peak B_1 at about -1.2 V.

To minimize the influence of overpotentials and potential drops due to cell resistance, cyclic voltammetry experiments with three electrodes were performed. Cyclic voltammogram with the three electrode system recorded on a Kanthal wire without the $CaWO_4$ pellet is given in Figure 4.10. The potential between Kanthal wire and the reference tungsten electrode was scanned in the 0 to -3 V range, at a rate of 20 mV/s. It is clearly seen that current values increased nearly linear with the increase in potential and followed more or less the same path upon reversal of the potential. This behavior indicates the stability of Kanthal lead wire in the cell used to make CV measurements. Therefore, the peaks observed in CV scans of Kanthal wire holding the pellet can directly be attributed to reactions of the $CaWO_4$ pellet.
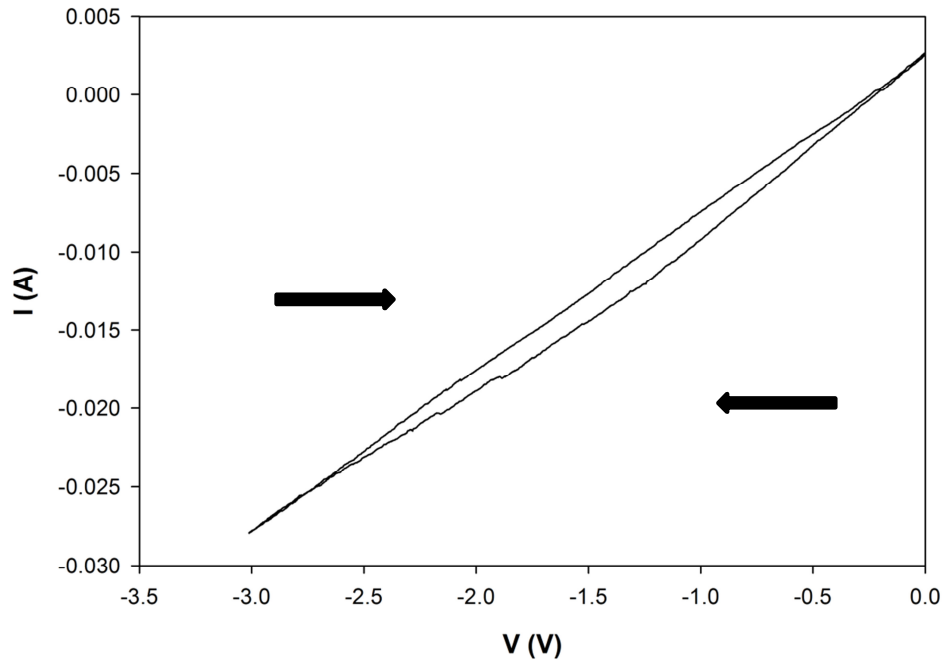

Figure 4.10: CV result between the Kanthal wire without the CaWO$_4$ pellet and tungsten wire reference electrode. Scan rate; 20 mV/s; scan range: 0 to -3.5 V, temperature; 600°C and electrolyte; eutectic CaCl$_2$-NaCl solution. The arrows indicate the scan directions.

In Figure 4.11, the CV result, recorded on an assembled electrode of $CaWO_4$ attached to a Kanthal wire versus tungsten reference electrode; between 0 to -1.5 V was presented. The result of CV performed between the graphite rod and the tungsten wire reference in the 0 to 1.5 V range is given in Figure 4.12. Again, using the midpoints of the of the onset and peak potentials [48], a potential value of -0.3 V from Figure 4.11 and 0.8 V from Figure 4.12 were calculated. Therefore, the difference between the cathode and the anode electrode potentials is about -1.1 V.

An approach that can be used to test the results obtained from the cyclic voltammetry and constant voltage electrochemical reduction experiments is to carry constant current electrochemical reduction experiments. For this purpose, an experiment was performed at 0.1 A and observed potential values were recorded as a function of time. The related voltage-time graph is given in Figure 4.13. Similarly, rapid increase of the voltage values is most likely due to the resistance of the pellet, which becomes more important as reduction proceeds. It is clear that subtraction of E_{pellet}, $E_{electrolyte}$ and $E_{electrical\ connections}$ from the observed potential $E_{observed}$, should give $E_{reaction}+\eta$ value. Table 4.4 was obtained when the observed potential values corresponding to the passage of 0.0052 Faradays (about 10% theoretical reduction) and 0.035 Faradays (about 68% theoretical reduction) were used. As it can be seen from Table 4.4, subtraction of $E_{electrical\ connections}$, E_{pellet} and $E_{electrolyte}$ from $E_{observed}$, gave consistent $E_{reaction}+\eta$ values within the experimental error limits with the ones found by cyclic voltammetry and constant voltage electrochemical reduction experiments. In order to determine E_{pellet} and $E_{electrolyte}$, the resistance values obtained in constant voltage electrochemical reduction experiments were used and the resistance of the pellet was ignored for calculations at 10% theoretical reduction due to the reasons discussed above.

Figure 4.11: CV result between the $CaWO_4$ pellet and the tungsten wire reference electrode. Scan rate; 20 mv/s, temperature; 600°C, electrolyte; eutectic $CaCl_2$-NaCl molten salt solution and scan range; 0 to -1.5 V. The arrows indicate the scan directions. Reproduced from [42] by the license obtained from Springer.

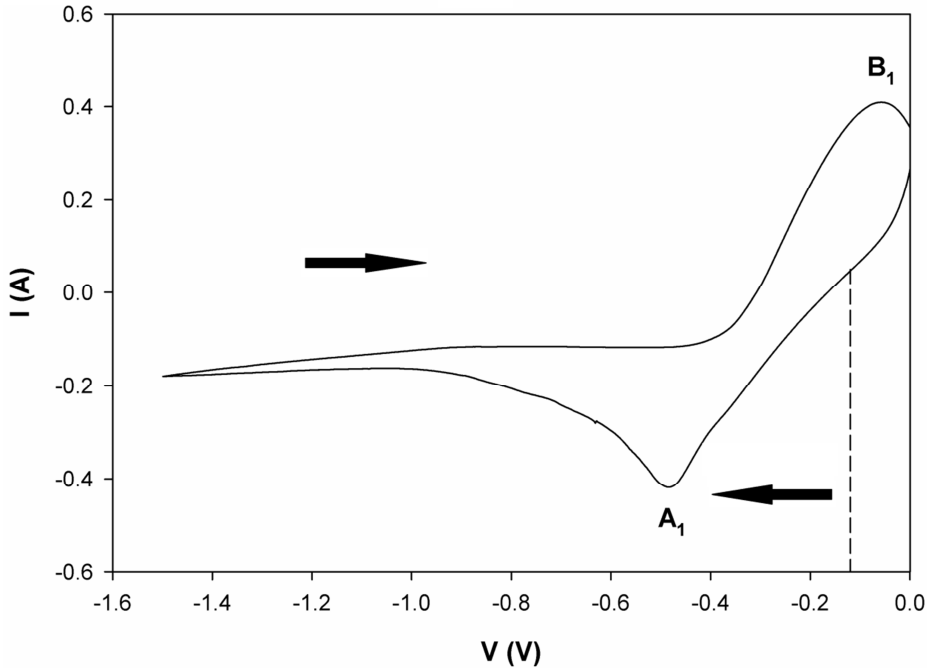**Figure 4.12: CV results between graphite rod and the tungsten wire reference electrode. Scan rate; 20 mv/s, temperature; 600°C, electrolyte; eutectic $CaCl_2$-NaCl molten salt solution, scan range; 0 to 1.5 V. The arrows indicate the scan directions. Reproduced from [42] by the license obtained from Springer.**
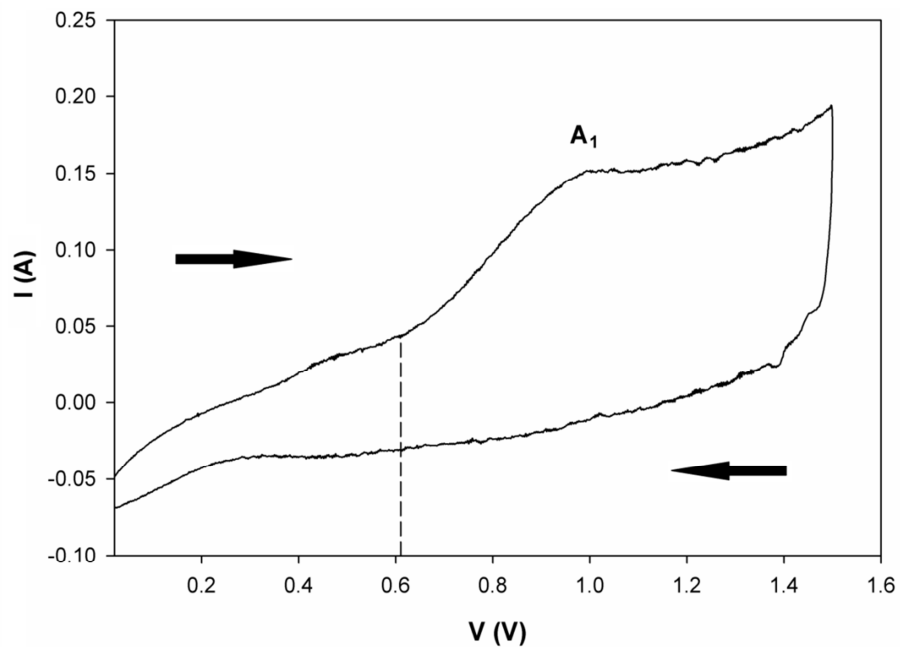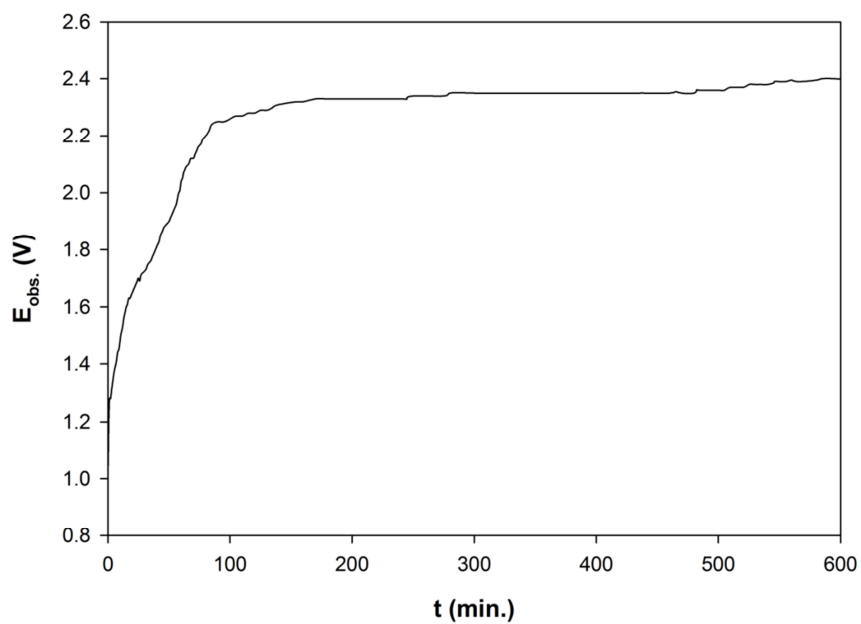

Figure 4.13: Observed potential values as a function of time at 0.1 A constant current.
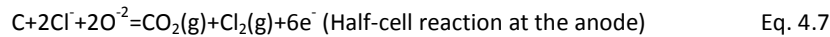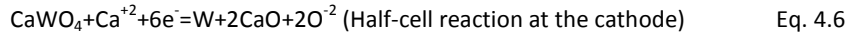
Table 4.4: $E_{reaction}+\eta$ values obtained when 0.0052 and 0.035 Faradays of electrical charge passed.

Q (F)	$E_{observed}$ (V)	$E_{electrical\ connections}$ (V)	$E_{electrolyte}$ (V)	E_{pellet} (V)	$E_{reaction}+\eta$ (V)
0.0052	2.23	0.030	0.035	0	2.17
0.035	2.39	0.030	0.035	0.057	2.27

In the reduction experiments, a significant amount of Cl_2 release was detected from the specific odor of the gas in spite of the fact that the applied potentials were low for $CaCl_2$ and/or NaCl decomposition. Furthermore, presence of $CaCO_3$ in the X-ray diffraction results of the reduced specimens [31, 35] could only be explained by the evolution of CO_2 at the anode. Therefore, it has been thought that, among the whole reactions that can occur in the molten salt, the ones having CO_2 and Cl_2 as the anodic products are most likely to occur during electrolysis. Also, presence of $CaCO_3$ and $Ca(OH)_2$, after treating the samples with water, can be explained by the reactions which produce Ca and/or CaO in addition to tungsten. Furthermore, there is no indication that the reaction mechanism involves more than one step. Cyclic voltammetry tests (see Figure 4.9 and Figure 4.11) and X-ray diffraction results of partially reduced samples [4, 35] did not show the presence of any intermediate compounds. Finally, half-cell potentials obtained by cyclic voltammetry tests (see Figure 4.11 and Figure 4.12), which excluded the IR drop and polarizations, pointed out about 1.1 V for the potential requirement of the reduction reaction. Due to the voltage drops in cyclic voltammetry experiments with three electrodes as a result of the uncompensated resistance (UR) coming from the solution and the resistance of the working electrode, reversible potential of the reduction reaction to be suggested could be somewhat more positive than -1.1 V, but it cannot be more negative than this value. Based on these observations, among all the possible reactions that can occur in the present system, the following reaction could be suggested:

$$CaWO_4(s) + C(s) + CaCl_2(l) = W(s) + 2CaO(s) + CO_2(g) + Cl_2(g) \quad E^o = -0.85\ V\ [32, 33] \quad \text{Eq. 4.5}$$
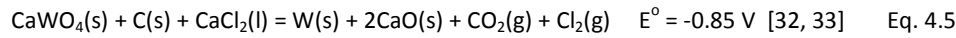
Potential requirement of the above reaction will get 40 mV closer to 1.1 V when the activity of $CaCl_2$ ($\approx$0.35) in eutectic $NaCl$-$CaCl_2$ molten salt solution is also considered [50]. The electrode reactions of the $CaWO_4$ pellet and graphite can be expressed by the following:

$$CaWO_4 + Ca^{+2} + 6e^- = W + 2CaO + 2O^{-2} \text{ (Half-cell reaction at the cathode)} \quad \text{Eq. 4.6}$$

$$C + 2Cl^- + 2O^{-2} = CO_2(g) + Cl_2(g) + 6e^- \text{ (Half-cell reaction at the anode)} \quad \text{Eq. 4.7}$$

From this discussion, it can be deduced that there are high overpotentials when 2.2 V measured cell potential between $CaWO_4$ cathode and graphite anode is compared with the theoretical reduction potential of Eq. 4.5. This was also supported by the cell potential calculated from the results of CV's recorded between cathode-reference and anode-reference cells given in Figure 4.11 and Figure 4.12. About 1.35 V difference was thought to be mainly caused by the CO_2 overpotential on graphite anode. There are not sufficient data in the literature about the value of this overpotential especially at low temperatures.

4.3 Effects of Voltage, Temperature and the Length of Kanthal Wire Winding on the Reduction Rate of CaWO$_4$

An experimental procedure was designed to examine the effects of temperature (T), applied voltage (E), and the length of Kanthal wire winding (L$_w$) on the reduction rate of CaWO$_4$ in the cell used for constant potential reduction experiments. The minimum and the maximum values of three process parameters were determined prior to experimental design. The parameters and their limits are given in Table 4.5. Kanthal wire winding of the pellets were reported to increase the reduction rate of SiO$_2$ in a similar process [23]. The wire used had 0.15 mm diameter and winded onto the pellets as shown in Figure 4.14. As L$_w$, the length of the wire which was in contact with CaWO$_4$ pellet was taken.

Table 4.5: Selected parameters and their limits.

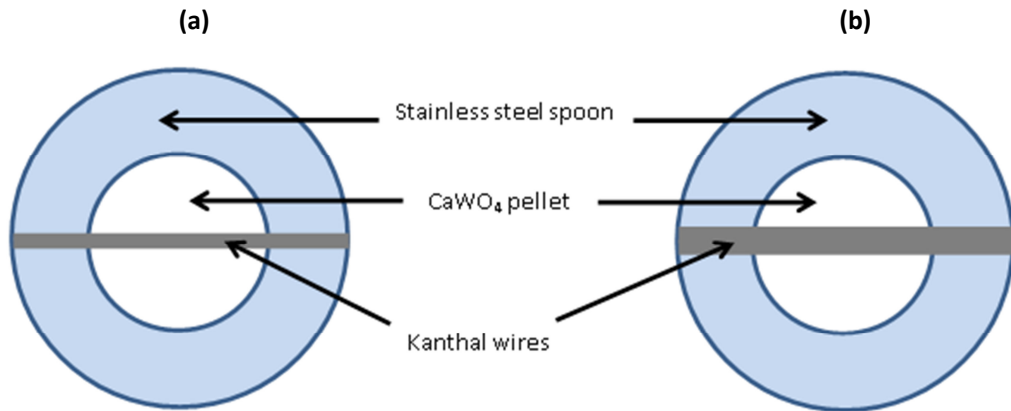| Parameter	Minimum (0)	Maximum (1)
E (V)	2.6 (0)	3.2 (1)
T (^{o}C)	575 (0)	675 (1)
L$_w$ (cm)	0 (0)	20 (1)

Figure 4.14: Top views of the cathodes used in the electrolysis experiments where Kanthal wire winding was (a) 10 cm and (b) 20 cm.

The experimental conditions determined according to the design are given in Figure 4.15. The levels of the parameters (within predetermined limits, 0 for minimum and 1 for maximum) and their combinations were chosen so as to represent a coordinate point in an equilateral triangle. Absolute values of the parameters, corresponding to the points shown in Figure 4.15 and conditions for all of the experiments are given in Table 4.6.

The currents passing through the cell were recorded as a function of time during each experiment. The current vs. time graph recorded in Experiment 9, which represents the typical shape of the curve for all experiments, is given in Figure 4.16. All the remaining current vs. time and total charge vs. time graphs are given in Figure 4.17 and Figure 4.18, respectively. Total charge vs. time graphs were plotted to show results more clearly and associate measured current values with theoretical amount of reduction. Accumulative total charge, Q, passed through the cell can be calculated from the following equation when 100% current efficiency is assumed:

$$Q = \int_{t=0}^{t} I \, dt = \frac{WnF}{M}$$ Eq. 4.8

where, W is the theoretical amount of reduction, n is the number of electrons involved in the reaction, F is the Faraday's constant and M is the molecular weight of $CaWO_4$. It can be calculated from Eq. 4.8 that, 5026 coulombs of electrical charge is required for complete theoretical reduction of 2.5 g of $CaWO_4$.

3-D contour plots of T-L_w-E were constructed for currents in amperes in Figure 4.19. The values in this figure are currents passing through the cell at the time when 2513 Coulombs of accumulative charge was passed. This corresponds to the instance when nearly 50% theoretical reductions of pellets took place under the conditions indicated by the coordinates of points in the triangle.

3-D contour plots of T-L_w-E for the time, in minutes, it took to pass 5025 Coulombs of accumulative charge through the cell is given in Figure 4.20. From above information, it can be seen that values given in this figure, corresponds to the time in minutes for theoretical complete reductions of pellets under the conditions indicated by the coordinates of points in the triangle.

From the examination of Figure 4.19 and Figure 4.20, it can be seen that temperature and applied voltage are the dominant parameters. When Kanthal wire winding was introduced, either voltage or temperature or both should decrease in order to place the coordinate into the triangle. As a result, although Kanthal wire winding seems to have no positive influence on the reduction rate, it could be due to the negative effect of the decrease of other parameters. Therefore, the optimum reduction parameters for the fastest reduction were determined as; $640^{\circ}C$ and 2.81 V without Kanthal wire winding.
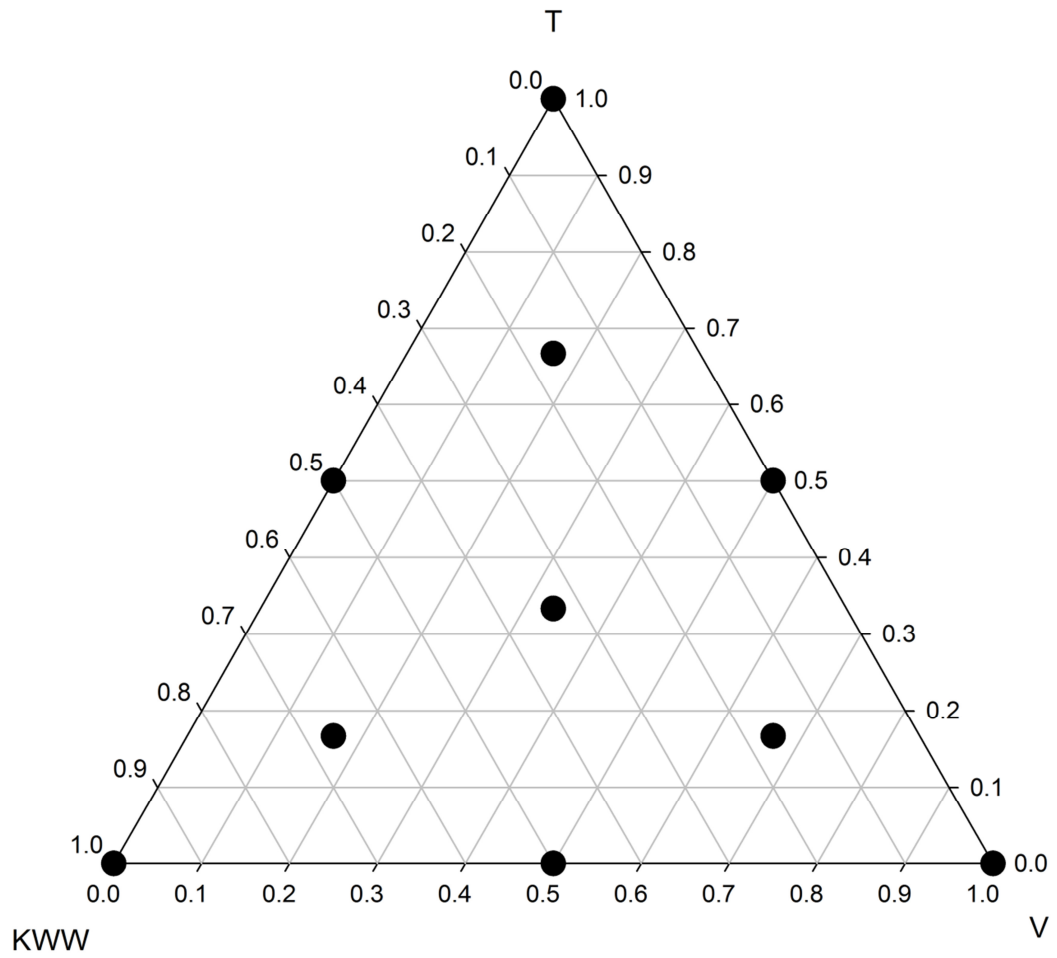
Figure 4.15: Experimental design created for three parameters and three levels. The levels of the parameters (within predetermined limits) and their combinations were chosen so as to represent a coordinate point in an equilateral triangle.

Table 4.6: Absolute values of the parameters, corresponding to the points shown in Figure 4.15 and conditions for all of the experiments

Exp. No:	T	Lw	V
1	0.5 (625°C)	0 (0 cm)	0.5 (2.9 V)
2	0 (575°C)	0 (0 cm)	1 (3.2 V)
3	0.5 (625°C)	0.5 (10 cm)	0 (2.6 V)
4	0 (575°C)	0.5 (10 cm)	0.5 (2.9 V
5	1 (675°C)	0 (0 cm)	0 (2.6 V)
6	0 (575°C)	1 (20 cm)	0 (2.6 V)
7	0.167 (592°C)	0.167 (3.34 cm)	0.667 (3 V)
8	0.667 (642°C)	0.167 (3.34 cm)	0.167 (2.7 V)
9	0.333 (608°C)	0.333 (6.66 cm)	0.333 (2.8 V)
10	0.167 (592°C)	0.667 (13.34 cm)	0.167 (2.7 V)
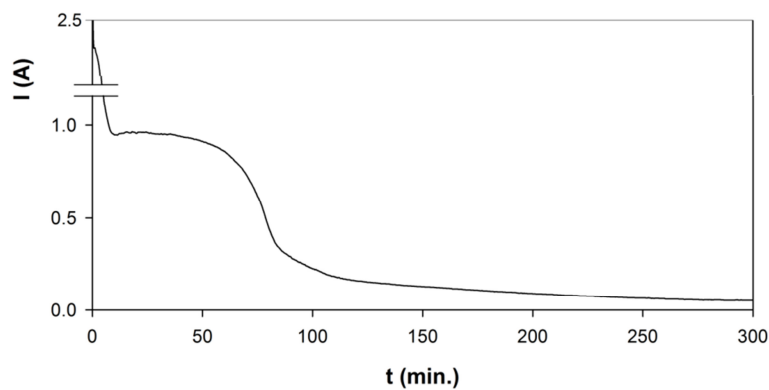
Figure 4.16: I-t graph recorded during Experiment 9; T: 608 °C, L_w: 6.66 cm, E: 2.8 V
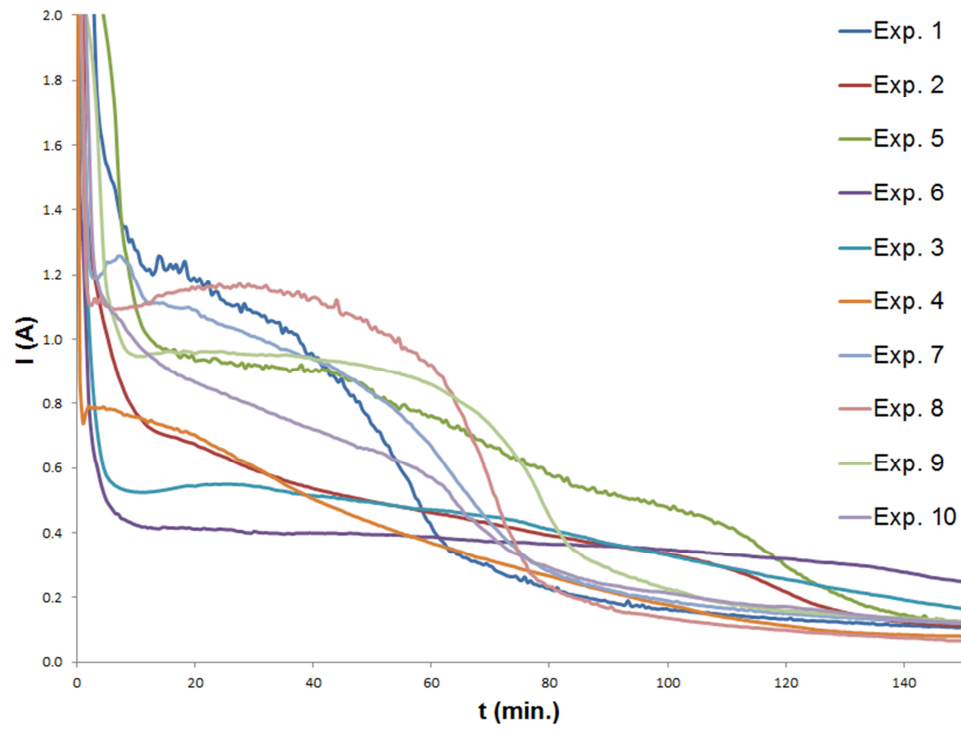
Figure 4.17: I vs. t graphs of all experiments done according to the Experimental design given in Table 4.6.
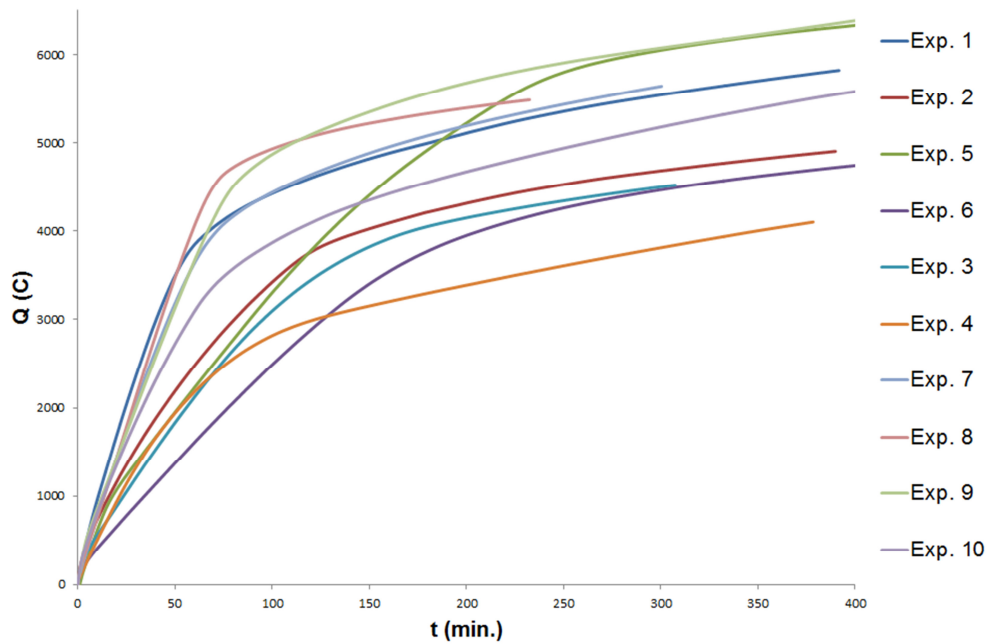
Figure 4.18: Q vs.t graphs of all experiments conducted according to the experimental design given in Table 4.6.
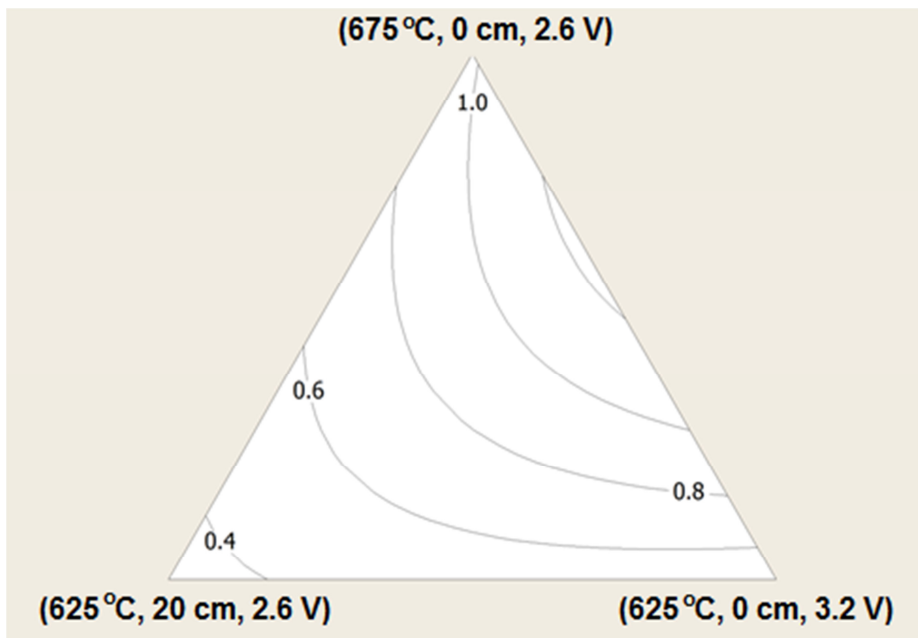
Figure 4.19: 3-D contour plot of the variables T-L_w-E for currents in amperes at the time when 2513 Coulombs of accumulative charge was passed. This corresponds to the instance when about 50% theoretical reductions of pellets took place.
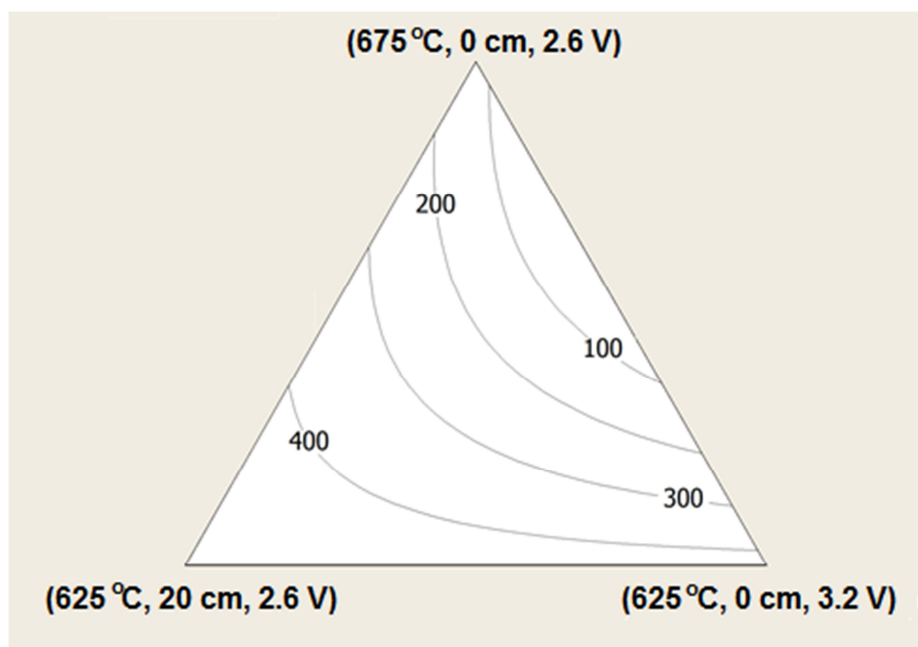
Figure 4.20: 3-D contour plot of the variables T-L_w-E for the time, in minutes, it took to pass 5025 Coulombs of accumulative charge through the cell, corresponding to complete theoretical reductions. Some of the values for complete reductions were obtained by extrapolation of the related I-t graphs.

4.4 Large Scale Tungsten Production Tests

It was seen that, presence of Na (see Figure 3.15) caused to form bubbles while introducing $CaWO_4$ to the electrolyte at 600^oC. For this reason, the powder was cleaned with 0.1 M HCl solution prior to experiments and dried in an oven at 200^oC for 12 hours. The EDX analysis result after HCl treatment, which shows Na was completely removed, can be seen in Figure 4.21. As received $CaWO_4$ was used ın the first test given below, but cleaned powder was used in other experiments.

In the first test, about 21.6 kg of salt mixture consisting of 11.65 kg $CaCl_2$ and 6.14 kg NaCl (balance H_2O) was placed into the bath so as to provide 8 cm electrolyte depth. This constitution corresponds to the eutectic composition and results in a salt solution which melts at 504^oC. The $CaCl_2$ salt contained 2 moles of H_2O per mole; therefore, 15.46 kg of $CaCl_2.2H_2O$ was at the used beginning. The $CaCl_2$ was dehydrated after 3.81 kg of H_2O was removed during heating. The $CaWO_4$ powder, weighing 1 kg, was placed onto the stainless steel cathode tray and immersed into the electrolyte, when the temperature reached the target temperature of 600^oC. Upon immersing the cathode, it was observed that the molten salt started to form bubbles and the powder was dispersed in the electrolyte. The graphite rod was also immersed into the electrolyte and the process was initiated by application of a potential difference of 2.8 V between the cathode and the anode. The experiment was carried on for about 18 hours. The applied potential during the process was altered time to time, but it did not exceed 3.2 V.

After the experiment, the reduced sample was taken out from the vessel within the tray. This shows that the $CaWO_4$ powder probably settled down on the tray after a certain period of time. Produced powder was washed with tap water to remove the solidified salt around it so that it could be taken out of the tray. It was then cleaned by 30 liters of a 0.2 M HCl solution for 30 minutes and pulp was formed. The pulp was filtered by a box filter under vacuum and dried to obtain the reduced powder. The XRD result of the powder is given in Figure 4.22. It can be seen in this figure that tungsten could be produced but the reduction was incomplete. Presence of small amount of $Ca(OH)_2$ was probably because of the incomplete leaching by HCl. Optimization of cleaning process for reduced product was performed in small scale but was not adapted to larger volumes in this study.

In addition to incomplete reduction of $CaWO_4$, there were other problems related to the materials used in the construction of the cell. After the experiment, it was seen that commercially available AISI 306 stainless steel parts, purchased from shops selling kitchenware were deteriorated because of the very corrosive environment constituted by high temperature, molten salts and gaseous electrolysis products. The photographs of the vessel and the cathode tray after the experiment are given in Figure 4.23. As it can be seen, both the tray (a) and the vessel (b) were heavily corroded and they were not used for subsequent runs.

The other problem was the oxidation of graphite anode inside the furnace above the electrolyte level. The slow rate of electrochemical reduction could not produce large volume of CO_2 to build enough positive pressure inside the cell to stop penetration of air into the system. As it can be seen from the photograph of the graphite rod after electrolysis given in Figure 4.24, air penetrated through open spaces present especially around the hole where graphite electrode was introduced into the system.
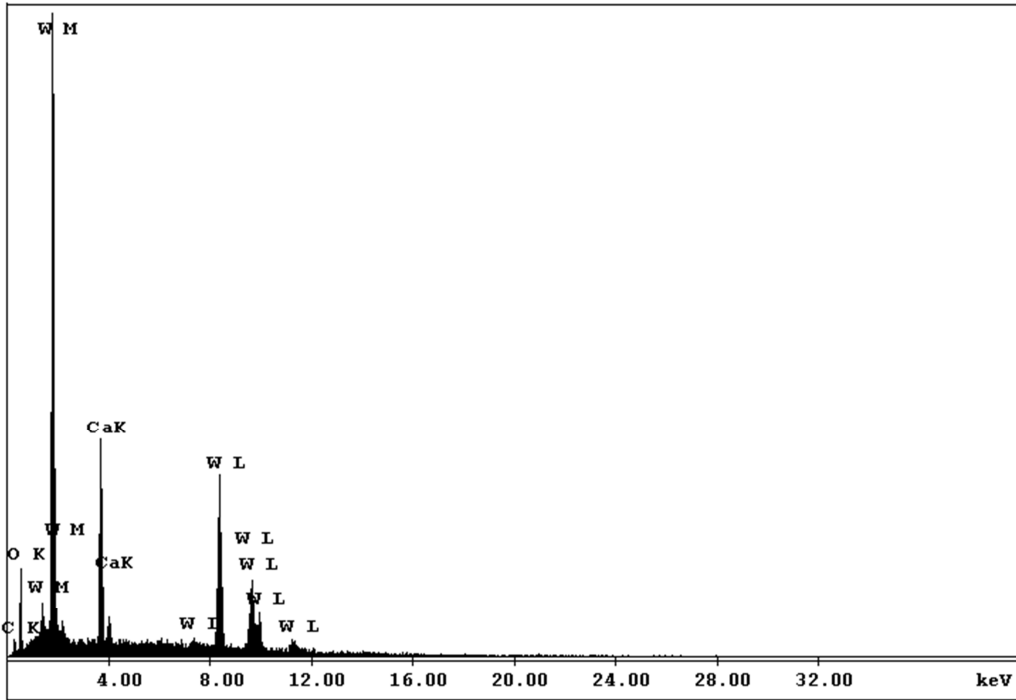
```
EDAX ZAF Quantification (Standardless)
Element Normalized
SEC Table : Default

Element   Wt %    At %    K-Ratio    Z        A        F
   C K     6.56   21.37   0.0163   1.1591   0.2148   1.0003
   O K    21.71   53.07   0.0352   1.1424   0.1419   1.0000
   CaK    13.51   13.18   0.0775   1.1108   0.5140   1.0052
   W L    58.21   12.38   0.5160   0.8429   1.0515   1.0000
   Total 100.00  100.00

Element   Net Inte.    Bkgd Inte.   Inte. Error     P/B
   C K      15.11         4.10         9.76         3.68
   O K      89.82         6.62         3.45        13.56
   CaK     370.92        26.86         1.70        13.81
   W L     392.84        28.07         1.65        13.99
```

Figure 4.21: EDX analysis of the CaWO$_4$ (Noah, 18418) powder after 0.1 M HCl treatment.

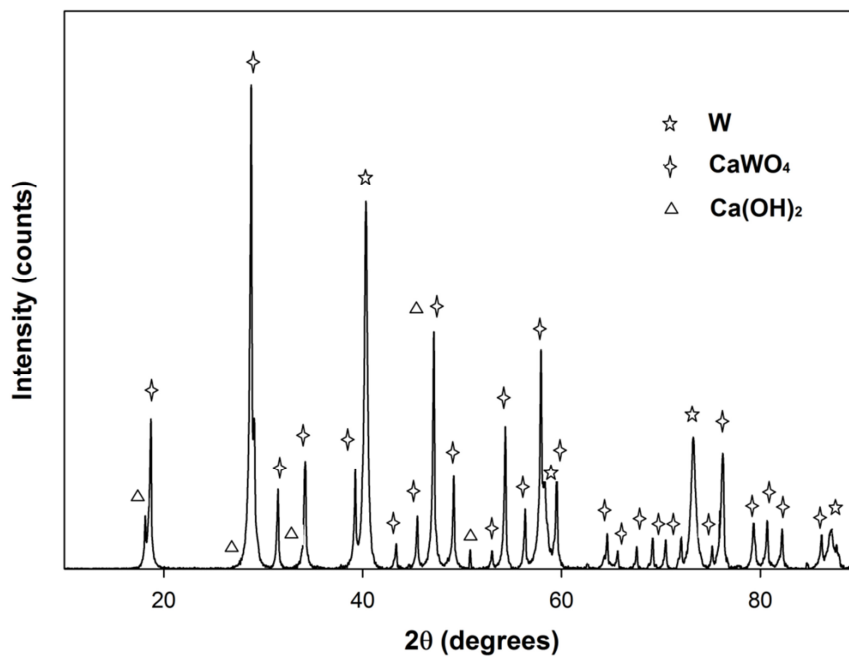**Figure 4.22: The XRD result of the sample from the preliminary test after HCl cleaning.**

(a)   (b)

Figure 4.23: Photographs of the (a) cathode tray and (b) the vessel after 18 hours of electrolysis.

Figure 4.24: Photograph of the graphite rod after electrolysis in the preliminary large scale test.

In the light of above findings, the setup was redesigned to overcome the problems encountered in the first production test. First of all, the stainless steel parts were manufactured specifically for this purpose from 4 mm thick AISI 316 Ti steel. Secondly, the impermeability of the reactor was improved to prevent penetration of oxygen into the furnace and a continuous flow of nitrogen gas at a rate of 800 cc/min was provided during the reduction process. Thirdly, the bubble formation in the molten salt mixture upon immersion of $CaWO_4$ was believed to be caused by the evaporation of H_2O which the $CaWO_4$ powder contained. Therefore it was dried at $200^{o}C$ in a drying oven for 12 hours prior to introduction into the cell for electrolysis. It was seen that the $CaWO_4$ powder contained approximately 1 wt. % H_2O which was removed by drying.

After the electrolysis experiments, it was observed that the new materials used in the construction of cell vessel and cathode tray had adequate resistance to the environment formed inside the furnace and suitable for the present process. Therefore, it was possible to use them in subsequent runs. Furthermore with the improvements in the setup, oxidation of graphite was considerably reduced. However, despite all the modifications made on the electrodes and electrolysis system, complete reduction could not be achieved with 1 kg $CaWO_4$ powder and 8 cm electrolyte depth. It was thought that, the reason for incomplete reduction could be the lower weight ratio of $CaCl_2$-NaCl molten salt electrolyte to $CaWO_4$ when compared to laboratory experiments because rate of electrochemical reduction is proportional to oxygen solubility of the electrolyte as observed from different salt compositions used in laboratory tests [22, 51, 52]. From this point of view, in the following experiments, the depth of the electrolyte was fixed at 5 cm and $CaWO_4$ amount was varied so as to provide weight ratios of 10, 20 and 30 between the electrolyte and $CaWO_4$. The constitutions of reduced samples are compared in Figure 4.25. All the reduced samples were cleaned by 30 liters of a 0.2 M HCl solution for 30 minutes.

(a)

(b)

61

(c)
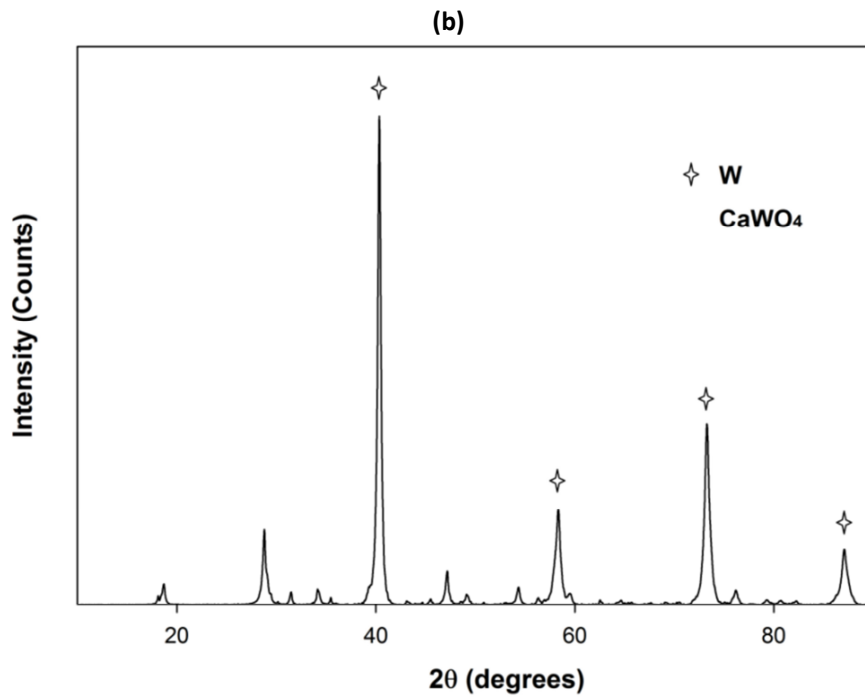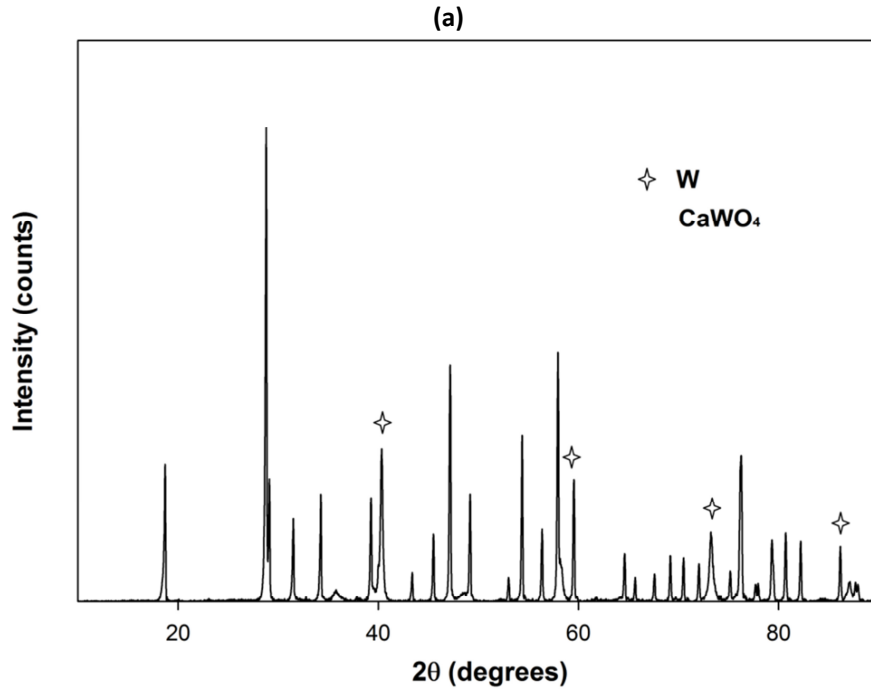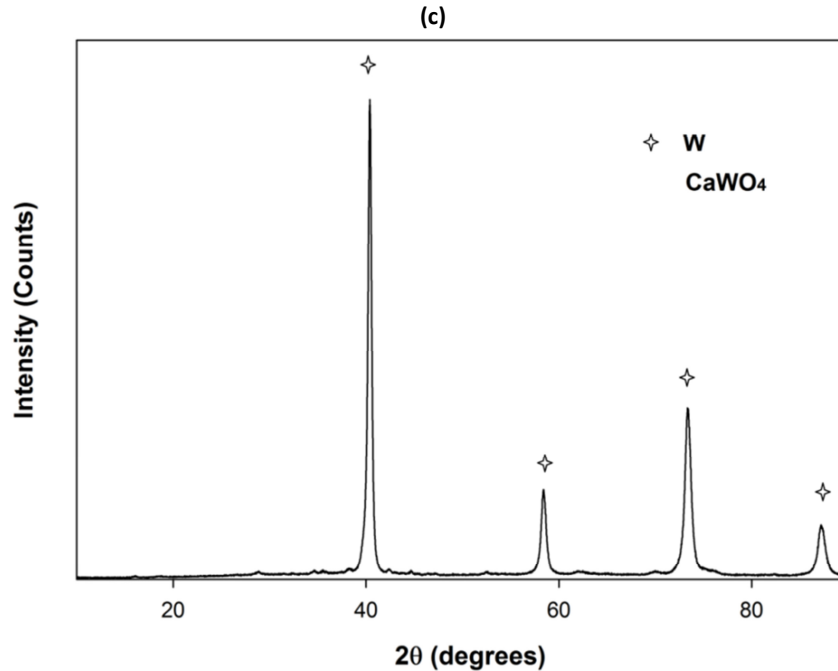
Figure 4.25: X-ray diffraction results of the reduced samples after HCl cleaning procedure when weight ratio of the electrolyte to $CaWO_4$ was (a) 10 (b) 20 and (c) 30. Only tungsten peaks were marked, all the remaining unmarked peaks belong to $CaWO_4$.

As it can be seen in Figure 4.25, less $CaWO_4$ was left as the weight ratio of the $CaCl_2$-NaCl electrolyte to $CaWO_4$ got closer to the laboratory scale experiments in which 2.5 grams of $CaWO_4$ was reduced in 100 grams of electrolyte.

4.5 Investigation of the HCl Cleaning Process of the Reduced Samples

The reduction product of $CaWO_4$ inevitably contains some calcium compounds. These compounds can be $Ca(OH)_2$ and/or $CaCO_3$ which are produced as byproducts during reduction and $CaWO_4$ which may be left unreduced. Normally, the reduction was completed when small samples (2.5 g) were used in experiments. But presence of unreduced $CaWO_4$ were found in the reduced samples of large scale tests. Cleaning process was performed by using a stock obtained from large scale tests to observe calcium removal. From mass balance considerations, about 26 % of Ca was taught to be originated from $CaWO_4$ reduction and remaining Ca from other sources. Since it is easier to remove Ca compounds coming from byproducts of reduction reaction, attention was placed more on their removal. As mentioned previously, a dilute HCl solution treatment could be used to isolate tungsten from the undesired Ca compounds. A series of experiments were conducted according to full factorial experiment design (see Table 3.1) to analyze the effects of acid concentration, temperature and time on the removal of Ca from the reduced tungsten powder. Ca contents of the HCl treated samples were determined after each experiment by XRF analyses. The results are given in Table 4.7 together with the experimental conditions which were suggested by full factorial experiment design.

Table 4.7: Ca contents of the as reduced and HCl treated samples.

Exp. No	T (^{o}C)	C (M)	t (min.)	Ca (%)
As reduced powder (stock)				33.4
1	55	0.2	60	6.5
2	55	0.4	120	2.1
3	40	0.2	60	6.7
4	55	0.1	60	18.1
5	25	0.4	30	10.2
6	55	0.2	30	7.1
7	40	0.2	120	5.0
8	55	0.4	60	2.6
9	40	0.4	120	3.2
10	25	0.2	30	16.4
11	55	0.1	30	13.7
12	55	0.2	120	5.3
13	40	0.1	120	18.7
14	40	0.4	30	3.6
15	25	0.1	30	26.6
16	25	0.2	120	8.5
17	55	0.1	120	17.0
18	25	0.2	60	9.3
19	25	0.1	120	26.3
20	40	0.2	30	8.2
21	25	0.4	120	3.2
22	25	0.4	60	5.2
23	25	0.1	60	26.3
24	40	0.1	30	25.7
25	40	0.1	60	24.4
26	40	0.4	60	3.4
27	55	0.4	30	3.0

The graphs presented in Figure 4.26 represent the main effects of the parameters on the Ca content of the HCl solution treated samples. As expected, weight percent of Ca in the samples decrease with increase in acid concentration, temperature and exposure time. The decrease got slower from level 2 to level 3 for concentration and time. However, this was not the case for temperature which was probably because more $CaWO_4$ was dissolved at higher temperatures. Binary interactions of the parameters are given in Figure 4.27.
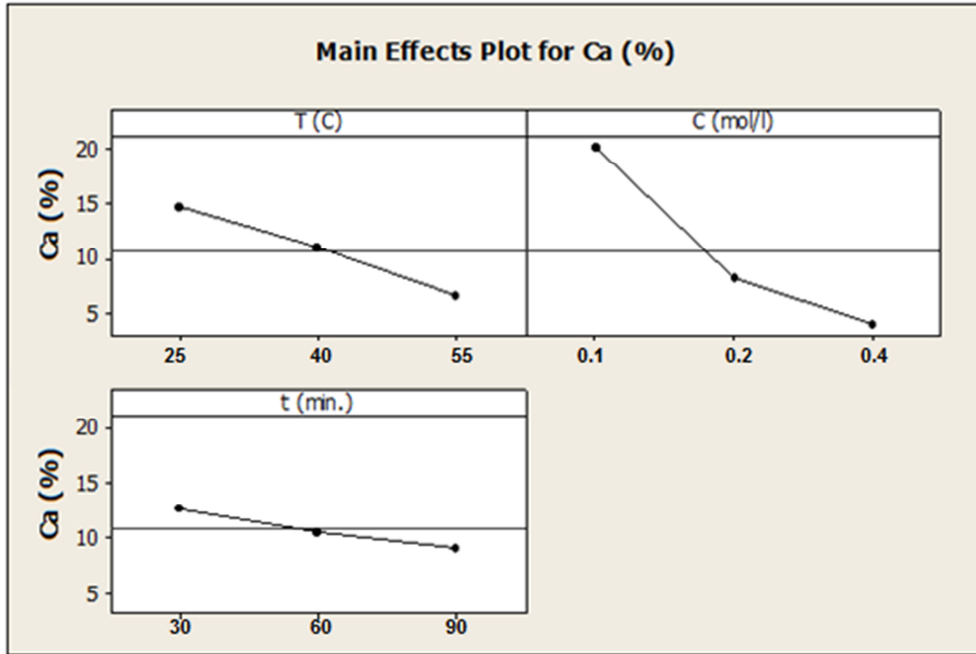
Figure 4.26: Main effects of the parameters on the Ca content of the HCl solution treated samples.

The regression equation to estimate Ca content of the reduced sample for different values of the selected parameters within the predetermined levels is given in Eq. 4.9. In Eq. 4.9, Ca (%) can be calculated for any parameter combination by giving numbers between 1 and 3 to the parameters T, C and t; where, numbers between 1 and 3 correspond to the levels determined prior to the experiments as shown in **Error! Not a valid bookmark self-reference.**. Values of the parameters corresponding to levels between 1 and 3 can be calculated by simple proportioning.

$$Ca\ (\%) = 38.5 - 3.99\ T - 8.06\ C - 1.80\ t \qquad \text{Eq. 4.9}$$

Table 4.8: Absolute values of the parameter levels which were denoted as 1, 2 and 3.

Levels	1	2	3
T (^{o}C)	25	40	55
C (M)	0.1	0.2	0.4
t (min.)	30	60	120
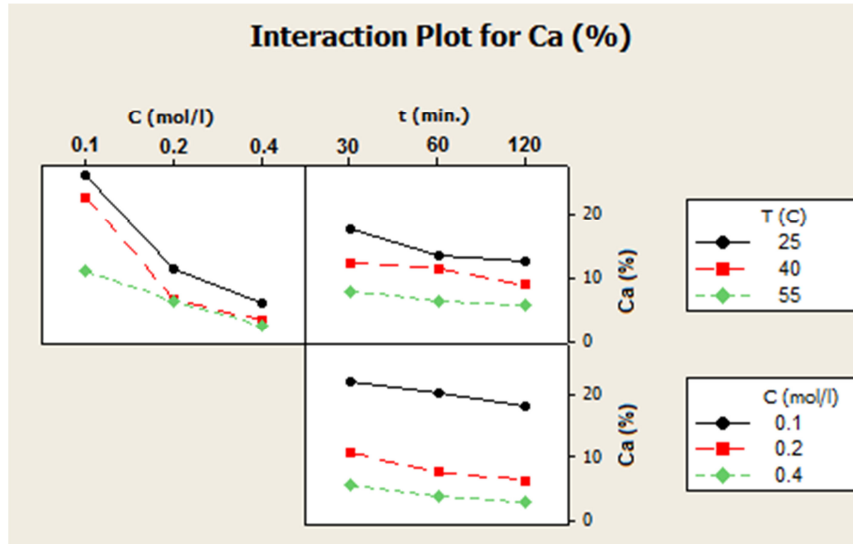
Figure 4.27: Binary interactions of the selected parameters in HCl cleaning treatment.

4.6 Tungsten Production Tests From Uludağ Scheelite Mineral

As it was stated previously, the new tungsten production technique introduced recently [5-7], has the potential to be directly applied to scheelite concentrates. For this purpose, rich and flotation concentrates obtained from Uludağ Etibank Volfram Plant, which aborted its production in 1989, were used. The compositions of the concentrates were already given in Table 2.5. As it can be seen in Table 2.5, both concentrates have similar ingredients. However, flotation concentrate contains a very high amount of $CaCO_3$ (45-50 %) when compared to that of rich concentrate (1-2 %).

Pellets having 2.5 g in weight were prepared from both concentrates according to the pellet preparation procedure given in section 3.1.1. Electrochemical reduction experiments were performed at 600°C at 2.8 V constant potential. The results are given in Figure 4.28 and Figure 4.29.

Figure 4.28: X-ray diffraction results of the electrochemical reduction experiments with Uludağ rich scheelite concentrate.

Figure 4.29: X-ray diffraction results of the electrochemical reduction experiments with Uludağ flotation scheelite concentrates.

As it can be seen in Figure 4.28 and Figure 4.29 tungsten could be produced by electrochemical reduction of both concentrates. Presence of metallic Fe, which can be seen in both figures, can be explained by the electrochemical reduct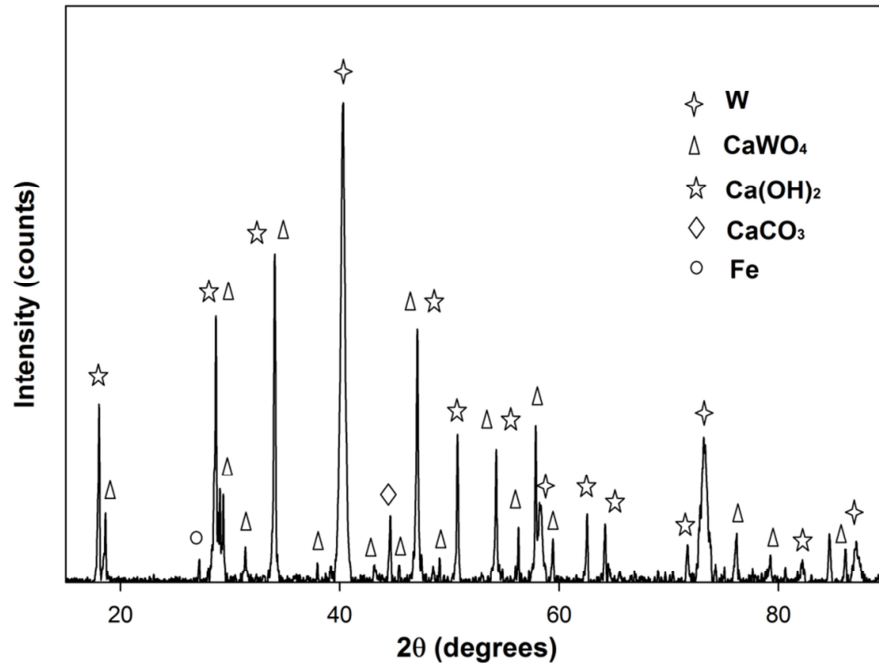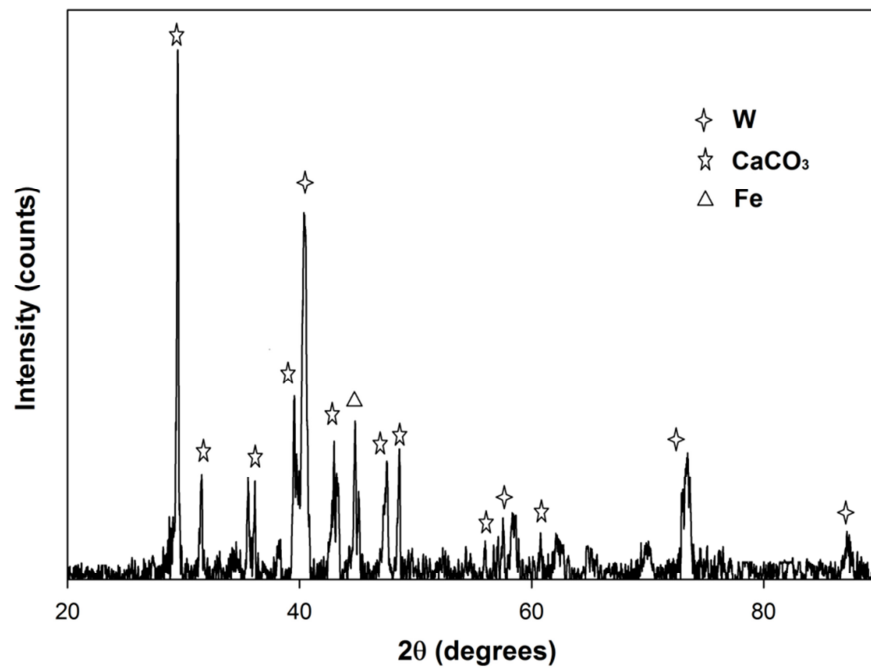ion of iron containing compounds (see Table 2.5) in the concentrates. $CaWO_4$ peaks seen in Figure 4.28, indicates incomplete reduction. Complete reduction can be achieved by increasing reduction time. Majority of $CaCO_3$ peaks seen in Figure 4.29 were originated from the flotation concentrate as can be seen in Table 2.5. $CaCO_3$ can completely be removed by dilute HCl solutions either before or after electrochemical reduction experiments.

4.7 A Model for the Electrochemical Reduction of $CaWO_4$ to W

A basic diffusion model in the electrolyte was developed to better understand the decrease in current values (see Figure 4.5) and incomplete reduction when weight ratio of electrolyte to input $CaWO_4$ exceeds a critical value (see Figure 4.25).

In the electrochemical reduction of $CaWO_4$, oxygen in $CaWO_4$ is ionized under the influence of the applied potential and diffuses through the molten salt to the anode. In other words, part of the current is carried by the oxygen ions in the electrolyte. In order to relate current to the movement of oxygen ions, the diffusion coefficient of oxygen in $CaCl_2$-NaCl eutectic solution should be calculated first.

As in other transport processes, movement of oxygen consists of hole formation which was followed by a particle jumping into the hole. When a particle jumps, another hole is created in its previous position. Therefore, instead of dealing with jumping particles, the transport process could be defined by the movement of holes [53]. The Stoke's law for the diffusion coefficient of holes is written as [53]:

$$D = \frac{kT}{6\pi(r_h)\gamma}$$

Eq. 4.10

where; k is Boltzmann constant, r_h is the radius of the hole and γ is the viscosity of the electrolyte. The viscosity, γ, of the $CaCl_2$-NaCl eutectic mixture was reported as 0.054 poise ($kg.m^{-1}.s^{-1}$) [47]. When a value of 128 pm [54] is used for the ionic radius of oxygen, diffusion coefficient of oxygen can be calculated as 9.25×10^{-5} $cm^2.s^{-1}$ from Eq. 4.10 at $600^{\circ}C$.

There is a thin layer (δ) at the reaction front where a concentration gradient of oxygen occurs during electrochemical reduction of $CaWO_4$ as can be seen in Figure 4.30. The current density, i, of the cell can be calculated within this thin layer as follows:

$$i = \frac{\Delta C \times D \times nF}{(1-t) \times \delta}$$

Eq. 4.11

where, ΔC is the concentration difference between the ends of the thin layer and t is the transference number. Concentration of oxygen at the reaction front can be taken as the saturation oxygen concentration of the molten salt, C_O^S, because oxygen ions will continuously be generated as a result of the reduction reaction. The oxygen concentration at the end of the thin layer at any time is represented by C_O^E.
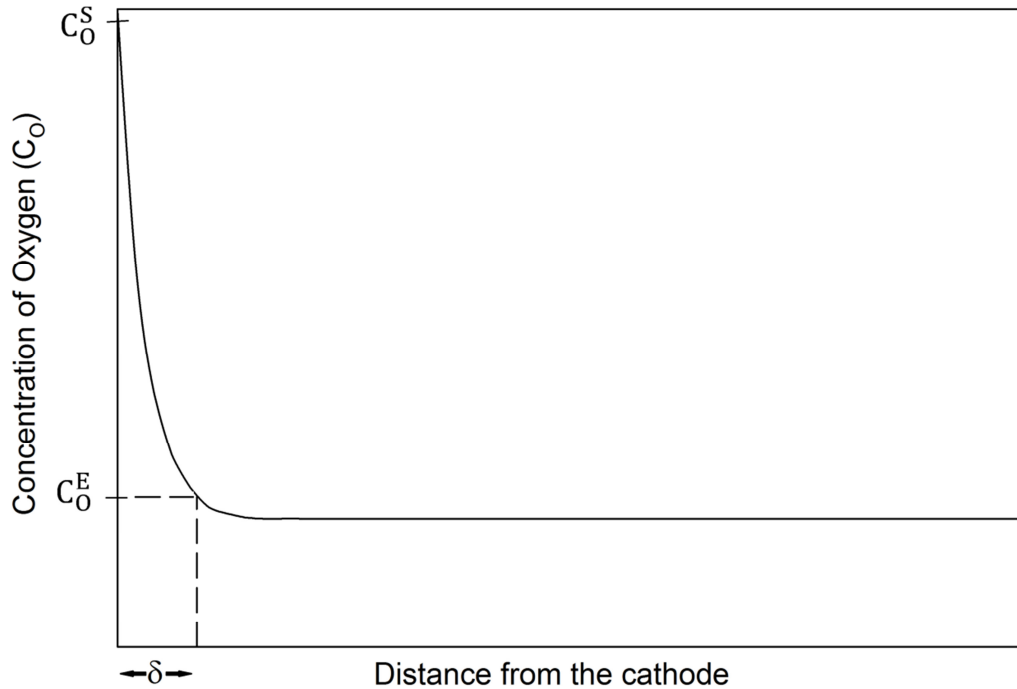
Figure 4.30: Schematic concentration profile of oxygen as a function of distance from the cathode.

In order to find the concentration gradient between the ends of the thin layer as a function of time, oxygen balance in the molten electrolyte was done as follows:

$$O\ (in)-O(out)=O(accumulation) \qquad\qquad \text{Eq. 4.12}$$

Eq. 4.12 can be rewritten as:

$$-D\frac{\partial C}{\partial x}A - O(out) = \frac{\partial C}{\partial t}V \qquad\qquad \text{Eq. 4.13}$$

Using thin film model and doing necessary simplifications, Eq. 4.14 can be obtained.

$$\frac{D}{\delta}(C_O^S - C_O^E - \frac{\delta O(out)}{DA}) = \frac{\partial C_O^E}{\partial t}l \qquad\qquad \text{Eq. 4.14}$$

where l represents the distance between anode and cathode. Rearrangement of the terms leads;

68

$$\int_{t=0}^{t} \frac{D}{\delta x l} dt = \int_{C_O^E = c_{O(initial)}^E}^{C_O^E} \frac{\partial C_O^E}{(C_O^S - C_O^E - \frac{\delta O(out)}{DA})}$$ Eq. 4.15

Integration yields:

$$-\frac{D}{\delta x l} t = \ln(C_O^S - C_O^E - \frac{\delta O(out)}{DA}) - \ln(C_O^S - C_{O(initial)}^E - \frac{\delta O(out)}{DA})$$ Eq. 4.16

Therefore, C_O^E can be calculated for any t value as follows:

$$C_O^E = -e^{\left(\ln\left(C_O^S - C_{O(initial)}^E - \frac{\delta O(out)}{DA}\right) - \frac{Dt}{\delta l}\right)} + C_O^S - \frac{\delta O(out)}{DA}$$ Eq. 4.17

Oxygen solubility of the eutectic $CaCl_2$-NaCl salt solution can be calculated as 9.9% mole from the ternary $CaCl_2$-NaCl-CaO system [55]. 100 grams eutectic $CaCl_2$-NaCl salt solution is nearly 47.3 cc and contains 1.18 moles $CaCl_2$ and NaCl. As a result, oxygen concentration of the electrolyte after saturation, C_O^S, can be calculated in moles.cm^{-3} as follows:

$$C_O^S = \frac{1.18 \times 9.92}{100 \times 47.3}$$ Eq. 4.18

Current values were calculated as a function of time by combining Eq. 4.11 and Eq. 4.17. The resulting I vs. t graphs obtained by the model for 2.5 V and 2.65 V and comparison with the experimental data are given in Figure 4.31 and Figure 4.32, respectively. $O(out)$ values in mol.s^{-1} were calculated by using the current values recorded at the plateau regions (0.2 A and 0.37 A), which can be seen in Figure 4.31 and Figure 4.32, according to the below formula, assuming 100% current efficiency:

$$O(out) = \frac{I}{6 x 96500} x2$$ Eq. 4.19

Values of constants used in the calculations are given in Table 4.9. Saturation concentration was calculated from Eq. 4.18 and about 88% saturation was used as the initial oxygen concentration to fit the model to experimental data. This indicates that, a high amount of dissolved CaO could be present in the electrolyte; nevertheless, the salts were dried carefully. The value, 0.05 cm, used as the film thickness is acceptable when compared to typical mass transfer processes in which values around 10^{-2} cm were reported [56, 57]. 0.5 was assumed as the transference number of oxygen. The experiments at 2.8 and 2.95 V were not used for comparison because of the absence of steady state in these experiments as can be seen in Figure 4.5.
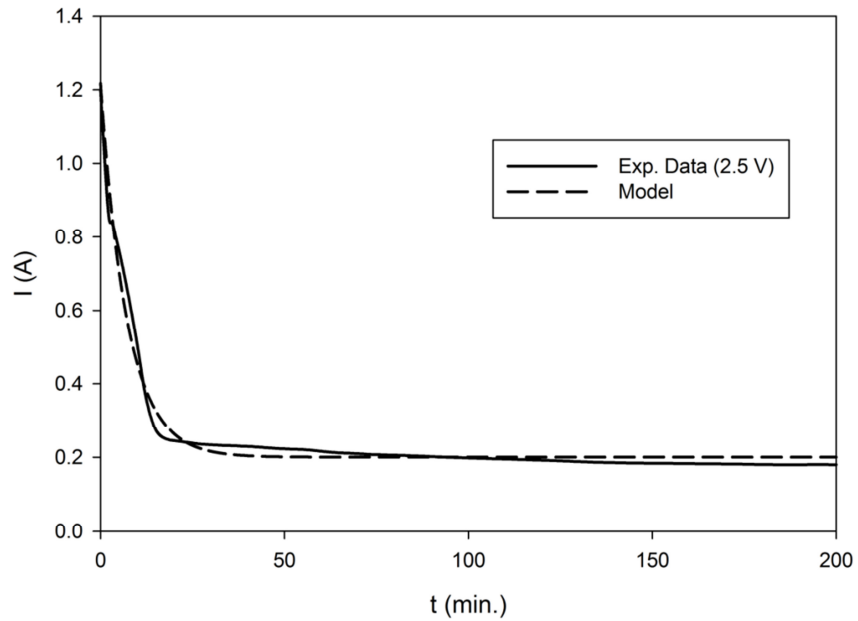
Figure 4.31: Current vs. time graph calculated by the model for the initial 200 minutes of the reduction and comparison of it with the experiment conducted at 2.5 V volts.
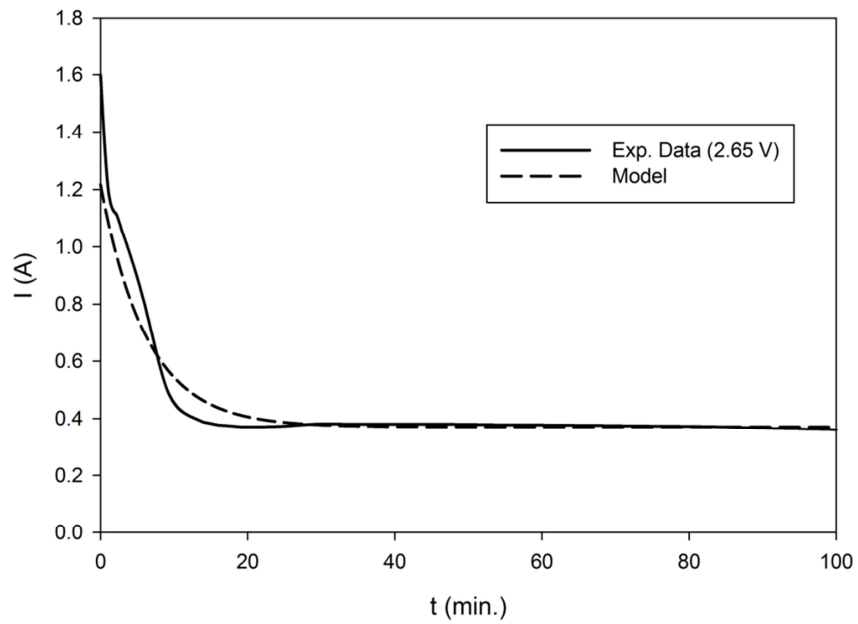
Figure 4.32: Current vs. time graph calculated by the model for the first 100 minutes of the reduction and comparison of it with the experiment conducted at 2.65 V volts.

Table 4.9: Constants used in the calculations.

D (cm^2.sec^{-1})		9.24×10^{-05}
δ (cm)		0.05
l (cm		1
C_O^S (mol.cm^{-3})		0.00248
$C_{O(initial)}^E$ (mol.cm^{-3})		0.0021824
t		0.5
$O(out)$ (mol.s^{-1})	2.5 V	6.91×10^{-7}
	2.65 V	1.28×10^{-6}

CHAPTER 5

CONCLUSIONS

X-ray diffraction results of the electroreduced synthetic and commercially available $CaWO_4$ in molten $CaCl_2$–NaCl (48% mole NaCl) eutectic salt mixture at 600°C demonstrated that metallic tungsten could be obtained with significant concentrations of calcium compounds. Tungsten could be isolated from these compounds by treating the reduced samples with dilute HCl solutions.

Higher current values recorded with the non-sintered pellets indicated the faster reduction of non-sintered pellets.

The electrochemical reduction mechanism of $CaWO_4$ to W in eutectic $CaCl_2$-NaCl salt solution at 600°C was investigated by means of constant potential/current electrochemical reduction and cyclic voltammetry experiments. It has been shown that approximately 2.2 V makes up the sum of theoretical reduction voltage and the overvoltages. The difference between 2.2 V and the reversible reduction potential requirement of the suggested reaction, 0.89 V, was attributed mainly to the overvoltage for CO_2 evolution on graphite anode.

Ten experiments were performed as suggested by the mixture design to examine the effects of three parameters; voltage, temperature and the length of Kanthal wire windings. The results showed that temperature and voltage had strong influences on the output current. An optimum between the applied voltage and process temperature in terms of reduction rate was determined. Kanthal wire windings had no or very small effect on the reduction rate when compared to the other parameters.

HCl cleaning treatment to remove Ca compounds which were found in the reduced samples was investigated by full factorial experiment design. Main effects and binary interactions of temperature, acid concentration and exposure time on the Ca content of the samples were determined. An equation giving Ca weight percent after HCl treatment was developed as a function of temperature, concentration and time within the predetermined limits.

Metallic tungsten powder was produced together with iron directly from rich and flotation scheelite concentrates of Uludağ, by the electrochemical reduction method.

A tungsten production line was designed and manufactured with a capacity of 300 g tungsten production per day. Electrode materials which can withstand the highly corrosive environment constituted by the molten salt, high temperature and gaseous electrolysis products were determined for industrial production.

A basic model based on the diffusion of oxygen ions was developed for electrochemical reduction of $CaWO_4$ pellets. The model was used to simulate the experimental data recorded during reduction experiments at 2.5 and 2.65 V.

Original Contributions;

The production technique described in the thesis is a novel process. As a result, most of the studies done on the process are new and can be regarded as original contributions of the authors to the literature. Some of which can be compiled as follows:

- M^1M^2X type materials were used at the cathode to produce a metal for the first time in electrodeoxidation process. M^1 represents the first metal like Ca, M^2 represents the second metal like W and X is the non-metallic substance like O.
- Metallic tungsten powder at nano and micro scale was produced for the first time in $CaCl_2$ containing molten salt solutions by electrochemical reduction of $CaWO_4$ at solid state.
- Metallic tungsten powder was produced from scheelite concentrates for the first time in $CaCl_2$ containing molten salt solutions by electrochemical reduction at solid state. It is thought that tungsten produced directly from scheelite concentrate could be used in such applications where purity requirement is less stringent. Non-sintered pellets were used instead of sintered pellets for the first time in electrodeoxidation experiments.
- Electrochemical reduction mechanism of $CaWO_4$ to W was illustrated.

For future work;

- Different cell geometries like anode-cathode positions and advanced electrochemical techniques such as pulse current and/or pulse voltage can be tested to increase electrochemical reduction rate of $CaWO_4$.
- Expectation of decrease in electroreduction time of smaller particles may be tested in the future.
- Possible causes of incomplete reduction at larger scale such as the dispersion of graphite particles into the electrolyte should be investigated and solutions should be searched.
- A production line, which will enable continuous removal of the solid products from the cathode while continuously feeding it with the raw material, should be designed.
- Pressing and sintering of the electrochemically produced tungsten powder to obtain end products should be studied to test the performance of the powder.

REFERENCES

[1] Missile Technology Control Regime (MTCR), http://www.mtcr.info/english/index.html, last accessed: January 2013.

[2] Wassenaar Arrangement, http://www.wassenaar.org/, last accessed: January 2013.

[3] Tungsten, International Tungsten Industry Association, 2009.

[4] D. Tang, W. Xiao, H. Yin, L. Tian, D. Wang, Journal of the Electrochemical Society, 159 (2012) E139.

[5] İ. Karakaya, M. Erdoğan, patent, TR 2007 07197 B,: T.P. Enstitüsü, Türkiye, 2007.

[6] İ. Karakaya, M. Erdoğan, patent, 2463387: R.P. Office, Russia, 2012.

[7] İ. Karakaya, M. Erdoğan, patent, 2,703,400 C.P. Office, Canada, 2012.

[8] London Metal Bulletin.

[9] Mineral Commodity Summaries, U.S. Geological Survey, 2012.

[10] Sekizinci Beş Yıllık Kalkınma Planı 2001-2005, DPT.

[11] Türkiye Volfram Envanteri, Maden Tetkik ve Arama Enstitüsü Yayınlarından, Ankara, 1978.

[12] Y. Topkaya, H. Eriç, G. A, M. Timuçin, N. Koç, Etibank Uludağ Volfram İşletmesi Konsantrelerinden APT Üretim Parametrelerinin Araştırılması Raporu, 1981.

[13] T. Rosenqvist, Thermochemical Data for Metallurgists, Tapir, 1970.

[14] D.J. Fray, T.W. Farthing, G.Z. Chen, patent, WO 99/646381999, World patent, 1999.

[15] R.G. Ward, T.P. Hoar, Journal Institute of Metals, 90 (1961) 6.

[16] T.H. Okabe, R.O. Suzuki, T. Oishi, K. Ono, Tetsuto Hagane (J. Iron Steel Inst. Japan), 77 (1991) 93.

[17] T.H. Okabe, T. Oishi, K. Ono, Journal of Alloys and Compounds, 184 (1992) 43.

[18] T.H. Okabe, M. Ikezawa, R.O. Suzuki, T. Oishi, K. Ono, CAMP ISIJ (Proc Annual Meeting of the Iron and Steel Institute of Japan), 3 (1990) 101.

[19] G.Z. Chen, D.J. Fray, Journal of Applied Electrochemistry, 31 (2001) 155.

[20] G.Z. Chen, D.J. Fray, T.W. Farthing, Metallurgical and Materials Transactions B, 32 (2001) 1041.

[21] G.Z. Chen, D.J. Fray, T.W. Farthing, Nature, 407 (2000) 361.

[22] G. Elena, G.Z. Chen, D.J. Fray, Electrochimica Acta, 49 (2004) 2195.

[23] E. Ergül, İ. Karakaya, M. Erdoğan, Journal of Alloys and Compounds, 509 (2011) 899.

[24] W.K. Han, J.W. Choi, G.H. Hwang, S.J. Hong, J.S. Lee, S.G. Kang, Applied Surface Science, 252 (2006) 2832.

[25] G.Z. Chen, D.J. Fray, in: Progress in Molten Salt Chemistry 1, 2000, pp. 157-162.

[26] G.Z. Chen, D.J. Fray, in: TMS Light Metals, New York, 2001, pp. 1147-1152.

[27] X.Y. Yan, D.J. Fray, Metallurgical and Materials Transactions B, 33B (2002) 685.

[28] A.M. Abdelkader, A. Daher, E. El-Kashif, Metallurgical and Materials Transactions B, 38B (2007) 35.

[29] K. Dring, R. Bhagat, M. Jackson, D. Inman, R. Dashwood, Journal of Alloys and Compounds, 419 (2006) 103.

[30] R. Bhagat, K. Dring, M. Jackson, D. Inman, R. Dashwood, The Electrochemical Society, 156 (2009) E1.

[31] M. Erdoğan, İ. Karakaya, Metallurgical and Materials Transactions B, 41 (2010) 798.

[32] İ. Barın, O. Knacke, Thermochemical Properties of Inorganic Substances, Springer-Verlag, Berlin, 1973.

[33] W.T. Thompson, C.W. Bale, and A.D. Pelton: Facility for the Analysis of Chemical Thermodynamics (FACT), McGill University Montreal, Royal Military College of Canada in Kingston, Ecole Polytechnique, Montreal, Canada, 1985.

[34] A. Packter, B.N. Roy, Kristall Und Technik-Crystal Research and Technology, 6 (1971) 39.

[35] M. Erdoğan, Masters Thesis, Department of Metallurgical and Materials Engineering, Middle East Technical University, Ankara, Türkiye, 2007.

[36] D.O. Voight, H. Neels, Kristall und Technik-Crystal Research and Technology, 6 (1971) 651.

[37] T. Hattori, H. Ikezawa, R. Hirano, J. Machinaga, Nippon Kagaku Kaishi, 6 (1982) 952.

[38] J.W. Kim, N.D. Lee, Daehan Hwahak Hwoejee, 10 (1966) 32.

[39] H.L. Slatin, patent, 3,297,554, U.S.P. Office, U.S., 1967.

[40] W. Xu, C. Liao, International Journal of Refractory Metals and Hard Materials, (2011), DOI: 10.1016/j.ijrmhm.2011.11.004.

[41] İ. Karakaya, PhD Thesis, Department of Mining and Metallurgical Engineering, McGill University, Montreal, Canada, 1985.

[42] M. Erdoğan, İ. Karakaya, Metallurgical and Materials Transactions B, 43 (2012) 667.

[43] K.S. Mohandas, D.J. Fray, Metallurgical and Materials Transactions B, 40B (2009) 685.

[44] C. Schwandt, D.J. Fray, Electrochimica Acta, 51 (2005) 66.

[45] Bruker, http://www.bruker.com/products/x-ray-diffraction-and-elemental-analysis/x-ray-spectrometry/s8-tiger/applications.html, last accessed: January 2013.

[46] W. Xiao, X. Jin, Y. Deng, D. Wang, X. Hu, G.Z. Chen, ChemPhysChem, 7 (2006) 1750.

[47] K.L. Strelets, Electrolytic Production of Magnesium, Keter Publishing House, Jerusalem, 1977.

[48] A.J. Bard, L.R. Faulkner, Electrochemical Methods Fundamentals and Applications, John Wiley & Sons, Inc., New York, 2001.

[49] Kanthal Handbook Heating Alloys for Electric Household Appliances, Hallstahammar: Kanthal AB, 2003.

[50] İ. Karakaya, W.T. Thompson, Canadian Metallurgical Quarterly, 25 (1986) 307.

[51] Q. Xu, L.-Q. Deng, Y. Wu, T. Ma, Journal of Alloys and Compounds, 396 (2005) 288.

[52] B.A. Glowacki, D.J. Fray, X.-Y. Yan, G. Chen, Physica C, 387 (2003) 242.

[53] J.O.M. Bockris, A.K.N. Reddy, Modern Electrochemistry 1, Plenum Press, New York, 1973.

[54] Web elements, http://www.webelements.com/oxygen/atom_sizes.html, last accessed: January 2013.

[55] E.B. Freidina, D.J. Fray, Thermochimica Acta, 354 (2000) 59.

[56] E.L. Cussler, Diffusion Mass Transfer in Fluid Systems, Cambridge University Press, Cambridge, 1997.

[57] J. Szekely, N.J. Themelis, Rate Phenomena in Process Metallurgy, Wiley-Interscience, a Division of John Wiley & Sons, Inc., New York, 1959.

CURRICULUM VITAE

Personal information

First name, Surname	**Metehan Erdoğan**
Address	46. Sokak 77/6 Bahçelievler 06490 Ankara/Türkiye.
Telephone	+90(312) 210 5912 Mobile:+90(533) 634 5752
Fax	+90(312) 210 2518
E-mail	metehan@metu.edu.tr, bilgi@megap.com.tr
Nationality	Turkish
Date of birth	25.05.1981
Gender	Male

Work experience

Dates	November 2004-August 2011
Occupation or position held	Research Assistant
Name and address of employer	Metallurgical and Materials Engineering Department, Middle East Technical University (METU), 06800, Ankara/Türkiye.

Dates	August 2008 onwards
Occupation or position held	General Manager (May 2009 onwards).
Name and address of employer	MEGAP Ltd. Co., Middle East Technical University (METU), METU-Technopolis, Silver Blocks, No: 15-A, 06800, Ankara, Türkiye.

Education and training

Dates	February 2007-February 2013
Title of qualification awarded	PhD.
Name and type of organisation providing education and training	Middle East Technical University, Metallurgical and Materials Engineering Department.

Dates	September 2004-January 2007
Title of qualification awarded	MSc.
Name and type of organisation providing education and training	Middle East Technical University, Metallurgical and Materials Engineering Department.
Dates	September 1999-June 2004
Title of qualification awarded	BSc.
Name and type of organisation providing education and training	Middle East Technical University, Metallurgical and Materials Engineering Department.
Dates	September 1995-June 1999
Title of qualification awarded	High School
Name and type of organisation providing education and training	Cumhuriyet High School

Foreign Language	
English	Proficient

Publications	
Patents	1. İ. Karakaya, M. Erdoğan, patent, TR 2007 07197 B,: T.P. Enstitüsü, Türkiye, 2007. 2. İ. Karakaya, M. Erdoğan, patent, 2463387: R.P. Office, Russia, 2012. 3. İ. Karakaya, M. Erdoğan, patent, 2,703,400 C.P. Office, Canada, 2012.
Papers	1. M. Erdoğan, İ. Karakaya, Metallurgical and Materials Transactions B, 41 (2010) 798. 2. M. Erdoğan, İ. Karakaya, Metallurgical and Materials Transactions B, 43 (2012) 667. 3. E. Ergül, İ. Karakaya, M. Erdoğan, Journal of Alloys and Compounds, 509 (2011) 899. 4. A. Sultan, İ. Karakaya, M. Erdoğan, Materials and Corrosion, 63 (2012) 119.
References	1) Prof. Dr. İshak Karakaya 2) Prof. Dr. Muharrem Timuçin 3) Prof. Dr. Naci Sevinç